FCS investigations on the diffusional behaviour of TNF-Receptors upon stimulation in living cells

Margarita Gerken

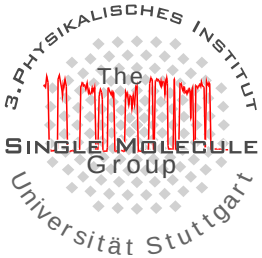

FCS investigations on the diffusional behaviour of TNF-Receptors upon stimulation in Living Cells

Von der Fakultät Mathematik und Physik der
Universität Stuttgart zur Erlangung der Würde eines Doktors der
Naturwissenschaften (Dr. rer. nat.) genehmigte Abhandlung

Vorgelegt von
Margarita Gerken
aus Eriwan

Hauptberichter:	Prof. Dr. Jörg Wrachtrup
Mitberichter:	Prof. Dr. Peter Scheurich
Prüfungsvorsitzender:	Prof. Dr. Udo Seifert
Tag der mündlichen Prüfung:	13. Februar 2008

3. Physikalisches Institut der Universität Stuttgart
2008

Table of contents

Abbreviations

1PE	one-photon excitation
2PE	two-photon excitation
ACF	autocorrelation function
APD	avalanche photo diode
CLD	caveolae like domains
CRD	cysteine rich domains
CT-B	cholera toxin subunit B
cysTNF	CysHisTNF D143N/A145R
cytD	cytochalasin D
DD	death domain
DHPC	diheptanoyl-*sn*-phosphatidylcholine
DOPC	dioleoyl-phosphatidylcholine
DOPE	dioleoyl- phosphatidylethanolamine
DRM	detergent-resistant membrane
ECFP	enhanced cyan fluorescence protein
EGFP	enhanced green fluorescence protein
EYFP	enhanced yelow fluorescent protein
EM	electron microscopy
FADD	Fas-associated death domain
FCS	fluorescence correlation spectroscopy
FLIM	fluorescence lifetime imaging microscopy
FLIP	fluorescence loss in photobleaching
FRAP	fluorescence recovery after photobleaching
FRET	fluorescence resonance energy transfer
GPI	glycosyl-phosphatidyl-inositol
GSL	glycosphingolipids
GUVs	giant unilamellar vesicles
HeLa80	overexpressing with TNF-R2 human cervix carcinoma cell line

l_o	liquid ordered
l_d	liquid disordered
MF TNF-R1/TNF-R2 (-/-; -/-)	immortalized murine fibroblasts
MβCD	methyl-β-cyclodextrin
MPEFM	multiple-photon excitation fluorescence microscopy
NF-κB	nuclear factor κB
PBS	phosphate buffered saline
PSF	point spread function
Rh-PE	rhodamine 6G marked phosphatidylethanolamine
RIP	receptor-interacting protein
SFVI	single-fluorescent molecule video imaging
SM	sphingomyelin
SPT	single-particle tracking
TACE	TNF-converting enzyme
TIRFM	total internal reflection fluorescence microscopy
TNF	tumour necrosis factor
TNF-R1	tumour necrosis factor receptor type 1
TNF-R2	tumour necrosis factor receptor type 2
TRADD	TNF-R-associated death domain
TRAF2	tumour necrosis factor receptor associated factor
wtHeLa	wild-type human cervix carcinoma cell lines
Φ_{fluo}	fluorescence quantum yield

Zusammenfassung

1. Einleitung

Diffusionsprozesse sind in Zellen an vielen biochemischen und biophysikalischen Vorgängen wie Signaltransduktion oder der Bildung von supramolekularen Komplexen beteiligt. Eine genaue Untersuchung dieser Prozesse, z.B. die Bestimmung der Diffusionskoeffizienten und Konzentration der beteiligten Moleküle, ist daher unerlässlich für deren Verständnis. Die geeignetste Methode zur Untersuchung von Diffusionsprozessen ist wohl die Fluoreszenz-Korrelationsspektroskopie (FCS). Bei dieser Methode wird die Autokorrelationsfunktion (*autocorrelation function*, ACF) der Fluoreszenzfluktuation in einem festen Beobachtungsvolumen bestimmt, aus deren Verlauf sich dann die relevanten Parameter bestimmen lassen.

In der vorliegenden Arbeit werden das Diffusionsverhalten der Tumor-Nekrose-Faktor Rezeptoren vom Typ 1 und 2 (TNF-R1, -R2) sowie des TNF-R assoziiertem Faktor Typ 2 (TRAF2) in lebenden Zellen untersucht. Diese Untersuchungen umfassen das Verhalten der Rezeptoren vor und nach Stimulation mit ihrem Liganden sTNF und cysTNF.
Die beiden membranständigen Rezeptoren sind Mitglieder der an der Apoptose beteiligten TNF-Rezeptorfamilie. Die Stimulation der Rezeptoren stellt dabei den ersten Schritt einer Signalkaskade dar, die schließlich das kontrollierte Absterben und die kontrollierte Entsorgung der toten Zelle und deren Bestandteile zur Folge hat. Das Protein TRAF2 hingegen ist ein cytoplasmatisches Protein, das durch Wechselwirkung mit TNF-R2 den Apoptoseprozess negativ regulieren kann. Zur Untersuchung mittels FCS lagen die Proteine als Fusionsproteine, fusioniert mit EGFP und ECFP, in der Zelle vor.

Der Einfluss der Mikroumgebung auf das Diffusionsverhalten der Proteine wurde ebenfalls untersucht. Dazu wurden die Zellen mit 2-Methylcyclodextrin (MβCD) sowie CytochalsinD (cytD) behandelt. Dies führt bei MβCD zu einer Verringerung des Cholesterinanteils in den Zellmembranen bzw. bei cytD zu einer Depolimerisation der Actinfilamente in der Zelle selbst. Weiterhin wurden die Zellen mit der fluoreszenzmarkierten Untereinheit B des Choleratoxins (CT-B) behandelt, das spezifisch an die Glycosphingolipide der Membranen, Bestandteile von Cholesterin-reichen Membranbereichen (sog. *lipid rafts*), bindet, um deren Rolle bei der Diffusion der Rezeptoren zu untersuchen.

2. Apoptose

Apoptose bezeichnet im Gegensatz zur Nekrose den programmierten Tod einer Zelle. Apoptose ist ein essentieller Prozess für alle multizellulären Organismen, da durch ihn unerwünschte, d.h. kranke und überflüssige, Zellen aus dem Organismus entfernt werden. Ist die Apoptose in ihrem Verlauf gestört oder vollständig unterdrückt, kann dies lebensbedrohliche Konsequenzen für den Gesamtorganismus haben. So führt eine unkontrollierte Vermehrung von Zellen und Geweben zu Krebserkrankungen oder Autoimmunstörungen wie Multiple Sklerose. Störungen des apoptotischen Prozesses tragen ebenfalls zum Verlauf der Autoimmunschwäche AIDS sowie zu neurodegenerativen Störungen wie der Alzheimerschen Krankheit bei, sind aber nicht deren Auslöser.

Eine wichtige Gruppe von Membranrezeptoren und deren Liganden, durch deren Zusammenwirken Apoptose ausgelöst werden kann, gehören zur Familie der Tumor Nekrose Faktoren (TNF). Allen Rezeptoren aus dieser Familie ist gemeinsam, dass sie extrazelluläre Domänen besitzen, die reich an Cysteinresten

sind. Die Rezeptoren, die für das Auslösen des Zelltodes verantwortlich sind, besitzen zusätzlich noch eine sog. Todesdomäne (*death domain*, DD) an ihrem zytoplasmatischen Bereich. Diese Domänen selbst bilden durch induzierte Oligomerisierung ihrer Rezeptoren eine Bindestelle für den TNF-Rezeptor assoziierten Todesdomänen (TRADD). Diese sind dann der Ausgangspunkt einer Kaskade, die letztendlich zum Zelltod führt. Die Oligomerisierung der Rezeptoren kann sowohl durch eine Überexpression der Rezeptoren als auch durch extrazelluläre Liganden, z.B. TNF ausgelöst werden.

3. FCS in lebenden Zellen

Die klassische Fluoreszenz-Korrelationsspektrokopie (FCS) und deren mathematische Modelle zur Beschreibung der Autokorrelationsfunktionen (ACF) wurden entwickelt, um die Diffusion, d.h. die Brownsche Bewegung, von Partikeln in viskosen Medien zu beschreiben. In biologischen Membranen und im Zellinneren sind diese Modelle i. A. nicht gültig, da dort die Beweglichkeit von Partikeln starken lokalen Schwankungen unterworfen ist. Diese Schwankungen werden hervorgerufen durch z.B. intrazelluläre Kompartimentierungen, massive Strukturen wie dem Zytoskelett, Membranmikrodomänen oder durch eine Wechselwirkung der Partikel untereinander. Diese Arten von gestörter Diffusion werden auch als anomale Diffusion (*anomalous / non-Brownian diffusion*) bezeichnet. Ein weiterer Typ der anomalen Diffusion ist der aktive Transport von Partikeln durch Proteine entlang filamentöser Strukturen in der Zelle.

Die mathematischen Beschreibungen solcher Diffusionsprozesse sind in Kap. 5.3 kurz skizziert. Die simulierten ACFn für solche Prozesse sind in Abb. 5.4 dargestellt. Man erkennt, dass es bis zu einem gewissen Grad möglich ist, anhand des exakten Kurvenverlaufes auf den jeweiligen Diffusionsprozess zu schließen.

Die Modelle zur Diffusion in Membranen sind allerdings nur dann streng anwendbar, wenn die Memranebene senkrecht zum Anregungsfokus liegt. Liegt diese nicht senkrecht oder hat sie eine nicht zu vernachlässigende Krümmung, so ist die vom Fokus eingeschlossene Fläche größer, und die gemessene Diffusionszeit erscheint daher ebenfalls größer als im senkrechten Fall. Bei einer Kippung der Membran von z.B. 30° beträgt die Abweichung der Diffusionszeit 63% im Vergleich zur senkrecht verlaufenden Membran (siehe Abb. 5.5). Um diese Einschränkung zu überwinden, wird in dieser Arbeit eine Erweiterung der ACF für den 2-dimensionalen Fall vorgestellt. Diese erlaubt es, den Winkel zwischen Membranebene und dem Anregungsfokus zu berücksichtigen. Die so erweiterte ACF wurde anhand des Diffusionsverhaltens von GFP-markierten Gap-Junction Kanälen in HeLa Zellmembranen getestet.

4. Ergebnisse

Diffusion des TNF-R2 Rezeptors. Das Diffusionsverhalten des Rezeptors TNF-R2 wurde in den Zelllinien wtHeLa, HeLa80 sowie MF untersucht. HeLa80 und MF zeichnen sich dadurch aus, dass diese Linien den Rezeptor überexprimieren (HeLa80) bzw. gar nicht exprimieren (MF). Der Wildtyp hingegen bildet TNF-R2 ungestört in normalen Konzentrationen in der Membran aus. Alle Zelllinien werden mit Vektoren transfiziert, die TNF-R2 als Fusionsprotein zusammen mit EGFP oder ECFP enthielten.

Die Messungen ergaben, dass in HeLa80 Zellen die gemessenen ACFn vor und nach Stimulation mit cysTNF ein 2-phasiges Verhalten zeigten. Der dazugehörige kleinere Diffusionskoeffizient war in beiden Fällen nahezu gleich ($\sim 2\times10^{-7}$ cm^2/s), während der größere Diffusionskoeffizient vor der Stimulation einen Mittelwert von $\overline{D} = (3.6 \pm 0.5)\times10^{-9}$ cm^2/s aufwies. Nach Stimulation der

Rezeptoren begannen die Diffusionskoeffizienten zu sinken und waren nach 50 min nicht mehr messbar, da die obere Auflösungsgrenze des Hardware-Korrelators erreicht wurde ($D < 10^{-10}\,cm^2/s$, siehe Fig. 6.7).

Als Ursache für diesen drastischen Abfall wurden untersucht: (1) ein möglicher Einfluß des Liganden auf die Viskosität der Zellmembran sowie (2) ein mögliche Aggregation der stimulierten Rezeptoren. Experimente mit Rhodamin-markierten Phospholipiden ergaben, dass die Viskosität der Membran unabhängig von der Gegenwart von cysTNF ist. Eine Abschätzung der Größe eines möglichen Proteinaggregates mit dem Saffman-Delbrück-Modell ergab eine nicht zu rechtfertigende Anzahl (~7000) von Rezeptormolekülen. Um Artefakte, verursacht durch die Überexpression der Rezeptoren, auszuschließen, wurde das Experiment in wtHeLa sowie MF Zellen wiederholt.

Die experimentell bestimmten ACFn zeigten wiederum ein 2-phasiges Verhalten vor und nach Stimulation der Rezeptoren. Der kleinere der beiden dazugehörigen Diffusionskoeffizienten entsprach dem der vorigen Messung. Eine Änderung gegenüber der Messung in wtHeLa zeigte sich nach Stimulation mit cysTNF. Die Diffusionskoeffizienten stiegen nach 30 min um eine Größenordnung, um nach weiteren 20 min auf ihren ursprünglichen Wert zurückzufallen. Dieser Vorgang könnte mit einer Internalisation der stimulierten Rezeptoren erklärt werden, müsste allerdings in Wellen verlaufen, was aber nicht beobachtet wurde. Neue Studien besagen, dass TNF-R2 nur als Dimer funktional ist. Eine Subpopulation aus Dimern könnte also nach Stimulation internalisiert werden und ließe nur nicht funktionale Monomere in der Membran zurück. Dieser Vorgang würde dann zu dem beobachteten Verlauf des Diffusionskoeffizienten führen. Die experimentellen Daten lassen allerdings keine Rückschlüsse auf die Massen der diffundierenden Partikel zu. Der genaue Grund für das beobachtete Verhalten bleibt somit ungeklärt (siehe Kap. 6.1.2).

Es wurde weiterhin untersucht, ob sich die TNF-R2 Rezeptoren vor oder nach ihrer Stimulation in Cholesterol-reichen Membrandomänen aufhalten. Diese

Domänen wurden dafür mittels MβCD aufgelöst und die Diffusionskoeffizienten der Rezeptoren bestimmt. Die experimentellen Ergebnisse zeigten aber keine Hinweise darauf, dass sich die Rezeptoren in solchen Mikrodomänen aufhalten (siehe Kap. 6.1.4). Ebenso wurde das Verhalten der TNF-R2 Rezeptoren auf mögliche Wechselwirkungen mit den Actinfilamenten des Membrangerüstes untersucht. Dazu wurden die Diffusionskoeffizienten von zwei Rezeptormutanten EGFP-TNF-R2Δcyt14aa sowie EGFP-TNF-R2Δcyt bestimmt. Beide Proteine besitzen Deletionen in ihren cytoplasmatischen Domänen. Einzig die Mutante EGFP-TNF-R2Δcyt, der der komplette cytoplasmatische Teil fehlt, zeigte eine Änderung ihres Diffusionsverhaltens nach der Behandlung der Zelle mit MβCD. Allerdings wurde dieses Verhalten als Artefakt gedeutet, da dieser Mutante die Lys-Lys-Lys-Pro Sequenz (Teile des cytoplasmatischen Bereiches) fehlt. Es wird angenommen, dass dieses Segment phospholipophil ist und für die korrekte Verankerung des Proteins in der Membran verantwortlich ist.

Diffusion des TNF-R1 Rezeptors. Das Diffusionsverhalten des TNF-R1 Rezeptors wurde nur in wtHeLa Zellen untersucht, da eine Überexpression dieses Rezeptors zur Induktion der Apoptose führen kann.
Es zeigte sich, dass das Diffusionsverhalten dieses Rezeptors völlig anders war als das des TNF-R2 Rezeptors. Die gemessenen Diffusionskoeffizienten zeigten eine breite Verteilung zwischen 2×10^{-10} bis 3×10^{-9} cm^2/s. Der Mittelwert der Verteilung lag bei $\overline{D} = (1.2 \pm 0.8) \times 10^{-9}$ cm^2/s und war damit 3-mal kleiner als der entsprechende Wert des TNF-R2 Rezeptors. Im Gegensatz zu TNF-R2 zeigte dieser Rezeptor eine Änderung im Diffusionsverhalten, stimuliert sowie unstimuliert, bei Behandlung der Zelle mit MβCD. Dies spricht dafür, dass der Rezeptor TNF-R1 in Cholesterol-reichen Membrandomänen anzutreffen ist.

Dieses Ergebnis konnte durch die Bestimmung der Diffusionskoeffizienten von CT-B, mit und ohne Stimulation der Rezeptoren, bestätigt werden.
Die Mutante EGFP-TNF-R1Δcyt, die eine vollständige Deletion des cytoplasmatischen Bereiches besitzt, wurde benutzt, um mögliche Wechselwirkungen mit dem Membrangerüst zu untersuchen. Es zeigte sich allerdings, dass die Abwesenheit des cytoplasmatischen Bereiches keine Auswirkung auf das Diffusionsverhalten des unstimulierten Rezeptors hat. Eine anschließende Stimulation des Rezeptors mit cysTNF sowie eine Behandlung der Zelle mit MβCD ergaben ebenfalls keine oder nur geringfügige Änderungen des Diffusionsverhaltens.

Diffusion des TRAF2 Proteins. Das Diffusionsverhalten von TRAF2 fusioniert mit EGFP wurde in der wtHeLa Zelllinie, mit und ohne Stimulation des TNF-R2 Rezeptors, untersucht Die Messungen ergaben, dass TRAF2 im Zytoplasma mit einem mittleren Diffusionskoeffizienten von $\overline{D} = (2.6 \pm 0.2) \times 10^{-7}$ cm^2/s diffundiert, während TRAF2, gemessen in der Nähe der Membran, einen mittleren Diffusionskoeffizienten von $\overline{D} = (0.3 \pm 0.2) \times 10^{-7}$ cm^2/s aufwies. Dies deutet auf eine Wechselwirkung des Proteins mit der Zellwand bzw. dem Zytoskelett hin. Nach der Stimulation der Rezeptoren konnte ein Abfall der Diffusionskoeffizienten beobachtet bis zu Werten von $(5 \pm 1) \times 10^{-10}$ cm^2/s werden. Diese liegen damit im Bereich der Daten, die aus den Messungen der Diffusion des TNF-R2 Rezeptors (in wtHeLa) erhalten wurden. Der zeitliche Verlauf der gemessenen Diffusionskoeffizienten nach der Stimulation war ebenfalls vergleichbar mit dem von TNF-R2. Die für TRAF2 gewonnenen experimentellen Daten sind somit konsistent mit den Daten für das Verhalten des TNF-R2 Rezeptors.

CHAPTER 1

Introduction

In a cell many biochemical and biophysical processes like signal transduction or the assembly of supramolecular structures are driven by diffusion. To gain insight in these processes it is necessary to obtain information about the diffusion coefficients and the concentrations of the involved molecules. The method of choice to observe diffusion processes and quantifying concentrations is the fluorescence correlation spectroscopy (FCS) which analyses the time-dependent intensity of a fluorescent molecule diffusing through the focus of a strongly focused laser beam by calculating the autocorrelation function (ACF) of the fluorescence. The ACF contains all relevant information about the diffusing molecules like the diffusion coefficient, concentration and other intramolecular properties which influences its fluorescence properties.

Derived and firstly applied to measure diffusion processes and chemical kinetics of DNA-drug intercalation in the early seventies [1;2] FCS has recently experienced growing popularity in physical, biochemical and biological applications. The non-invasive character of FCS combined with a lateral resolution of a few hundred nanometres makes this method also a powerful tool for investigations within living cells. It was demonstrated that the application of two-photon excitation (2PE) offers an alternative in biological applications of FCS [3;4]. Due to reduced photobleaching, light scattering and autofluorescence 2PE particularly impro-ves the signal in thick and turbid specimens such as cells and tissues.

Due to significantly improved signal-to-noise ratio and single molecule sensitivity [5] FCS became a widely used method in the field of single molecule physics. The applications of FCS include the investigation of binding of protein subunits [6], conformational changes [7;8], protein oligomerisation [9], as well as the observation of quantum effects like bunching and anti-bunching of photons emitted by a single quantum system [10;11].

In this work the diffusion behaviour of the *tumour necrosis factor receptor type 1* and *type 2* (TNF-R1, TNF-R2) have been examined in living cells before and after stimulation with their ligands sTNF and cysTNF, respectively, with FCS and 2PE. The transmembrane proteins TNF-R1 and TNF-R2 are members of the TNF receptor family capable of initiating apoptosis, the programmed and controlled cell death. Apoptosis plays an important role for the development of all multicellular organisms whereby unwanted or abnormal cells are eliminated during normal development of the organism. Stimulation of TNF-R1 and TNF-R2 represents the first step in the signalling cascade starting the apoptotic process of a cell. For investigating the function of the cytoplasmic domain of TNF-R1 and TNF-R2 the diffusion behaviour of mutants which lacked the complete cytoplasmic domain were investigated. It was also examined the

diffusion behaviour of the *tumour necrosis factor receptor associated factor type 2* (TRAF2) a cytoplasmic protein which appears to be capable of negatively regulating the apoptotic process by interacting with TNF-R2. For the investigations with FCS the cells were transiently transfected with a plasmid which bore the encoded protein, TNF-R1, TNF-R2 or TRAF2, fused with EGFP or ECFP as a fluorescent probe.

CHAPTER 2

Single Molecule Measurements in Cell Membranes

Living cells exchange information through physical and chemical processes that occur at different levels of spatial organization and on a multitude of time scales. The involved events may be extremely fast and highly localised, e.g. binding of signal molecules to membrane receptors, or may be slower and spatially expanded like in highly coordinated wave propagation and translocation of signalling molecules through the cytoplasm and the cell nucleus.

Single-molecule approaches have resulted in revolutionary changes in many areas of biology. Results from single-molecule experiments are highly complementary to ensemble methods. In many cases, the single molecule approach proves to be the unique way of tackling a scientific problem. Recent

advances in optical imaging have demonstrated that it is possible to make observations on the dynamic behavior of single molecules, to determine mechanisms of action at the level of an individual molecule, and to explore heterogeneity among different molecules within a population. These studies have the potential to provide fundamentally new information about biological processes and are critical for a better understanding of cellular function. High-resolution methods, such as x-ray crystallography and NMR, have provided a vast array of structural detail for biological molecules, yet the output of these methods is limited by its static molecular view and ensemble averaging. Single molecule methods provide an alternative set of approaches that will lead to a more direct view of the action of individual molecules without the need to infer process or function from static structures. Real-time measurements on the spatial and temporal fluctuations of single molecules in living cells, which are not possible using other methods, are a major goal of this initiative.

Measurements on single biomolecules fall into three categories: optical (fluorescence and nonlinear optical spectroscopy), electrical (e.g. patch clamp technique for ion channels), and mechanical force measurements. Each measurement type allows real time observation of dynamical processes of individual macromolecules. Single molecule manipulation techniques (atomic force microscopy, magnetic and optical tweezers, microfluidics, and biomembranes devices) provide a way to study molecular machineries and also to control their biological reactions and functions. Single molecule imaging with high spatial resolution (diffraction limited or nanometric) is now making it possible to track individual biomolecules with specific labels, and to follow their biochemical reactions in living cells. The extension of single molecule techniques to track and measure individual biomolecules in living cells has the potential to revolutionise our understanding of cell signaling.

2.1 Signalling in living cells

Various fluorescence microscopy based techniques, such as fluorescence recovery after photobleaching (FRAP) [12-15], fluorescence loss in photobleaching (FLIP) [14;16-19], fluorescence resonance energy transfer (FRET) [12;15;20], fluorescence correlation spectroscopy (FCS) [21-25], multiple-photon excitation fluorescence microscopy (MPEFM) [26-28] and spectroscopy (MPEFS) [3;4] fluorescence lifetime imaging microscopy (FLIM) [29], total internal reflection fluorescence microscopy (TIRFM) [30], single-fluorescent molecule video imaging (SFVI) [31], single-particle tracking (SPT) [32-35] and related techniques that have evolved in the past decade are, at the present time, probably the most sensitive techniques that can detect and identify single molecules in a cell and investigate dynamic processes on the plasma membrane.

Recently, FCS and other single molecule techniques have contributed considerably to our understanding of the physicochemical behaviour of membrane compositions and their influence on receptor partitioning in different membrane microdomains [33;36].

FCS, single molecule tracking and FRAP studies have the potential to provide important information to unravel the interplay between membrane protein dynamics and membrane structure.

For example, FCS experiments on the b2-AR receptor, a member of the family of G-protein coupled receptors, in A549 cells revealed three different diffusion coefficients [37]. In addition to the diffusion of free, unbound ligand with a diffusion coefficient $D_{free} = (2.11 \pm 0.04) \times 10^{-6}$ cm^2/s, two other distinct mobilities of receptor-ligand complexes were found. The higher diffusion coefficient $D_1 = (2.88 \pm 1.72) \times 10^{-8}$ cm^2/s most likely corresponds to the lateral mobility of the receptor-ligand complexes localized in caveolae, because resting b2-AR are

found mainly in caveolae [38;39]. Slower diffusion complexes with D_2 = (1.01 ± 0.46) × 10^{-9} cm^2/s were found to be restricted to the plasma membrane. During incubation, the occurrence of receptor-ligand complexes with D_2 was governed by a higher-order kinetic model and reached its maximum after ~15-20 min. In FRAP experiments, a diffusion coefficient of D = 4-12 × 10^{-9} cm^2/s was found for the b2-AR fused with GFP [40] whereas caveolae, associated with GFP tagged caveolin-1 fusion proteins, exhibited a diffusion coefficient of 1.0 × 10^{-10} cm^2/s [41].

Douglass et al. investigated the mobility of the transmembrane proteins CD2, LAT as well as Lck, in T cells with the FRAP method [42]. For the CD2 receptors the authors observed immobilisation and clustering upon activation. After treatment with MβCD no changes in the immobilisation and clustering behaviour were observed so the authors concluded that lipid rafts are unlikely to be the primary determinant of diffusional immobility or the formation of CD2/Lck/LAT clusters. Their study also revealed that T-cell receptor activation induces the formation of membrane subdomains, distinct from lipid rafts, built by a network of protein-protein interactions (see chapter 4.4) which is capable of trapping distinct signalling molecules. Experiments with mutant proteins, whose mutations interfere either with targeting to lipid rafts or with protein interactions suggested that the observed microdomains are created by a network of protein-protein interactions, rather than by lipid rafts or an underlying actin cytoskeleton.

In summary, the diffusional behaviour of different proteins in the T cell signalling pathway vary significantly and do not correlate with biochemical fractionation into lipid rafts.

Upon the ligand activation, many receptor molecules form clusters and subsequently induce the binding of cytoplasmic signalling molecules. The diffusion of these large signalling complexes are often greatly reduced as compared to those for the receptors before stimulation [43-45]. Recently, Fujiwara et al. investigated this issue by using both SFVI and SPT with a time

resolutions of up to 25 ms [33] and found that both the transmembrane protein transferrin receptor (TfR) and the unsaturated phospholipid dioleoylphosphorylethanolamine (DOPE) are confined within 230 nm compartments being comprised in larger 750 nm compartments [33;46]. The average residence time of DOPE in such a compartment was 13 ms, which is shorter than that of TfR (65 ms) by a factor of 5. The authors concluded that interactions with the membrane skeleton are primarily responsible for such temporary confinement (see chapter 4.4). Such membrane compartmentalization and hop diffusion of phospholipid molecules among these compartments were found in eight cell lines examined by Murase and co-workers [47]. They found that the cytoplasmic domains of transmembrane proteins collide with the membrane skeleton, which induces temporal confinement of these transmembrane proteins within the membrane skeleton mesh [35;48-50]. Therefore, the diffusion along the cell membrane is slow, not because the diffusion per se is slow (the diffusion rates within a compartment are as large as those found in artificial reconstituted membranes see [51;52], but because it takes time to hop across the compartment boundary between adjacent compartments.

However, Daumas et al. recently reported that the G-protein coupled receptor, m-opioid receptor (mOR), is almost totally confined within domains (with almost no probability of escape, i.e., no hop movements) that itself underwent very slow diffusion [53].

Other investigators also observed transient confinement behavior which appeared to be related to lipid raft association in some cases [32], but not in others [54].

Studies an the diffusion of the H-Ras protein, a membrane bound GTPase which is involved in the regulation of cell proliferation, differentiation and apoptosis [55-57] showed that inactive H-Ras is partially localized in 44 nm lipid rafts, that covered about 35% of the entire membrane surface whereas active H-Ras is

essentially absent from these structures. Electron microscopy (EM) studies recently revealed that active H-Ras seemed to be localized in small cholesterol independent microdomains with a diameter of 40 - 50 nm [58]. FRAP experiments showed, that there is an immobile fraction of H-Ras independent of the activation state. It was also shown, that cholesterol depletion increased the diffusion coefficient of non-activated wtRas by a factor of 2 indicating an association with lipid rafts [59;60]. FRET studies showed that the mobility of H-Ras is severely reduced upon activation of Ras, presumably by binding of activated Ras to specific scaffolding proteins [57]. Activation of H-Ras resulted in a severely reduced mobility at which half of the activated H-Ras molecules were found immobile and the remaining mobile H-Ras molecules were slowed down by a factor of 3 - 4. One possible explanation for the decrease in mobility of active H-Ras suggested by other studies is its transient binding to signalling complexes [57] or small non-raft domains [58-60].

Imaging of plasma membrane proteins by confocal microscopy and single-molecule techniques provide different but potentially complementary views of membrane structure and protein dynamics, but these two approaches have not been yet combined in a single study on a given cell type. Moreover, published single-molecule studies have focused on single proteins, but comparisons of several proteins can potentially provide new information on factors that influence protein mobility in the plasma membrane.

2.2 Microdomains and compartimentalisation in membranes

The mechanisms by which a cell adapts its functional membrane organization are until now poorly understood and therefore subject of ongoing investigations and

discussions. Lateral organization and the dynamics of lipids and proteins in the plasma membrane are important for many cellular processes such as signalling, endocytosis and intercellular interaction.

Investigations of lipid and protein dynamic in plasma membranes revealed that their diffusion times are reduced 5 up to 100 times compared to dynamic processes in artifical membranes [61-65]. Generally, this behaviour is attributed to lipid-lipid and lipid-protein interactions, due to the more complex composition of a biological membrane, as well as interactions of lipids and proteins with the membrane skeleton. A more detailed discussion of these interactions will be given at the end of this chapter. Alternatively, the existence of lipid microdomains, called rafts, is discussed to be responsible for the observed diffusional behaviour in biological membranes. Rafts are liquid ordered (l_o) membrane domains that are enriched in cholesterol and sphingolipids as well as in lipid-modified proteins, e.g. glycosyl-phosphatidyl-inositol (GPI)-anchored proteins and cholesterol-binding proteins such as caveolins [66]. Furthermore, raft domains are more thightly packed than the surrounding liquid disordered (l_d) phase of the bilayer [67-69] due to the saturated hydrocarbon chains of their lipids and protein membrane anchors resulting in a high degree of order. This contrasts with the disordered state of most lipids in the plasma membrane.

Despite much evidence supporting the concept and existence of lipid rafts their function is still debated [70]. Classically, rafts have been viewed as stable pre-existing cholesterol rich l_o domains in which proteins with appropriate anchors are able to partition [71-73]. An alternative view has been that these domains are unstable assemblies of saturated lipids and cholesterol which become stabilized by the presence of lipid anchored proteins [74;75]. However, it turned out that rafts are by no means static but dynamic structures, which means that proteins as well as lipids can move in and out of raft domains. Several transmembrane proteins, e.g. H-Ras [54-60], TCR [42] and EGFR [76;77], have been reported to associate with lipid rafts. Accordingly, several adaptor [78-80] and signalling

proteins [81;82] were found associated to rafts, too. Therefore, it is supposed that their main function consist of forming a platform to concentrate certain proteins which are required for distinct functions in membrane signalling processes [73;83].

The size of rafts domains is still not clear. Domain sizes of about 50 nm determined with photonic force microscopy experiments [71;84] indicates that larger membrane domains observed with fluorescence microscopy using raft markers are rather aggregates of rafts than single ones. But whatever the rafts real size is, it is supposed that they contain only a few proteins (3) and they have to cluster together to engage in membrane function.

The first biochemically definition of rafts was based on their insolubility in the non-ionic detergent Triton X-100 at 4^{o}C [85]. These isolated detergent-resistant membrane (DRM) fractions are believed to be aggregates of lipid rafts. Thus, their composition and size did not represent the native state of rafts in the cell membrane [86;87]. Caveolin was found to be part of the DRMs and it was shown that caveolae, flask-shaped membrane invaginations formed by their scaffolding protein caveolin, are one morphological identifiable raft structure [66;88].

Recent work revealed that rafts play an important role in the endocytic process. It was shown that crosslinked GPI-anchored proteins tended to translocate to caveolae and subsequently became endocytosed. Internalisation via the caveolin-mediated endocytic pathway was also shown for several other proteins like cholera toxin, folic acid and lactosyl ceramid [89]. Other experiments showed that raft-associated proteins are endocytosed by the other major internalisation pathway the clathrin-mediated endoctosis even though this pathway normally excludes lipid rafts [90].

Several immune receptors use lipid rafts as platforms wherein they interact with their signal transduction molecules starting the signalling cascade. This was demonstrated for the T-cell and IgE-receptor as well as for the receptor tyrosine

kinases. These receptors translocate to rafts upon activation and subsequent aggregation where they initiate a signalling cascade [91-93].

Raft formation and dynamics were also investigated in artifical model membranes. Many groups investigated the spatial and dynamical organization of lipids in giant unilamellar vesicles (GUVs) with fluorescence microscopy using fluorescent membrane probes [34;94]. In GUVs composed of ternary mixtures of cholesterol with phospholipids and sphingolipids a spatial separation of sphingolipid enriched l_o phases from phospholipid enriched l_d phases was observed when the the cholesterol content exceeded 10 mol%. The observation of these "artifical rafts" provided a tangible proof for the coexistence of l_o and l_d phases [34;94;95] in cells. The artifical rafts can exhibit several distinct shapes. Baumgart et al. presented stunning fluorescence images of raft domains in the shape of rods, stripes, circles and rings in cholesterol containing GUVs. Furthermore, it appeared that the l_d phases were particularly found in membrane areas of high curvatures, while the l_o phases were found in areas of lower curvatures [96].

FCS measurements in GUVs revealed the role of cholesterol in adjusting the lipid mobility in raft containing membranes. In GUVs, composed of cholesterol, the phospholipid DOPC and sphingomyelin (SM), the lipid mobility in the non-raft l_d phases is nearly 2 times faster than in GUVs devoid of cholesterol [97]. Lipid mobility in the SM-enriched l_d phases increased even by a factor of 8 when the the cholesterol concentration is raised form 10% to 33%. On the other hand, it was also found that the lipid mobility is almost unaffected by the SM level [34]. These results might imply that cells can modulate their membrane lipid and protein mobility by tuning the cholesterol level in the membrane. Other experiments used raft containing GUVs to investigate the effect of crossllinking membrane components upon their diffusional behaviour. It was shown, e.g. that the ganglioside GM1, the membrane receptor for cholera toxin, partitioned

strongly into the l_o domains [34;85] after crosslinking to four other GM1 molecules induced by the cholera toxin subunit B pentamer [98;99]. Although experiments on model membranes showed that cholesterol depeletion induced by methyl-β-cyclodextrin (MβCD) leads to raft disruption along with an increased mobility of raft proteins which were released from their confining domains, the effect of cholesterol depeletion upon cell mebranes is unexpectedly complex. While some studies reported that cholesterol depletion led to an increased diffusion of raft proteins [32;59;60;71], others reported a drop in mobility for both raft and non-raft proteins. Some authors also reported a drop in mobility [51] and even immobilisation of proteins and lipids in cholesterol depleted cells [36;54;100]. For example, in a study by Edidin et al. it was shown that cholestrol depletion led to an immobilisation of human leukocyte antigen (HLA) molecules in the cell membrane [100]. It was possible to reverse this effect by a treatment with cytochalasinD (cytD) which causes disruptions of the cytoskeletons actin filaments and inhibits further actin polymerization. The same effect could be mimicked by the sequestration of phosphoinistol-bisphosphate, a major regulator of the actin skeleton. These results indicate that cholesterol depletion may not function solely by breaking up raft domains but that cholesterol depletion triggers an interaction between the raft confined proteins and the membrane skeletons actin filaments.

Data from several experiments suggest that there are other kind of microdomains in cell membranes beside rafts. These domains are mainly characterized, in contrast to rafts, by their insensitivity to cholesterol depletion. It was shown that the inactive H-Ras protein partially localises in lipid rafts, but active H-Ras was found in cholesterol independent microdomains with a diameter of 40-50 nm which were also recently observed by electron microscopy [56;58-60]. SPT experiments with the fluorescently labelled H-Ras membrane targeting sequence indicates that 30-40% of the molecules are constrained in domains of about 200

nm which are insensitive to cholesterol depletion as well as actin depolymerisation [54].

Studies on the diffusional behaviour of cell membrane molecules revealed that lipids and membrane molecules, without being confined into lipid microdomains, undergo anomalous diffusion [33;35;47;48;101-103]. This kind of diffusion is neither isotropic nor homogeneous like simple Brownian diffusion but inhomogeneous and anisotropic on some timescales. For example, it was found that the rapid diffusion of dioleoyl-phosphatidylcholine (DOPC) molecules were confined within 230 nm compartments before the molecule hopped to a neighboured compartment. These hopping events, which is also called hop-diffusion, appeared every 11 ms on the average [35;48;104]. Anomalous diffusion is supposed to be the result of two main mechanisms. The first mechanism is the binding of transmembrane proteins with the actin filaments of the membrane skeleton. The immobilised proteins will act as pickets of a fence along the membrane skeleton meshwork. The pickets can confine membrane proteins as well as lipids through both steric hindrance and circumferential slowing resulting in a compartmentalisation of the cell membrane [105]. Membrane molecules can freely diffuse inside the compartments and can hop to a neighboured compartment when the membrane skeleton fluctuates and enlarges the distance between adjacent pickets. The other proposed mechanism is the collision of the cytoplasmic portion of transmembrane proteins with the cytoskeleton causing a temporary confinement of the transmembrane protein within the meshs of the membrane skeleton meshwork. In this model the transmembrane proteins can hop to a neighboured compartment when the skeleton fluctuates, transiently dissociates or when the proteins kinetic energy exceeds the barrier potential [33].

Whereas monomers of membrane molecules hop between adjacent compartments with relative ease, oligomers and molecular complexes have to

hop all at once which results in lower hopping diffusion rate for complexes and oligomers. Thus, the two described mechanisms provide an enhanced confinement of molecular complexes and oligomers within the compartments. Additionally, molecular complexes and oligomers possess a higher affinity to be bound or tethered to the membrane skeleton which also induces a temporary immobilisation or trapping of the molecules. All these mechanisms are supposed to be responsible for an effect called oligomersation-induced trapping, which describes the immediate arrest of molecular complexes within the membrane compartment where an extracellular signal was recieved [104;106]. Thus, protein barriers in the membrane, inuduced by bound protein pickets or temporary immobilised transmembrane proteins due to collisions with the membrane skeleton, may play a crucial role in localising receptors and intracellular signalling molecules at the site where an extracellular signal was recieved. This is an effect which is essential for polarised cell responses, such as phototaxis and cytoskeletal reorganisation.

CHAPTER 3

Structure and Function of the Investigated Proteins

All proteins which were investigated in this work are part of the signalling cascade of the programmed cell death also called apoptosis. Therefore this chapter will start with a short introduction to the principles of apoptosis. The structure and function of the investigated proteins will be given in the chapters 3.1.1, 3.1.2 and 3.1.3.

3.1 Apoptosis

Apoptosis, or programmed cell death, is a normal component of the development and health of multicellular organisms. Cells die in response to a variety of

stimuli and during apoptosis they do so in a controlled, regulated fashion. This makes apoptosis distinct from another form of cell death called necrosis. Necrosis is an uncontrolled cell death caused by e.g. viral or bacterial infections and physical damage which leads to lysis of cells, inflammatory responses and, potentially, to serious health problems (Fig. 3.1). In contrast apoptosis is a process in which cells play an active role in their own death. That is why apoptosis is often referred to as cell suicide. The term apoptosis was first used by Kerr et al. [107] and is of greek in origin, meaning 'falling (or dropping) off', in relation to petals from flowers or leaves from trees.

Apoptosis is an important process for all multicellular organisms whereby unwanted cells are eliminated during normal development. The inappropriate regulation of the apoptotic process therefore have severe consequences for the whole organism. The inability to induce apoptosis which leads to an uncontrolled proliferation of cells can cause cancer and autoimmune diseases like multiple sclerosis. In contrast, its inappropriate induction contributes to diseases such as the acquired immune deficiency syndrome (AIDS) and neurodegenerative disorders like the Alzheimer disease.

Cells undergoing apoptosis usually exhibit a characteristic morphology, typically including fragmentation of the cell into membrane-bound apoptotic bodies, nuclear and cytoplasmic condensation and cleavage of the DNA into small fragments. The cells or fragments are then phagocytosed by macrophages (Fig.3.1).

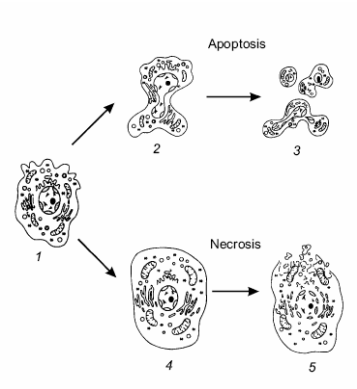

Figure 3.1. Changes in the cell structure resulting from necrosis and apoptosis: 1) a normal cell; 2) apoptotic cell shrinking with the formation of bubble-like protrusions; 3) cell fragmentation with the formation of apoptotic vesicles; 4) cell swelling during necrosis; 5) necrotic cell disintegration (according to [108]).

Apoptosis is a silent and altruistic form of programmed cell death that can be triggered by intracellular regulatory circuits, but also externally *via* membrane receptor stimulation. Prominent cell surface molecules capable of initiating the apoptotic process include several members of the tumour necrosis factor (TNF) family of ligands and receptors [109]) The members of the TNF receptor family are related to each other in possessing extracellular cysteine-rich domains. The death-inducing members of this family also contain a characteristic 80 amino acid cytoplasmic “death domain” (DD), a protein-protein interaction motif critical for engaging downstream components of the signal transduction machinery.

The ability of members of the TNF family of ligands and receptors to specifically trigger cell death was first shown for TNF itself, which transduces the apoptotic signal by binding to the TNF-receptor (TNF-R) [110]. Such mechanism is well understood, for example for TNF-R type 1 (TNF-R1). According to the accepted model, TNF-R1 forms oligomers upon TNF binding

[111], the TNF-R-associated death domain (TRADD) adaptor protein, then binds to the oligomers through the DD in the C-terminal region of TNF-R1. TRADD recruits signalling proteins that activate the apoptosis cascade [112-114]. Activation is also induced by the overexpression and self-aggregation of receptors [115].

The binding of TRADD to the DD of TNF-R1, also recruits additional adaptor proteins: receptor-interacting protein (RIP), TNF-R–associated factor 2 (TRAF2), and Fas-associated death domain (FADD) (Fig. 3.2).

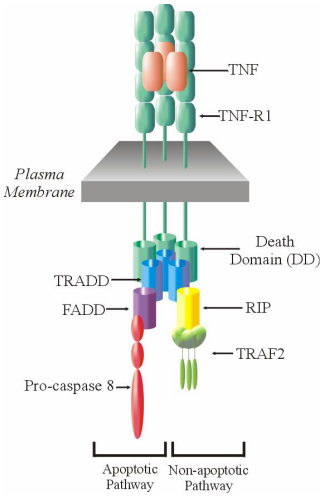

Figure 3.2. TNF-R1 signal transduction pathway. Interaction TNF ligand with TNF-R1 leads to the activation of two opposite pathways: non-apoptotic and apoptotic.

Recruitment of TRAF2 leads to the activation of the transcription factor, nuclear factor κB (NF-κB). This transcription factor is responsible for the expression of genes important for several biological processes, including cell growth and death.

Recruitment of FADD leads to the induction of apoptosis via the recruitment and cleavage of pro-caspase 8. Caspase-8 is a member of a family of cystein containing, aspartate directed proteases. Caspases may be divided into two subfamilies: the initiator caspases and the effector caspases. TNF-R1-mediated activation of apoptosis depends on a caspase cascade instigated by the initiator caspase-8 or initiator caspase-10 [116]. After cleavage and activation through the recruitment to TRADD-FADD, caspase-8 or caspase-10 activate downstream effector caspases-3 and 7 [117]. The activation of effector-caspases leads to cell death (Fig. 3.2).

3.1.1 TNF ligand superfamily

Most ligands of the TNF superfamily are expressed in a number of different tissues and occur both as soluble proteins as well as type II transmembrane proteins. Some of them are expressed in the immune system, where they play a major role in the regulation of proliferation and in the protective function of pathogen sensitive cells. These ligands typically form stable homotrimers capable of multimerizing their receptors [118]. This interaction plays an important role for intracellular signal induction such as recruitment of adaptor proteins (e.g. members of the TNF receptor-associated factor (TRAF) family or DD-containing proteins like TNF receptor-associated death domain protein (TRADD)). The recruitment of TRAF proteins leads to gene induction (cell proliferation), while the recruitment of FADD protein via TRADD leads to activation of the apoptotic program via the activation of initiator caspases.
Like with most members of the family there exist two forms of TNF, the membrane-bound form of TNF (mTNF) and the soluble cytokine (sTNF), which is derived from proteolytic cleavage of the 26 kDa membrane form [119].

Trimers of mTNF are already formed inside of the cell [120] and translocate to the plasma membrane where they can be processed by TACE (TNF-converting enzyme) to release soluble TNF-trimers [121]. Both ligand forms are bioactive only as self-assembled and stable, but non-covalently linked trimers [122]. Differences in bioactivity between the membrane bound and the soluble ligand form have been shown for TNF [119]. The soluble, mature form of TNF is able to bind to both TNF-R1 and TNF-R2, but only TNF-R1 is fully activated. In contrast, membrane bound TNF has been shown to activate TNF-R1 as well as TNF-R2 effectively [119;123]. The TNF interacts with cysteine rich domains (CRDs) 2 and 3 of the two TNFRs (see below).

Each TNF monomer subunit built up from β-sheets in a sandwich-like structure of antiparallel β-strands. The strands are arranged in a so called "jelly roll" arrangement [124]. A topology diagram is present in Fig. 3.3. The *core* of the "jelly roll" consists of two sheets of four β-strand. The "inner" sheet (strands **a**, **h**, **c**, and **f**) is involved in trimer contacts while the opposite sheets (**b**, **g**, **d**, and **e**) forms the outer surface of the trimer. Thus, both the inner and outer sheets comprise five β-strands each. The inner sheet facing the trimer axis is essentially flat while the outer sheet is highly curved. One of the β-sheets containing hydrophobic amino acids forms the interaction site with the two other subunit. The second β-sheet contains more hydrophilic residues. It also encompasses the receptor binding sites, which are located in the grooves formed by two of the three monomers, respectively. The trimeric ligands feature a triangular conical structure with the transmembrane domain sitting at the base of their pyramidal structure (Fig. 3.4 A).

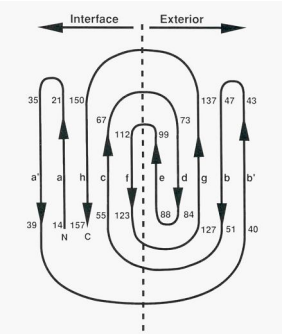

Figure 3.3. Topology diagram represent the "jelly-roll" connectivity of the β-sandwich. The TNF monomer is a β-sandwich composed of ten strands; the five strands to the left of the dashed line form the inner sheet of the sandwich, the five strands to the right form the outer sheet [124].

The membrane-integrated forms of the TNF family members are also believed to possess this homotrimeric structures. The membrane TNF analogue (cysTNF) was generated by introducing a histidine-tag with a cysteine residue to the N-terminus of TNF. This cystein residue allows the formation of disulfide bridges under non-reducing conditions leading to the formation of TNF oligomers by covalently linking two TNF monomers. This molecule was shown to possess membrane TNF-like activity [123].

3.1.2 TNF receptor superfamily

In contrast to the ligands, receptors of the TNFR family are typically type I transmembrane proteins. All members of TNF receptor family contain at least one copy of a cysteine rich domain (CRD) in their extracellular part, stabilized by three disulfid bonds [125].

The receptors TNF-R1 and TNF-R2 have four CRDs as shown in Fig. 3.4 B. The N-terminal CRD1 was identified to be responsible for ligand independent formation of dimers or trimers. CRD2 and CRD3 contain the TNF ligand binding sites (Fig. 3.4 C) whereas the function of CRD4 has not been identified yet.

As was mentioned above, two subclasses of receptors regarding their intracellular domains have been defined: the DD containing or death receptors (TNF-R1) and the non-death domain receptors (TNF-R2). TNF-R1 is expressed in all tissues whereas TNF-R2 is mainly expressed in lymphocytes and other cells of the immune system, endothelial cells and neurons.

After the latest model proposed by Micheau and Tschopp [126] the complex containing of TNF-R1–TRADD–RIP–TRAF2 and possibly other proteins, is rapidly assembled in lipid rafts after stimulation of TNF-R1 by TNF. Lipids rafts are conceived as glycosphingolipids (GSL) and cholesterol enriched and spatially differentiated microdomains in cell membranes. They have been termed lipid rafts based on their ability to float in a discontinuous density gradient after lysis in nonionic detergents (Munro, 2003; Simons and Toomre, 2000).

Within one hour after formation of this complex a large number of RIP and TRAF2 proteins dissociate from TNF-R1. Thus, the DD of TRADD becomes available for association with FADD leading to caspase-8 activation [126].

TNF-R2 is a typical member of non-death domain containing subgroup of the TNF receptor family. It directly binds TRAF2 protein leading to the activation of NF-κB-signalling pathways.

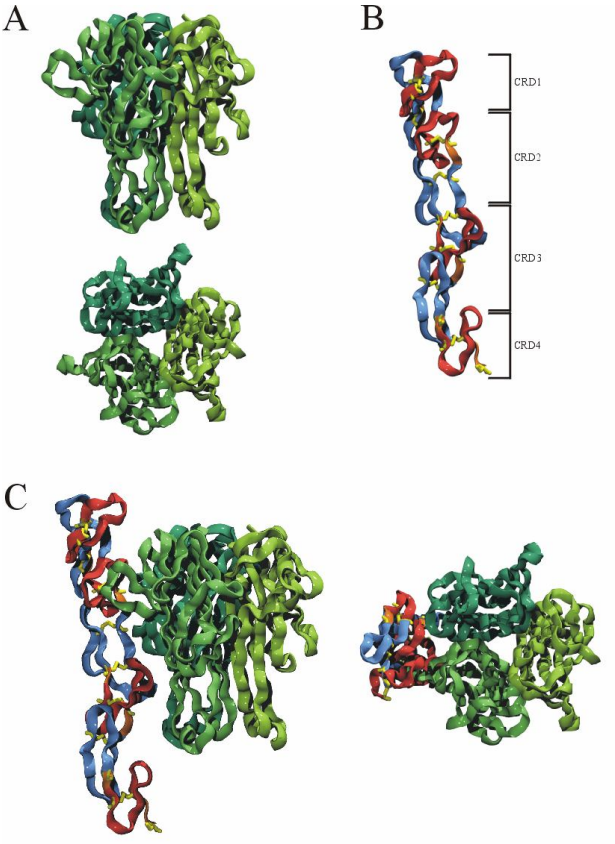

Figure 3.4. (**A**) Trimeric structure of TNF. Structure of the TNF trimer shown from the side (upper graph) and top (lower graph) views with each monomer differently green coloured. (**B**) Monomeric structure of the extracellular part of TNF-R1. (**C**) Structure of the liganded complex shown from the side (left) and top (right). Contact structure modeled on the interaction between a trimer of TNF and a monomer of TNF-R1 showing that the ligand contacts are made primarily in CRD2 and CRD3. Picture created with VMD [127].

The TNF-R2 possibly plays an important role in localized signalling during cell–cell interaction, but it induces apoptosis in some cells [128]. However, the

functional role of TNF-R2 is far from being understood. This might be due to the fact that TNF-R2 is fully activated only by mTNF, while TNF-R1 can be activated by sTNF as well as by mTNF [119].

3.1.3 TRAF protein superfamily

A family of cytoplasmic proteins has been identified that appears to be capable of negatively regulating apoptotic pathways as well as inducing the expression of genes that promotes cell survival. Members of this family of signal transduction molecules were first described because of there ability to bind to TNF-R2 and, therefore, were named TNF receptor-associated factors (TRAFs). Subsequent studies have demonstrated that TRAFs serve as adapter proteins for a wide variety of cell surface receptors and play important roles in regulating not only apoptosis but also stress responses.

One of the first member of the TRAF family was identified due to its association with the cytoplasmic tail of TNF-R2 and designated as TRAF2. Like all other members of this family, TRAF2 contains a conserved C-terminal domain of about 200 amino acids, called the TRAF domain. The TRAF domain can be further subdivided into a coiled-coil N-TRAF domain and a highly conserved C-TRAF domain (Fig. 3.5 A) [129].

The crystal structure of the TRAF2 revealed a trimeric, clover leaf like structure where the TRAF-C domains representing the leafs and the coiled-coil TRAF-N domains the stalk (Fig. 3.5 B, C) [130].

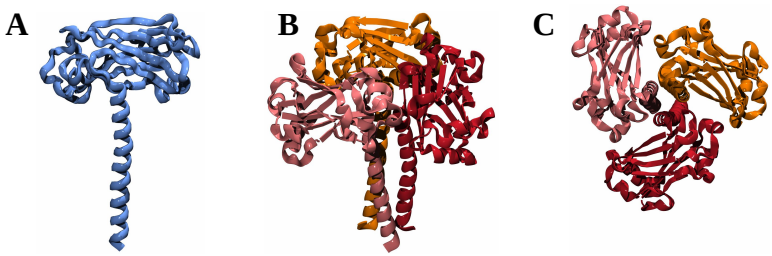

Figure 3.5. (**A**) Monomeric structure of TRAF2 protein. Clover leaf like trimeric structure of TRAF2 protein shown from the (**B**) side view and (**C**) top view. Picture created with VMD [127].

At the N-terminus TRAF2 has a RING finger structure plus five zinc fingers. A schematic sketch of the TRAF2 protein structure is shown in Fig. 3.6.

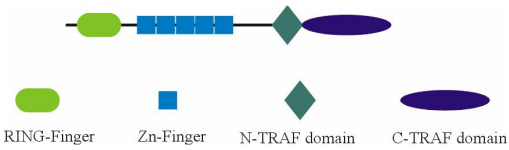

Figure 3.6. Schematic structure of TRAF2 protein.

Investigation of the TRAF2 protein show, that the TRAF domain is required for the TNF-R2 binding and is essential for the formation of TRAF homo- and heterotrimers, whereas the N-terminal part of the TRAF2 molecule is essential for signalling [131].

As mentioned above, TRAF2 can not bind directly to TNF-R1, it becomes part of the receptor signalling complex of TNF-R1 via interaction with TRADD and RIP. The crystal structure of the complex, consisting of the N-terminal part of TRADD (TRADD-N) and the TRAF domain of TRAF2, showed that TRADD-N binds stoichiometrically to the trimeric TRAF2 complex [132]. One TRADD-N

molecule interacts with the upper rim of the clover leaf formed by the C-TRAF domain.

3.2 The autofluorescent proteins GFP and CFP

The proteins investigated in this work were labelled with the green fluorescent protein (GFP) mutants EGFP and ECFP to examine the dynamics of TNF-R2 and TNF-R1 in plasma membrane as well as TRAF2 in the cytoplasm.

The green fluorescent protein was at first isolated from the pacific jellyfish *Aequorea victoria*. In this organism, it serves as the emitting species of the native bioluminescence system [133]. The GFP exhibits an intrinsic fluorescence, there is no cofactor required, from a fluorophore formed by covalent modification of three amino acid residues within its structure. Since its sequencing and cloning were performed [134], GFP and its spectral mutants can be expressed in bacterial, yeast, plant or animal cells and used as a natural fluorescent marker expressed with a selected protein. Therefore, in the last years GFP and its mutants have become powerful biological research tools.

The structure of GFP was resolved by Yang et al. with a resolution of 1.9 Å [134]. The protein consists of 238 amino acids with a molecular mass of 27 kDa. GFP is cylindrical shaped comprising 11 β-strands with an α-helix inside and short helical segments on the ends of the cylinder (Fig. 3.7). GFP has a length of 4.2 nm and a diameter of 2.4 nm. This particular motif with a β-structure on the outside and an α-helix on the inside is a unique structure which has not been found in nature before. Yang et al. named it the β-can.

The intrinsic fluorophore in wild-type GFP is a *p*-hydroxybenzylidene-imidazolidine derivative formed by a covalent modification of the sequence Ser65, Tyr66, and Gly67 and is located almost perfectly in the middle of the β-

structure (Fig. 3.7). The surrounding of the fluorophore inside the GFP is important for the function, because the modified tri-peptide Ser-Tyr-Gly is only fluorescent when it is embedded in the intact protein.

The spectral mutants enhanced green fluorescent protein (EGFP) and enhanced cyan fluorescent protein (ECFP) exhibit the substitutions Phe64Leu, Ser65Thr and Phe64Leu, Ser65Thr, Tyr66Trp, Asn146Ile, Met153Thr, Val163Ala, respectively, in the primary sequence the wild-type GFP [133].

A complete sequence and a detailed description of the structure and the properties of GFP and its mutants can be found in [133] and [135].

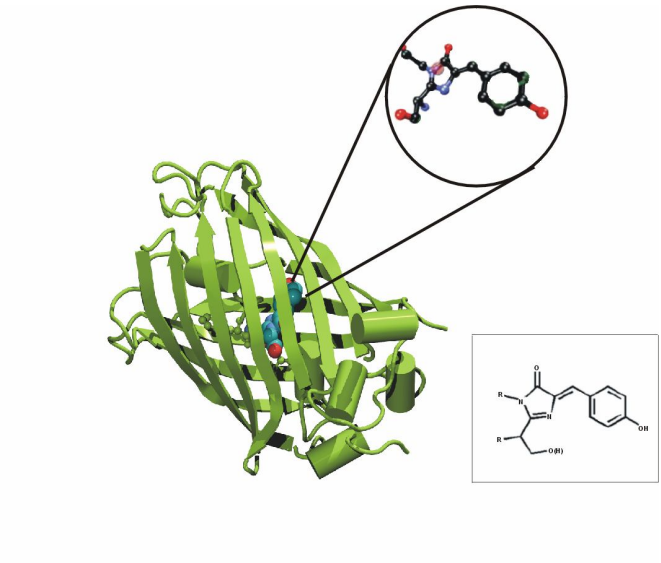

Figure 3.7. The chromophore inside GFP. The chromophore has the formal structure depicted in the lower right.

The excitation and emission spectra of EGFP and ECFP, the two mutants used in this work for labelling the proteins under investigation, are shown in Fig. 3.8.

The excitation and emission maxima as well as the extinction coefficient and fluorescence quantum yield for EGFP and ECFP are given in Table 3.1.

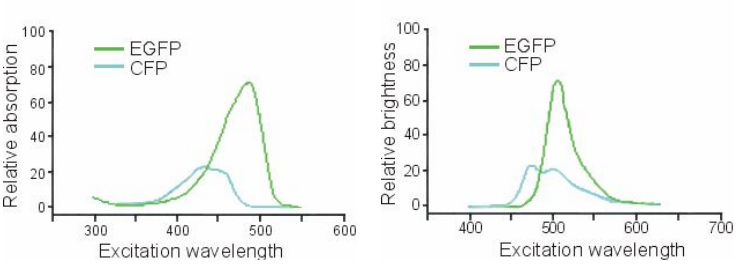

Figure 3.8. Excitation and emission spectra of EGFP and ECFP with their relative absorption and fluorescence brightness, respectively.

Table 3.1. Spectral characteristics of EGFP and ECFP [133].

Mutant	λ_{exc} / nm	ε / M^{-1} cm^{-1}	λ_{em} / nm	Φ_{fluo}
wtGFP	396 472	27500 12000	504	0.8
EGFP	488	56000	509	0.6
ECFP	434 452	32500	476 505	0.4

Although wtGFP has similar spectral characteristics compared with its mutant EGFP, wtGFP did not found large application in biology, because of complex photochemical properties and weak emission intensity due to low folding efficiency.

3.3. Gap junction (GJ) Hemichannels

Gap junctions (GJs) are specialized areas of the cell membranes that connect neighboring cells. They are organized collections of protein channels that allow ions and small molecules below 1000 Daltons to traverse between the connected cells in a passive fashion [136]. These allow for the "communicating" cells to equilibrate all of their critical regulatory ions and small molecules (e.g., Ca^{++}, glutathione) , as well as macro-molecular substrates (e.g. amino acids, sugars, nucleotides). These protein channels that make up the GJs consist of two hemi-channels or connexons which is a hexameric assembly of equal subunits called connexins (Fig. 3.9). Each connexon resides in the membrane of one cell and aligns and joins a connexon of the neighboring cell, forming a functional cell to cell or GJ channel [137;138].

These channels in turn assemble into larger clusters of more or less tightly packed particles that are known as gap junctions from electron microscopy.

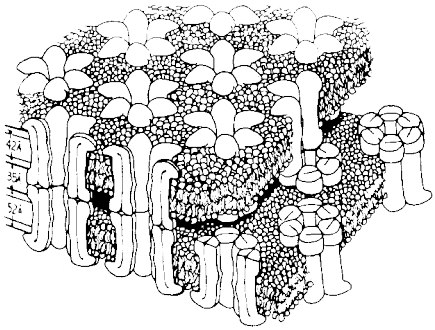

Figure 3.9. Ilustration of GJ connecting two plasma membranes of neighboring cells. Six connexin subunits oligomerize around a central pore to create a GJ hemichannel or connexon. Connexons from each of two neighboring cells dock through their extracellular interface to form a functional cell to cell or GJ channel. Figure taken from [139].

Connexins are synthesized in the rough ER and move across the Golgi apparatus where they oligomerize into hemichannels and are packaged into transport vesicles that move towards the plasma membrane. In some cells there is also a bypass route that omits the Golgi compartment and transports the connexons directly to the membrane [140]. The newly inserted connexons are thought to form a pool of free hemichannels that can be recruited to docking and assemble into gap junction plaque structures. Degradation takes place via lysosomal and proteasomal pathways [141] and is regulated by covalent protein modifications.

Recent advances in life imaging techniques (particularly GFP-fusing) have provided new insights into these processes. The transport vesicles from the Golgi towards the cell membrane have been shown to move along the microtubule network by time resolved laser-scanning microscopy [142;143]. By the same techniques, the GJ plaques were also proved to be very dynamic structures that constantly change their size, form, and location within the cell membrane [52;144-147]. Recent studies using fluorescence recovery after photobleaching (FRAP) on GJ plaques have shown that plaques grow from the periphery by accretion of (labeled) particles from the surrounding plasma membrane [143]. The same authors also have shown by FRAP that there is a freely diffusing pool of connexons in the plasma membrane that redistributes rapidly after photobleaching. However, they did not provide any quantitative data on the diffusion behavior of these particles in the plasma membrane.

CHAPTER 4

Experimental Set-Up and Sample Preparation

4.1 Confocal microscopy

A major problem in conventional microscopy is the fact, that micrographs of transparent samples like cells or tissues are normally blurred by light coming from regions out of the focal plane. To solve this problem, M. Minsky proposed the principle of the confocal microscope in 1957 [148] which is presented in Fig. 4.1. With a confocal microscope it is possible to achieve images from a thin section (≈1µm) within a thick transparent sample as shown in Fig. 4.2. This optical sectioning is a result of the combination of two effects: firstly, the

illumination is focused on a single point within a sample and secondly, the light coming from that point is collected and focused on a small aperture in front of the detector. This aperture, the confocal pinhole, prevents light which does not originate from the focal plane and which is therefore defocused in the plane of the pinhole from being detected.

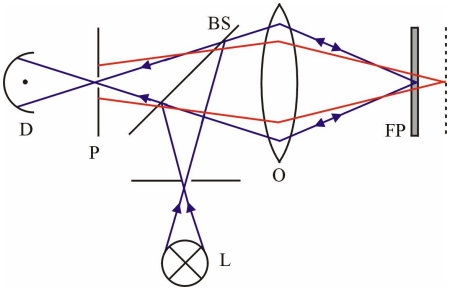

Figure 4.1. A schematic representation of a confocal microscope. L is the light source, O the objective lens, FP the focal plane, BS the beam splitter and D the detector. Only the light from the focal plane (blue line) can be detected whereas light from another plane is blocked by the pinhole (red line).

Thus, only the light from the focal plane contributes to the confocal image achieved by scanning the sample trough the focal plane. The axial and lateral resolving power of a confocal microscope can be deduced by considering the point-spread-function (PSF) for such a microscope. The PSF in lateral direction for a conventional microscope is given by the Airy function

$$p(\rho) = 2J_1^2(\rho)/\rho^2 \qquad (4.1)$$

where J_1 is the Bessel function of first order and ρ is the generalized radius

$$\rho = \frac{2\pi r}{\lambda} \cdot NA \tag{4.2}$$

where *NA* is the numerical aperture of the system and *r* the distance to the optical axis and λ the light wavelength.

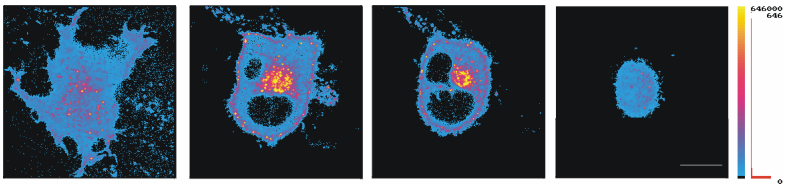

Figure 4.2. Series of miscoloured confocal images of a HeLa cell expressing ECFP-labelled connexones taken at different axial positions. Scale bar: 5µm.

For the special case of the confocal microscope the PSF changes to [149]

$$p_{conf}(\rho) = p(\rho) \times p(\rho). \tag{4.3}$$

The PSFs for the conventional and confocal case are shown in Fig. 4.3. The PSF for the confocal microscope exhibits steeper slope and almost no side maxima compared with the conventional PSF. With the PSFs eqn. (4.1) and (4.3) the application of Rayleigh's criterion yields for the lateral resolving power

$$\Delta r = 0.61 \frac{\lambda}{NA} \tag{4.4}$$

for a conventional microscope and

$$\Delta r_{conf} = 0.44\frac{\lambda}{NA} \tag{4.5}$$

for a confocal microscope.

The PSF in axial direction for a confocal microscope has the form [149]

$$p(\varsigma) = \left(\frac{\sin\frac{\varsigma}{4}}{\frac{\varsigma}{4}} \right)^2 \tag{4.6}$$

with the generalized z-coordinate

$$\varsigma = \frac{2\pi z}{\lambda n} \cdot NA^2 \tag{4.7}$$

where *n* is the diffraction index. The application of Rayleigh's criterion yields for the axial resolving power

$$\Delta z_{conf} = 1.5\frac{\lambda n}{NA^2} \tag{4.8}$$

which determines the effective thickness of an optical section.

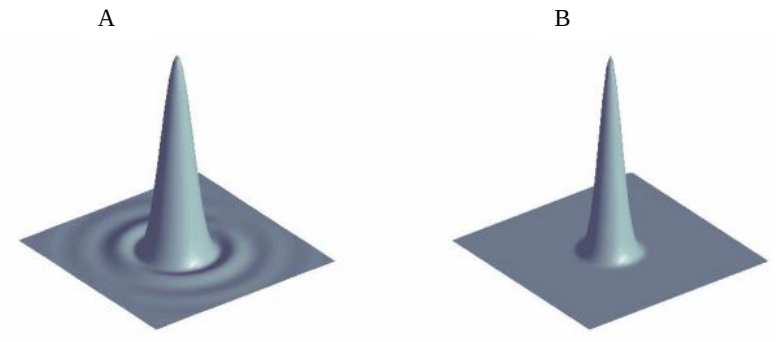

Figure 4.3. Normalized lateral point-spread-function (PSF) for (A) a conventional and (B) a confocal microscope.

A comprehensive description of the theory of confocal microscopy can be found in the text book of J. B. Pawley [150] and in the review of R. H. Webb [149].
In a confocal set-up with a given magnification M a reasonable choice for the pinhole radius could be

$$R_{pinhole} = 0.61\frac{\lambda}{NA}M \tag{4.9}$$

which corresponds to the first zeropoint of the radial PSF (eqn. (4.3)) in the plane of the pinhole. A pinhole of this size allows the central maximum of the PSF (98% of the whole signal intensity) to reach the detector. Generally, a pinhole is chosen with a size matching the experimental requirements, e.g. for Fluorescence Correlation Spectroscopy (FCS) a small stretch of the axial detection volume is needed to reach optimal S/N ratio, so a pinhole with a radius smaller than given in eqn. (4.9) is often used. In the case of two-photon excitation (2PE) it is even possible to work without a pinhole (see chapter 5).

4.2 Experimental set-up

The experiments were performed using a home-built confocal set-up which is illustrated in Fig. 4.4. The set-up consisted of a modified epi-fluorescence microscope (Olympus IX-70) with a high numerical aperture objective (Olympus UPLAPO 60x/NA 1.2, water immersion). The sample was mounted on a 3D piezo scanner (P517, Physik Instrumente) with a scanning range of 200 $\times$ 200 $\times$ $\times$ 20 μm^3. The sample was excited with laser light by using a quartz beam splitter through one of the optical side ports of the microscope. Because of a lens inside the Olympus microscope it was necessary to place a lens with a focal length of f = 60 mm (L1 in Fig. 4.4 and 4.5) in front of the optical side port to obtain a parallel beam entering the microscope objective.

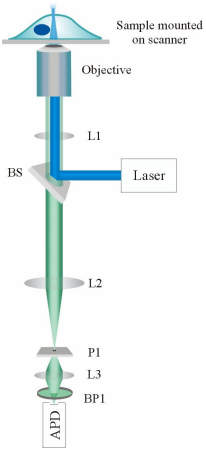

Figure 4.4. Home-built confocal set-up for the 1PE experiments. L1, L2, L3 are lenses, BS the beam splitter, P1 the pinhole, BP1 the bandpass filter and APD the avalanche photo diode.

The fluorescence of the sample was collected by the same microscope objective and detected with an actively quenched avalanche photo diode (APD) (EG&G SPCM-AQR 14). Bandpass filters adopted to the samples emission properties were installed between the pinhole and the APD. Data collection and visualization were done using a PC and custom software. Fluorescence ACFs was be recorded simultaneously with a hardware correlator (ALV-5000).

The set-up illustrated in Fig. 4.4. was used for the experiments with one-photon excitation (1PE) and single color fluorophores. For this experiments a pinhole with a diameter of 50 µm and a bandpass filter specially designed for the emmision caracteristics of EGFP (BP 528/20, Chroma Technology Corp.) were used. For experiments with two-photon excitation (2PE) the set-up was slightly modified as shown in Fig. 4.5. The main differences between this two set-ups were, that a dichroic mirror (AESP 750, Omega Optical Inc.) was used instead of the quartz beamsplitter, the pinhole was omitted and a different bandpass filter (BP 550/200, Chroma Technology Corp.) was used.

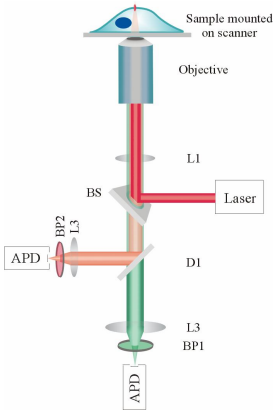

Figure 4.5. Modified confocal set-up for the 2PE experiments. L1, L3 are lenses, BS the beam splitter, D1 the dichroic mirror, BP1 and BP2 are bandpass filter and APD is the avalanche photo diode.

For the 2PE experiments with dual color fluorophors a dichroic mirror (630 DRLP, Omega Optical Inc.), a second APD and a second bandpass (BP 675/70, Chroma Technology Corp.) filter were installed in the detection beam path.
The sample was excited with an Ar^+ laser (Innova 90C, Coherent Inc.) for the 1PE applications and with a mode-locked titan sapphire laser (Mira 900D, Coherent Inc., pulse width 100fs @ 76MHz) for the 2PE applications.

4.3 Sample preparation

4.3.1. Cell preparation

The human cervix carcinoma cell lines HeLa wildtype (wtHeLa) and HeLa80, stably expres-sing TNF-R2, as well as immortalized murine fibroblasts (MF TNF-R1/TNF-R2 (-/-; -/-)) (which do not express TNF-R1/TNF-R2) were used for transient transfection. Cells were grown in RPMI 1640 medium supplemented with 5% (v/v) heat inactivated fetal calf serum and 2 mM L-glutamine. 2.5×10^5 cells were seeded into a 35 mm coverslip-bottom microwell dish (MatTek Corp.). The cells were allowed to adhere and grow overnight at 37 °C in an incubator under 5% CO_2 atmosphere. The next day cells were transiently transfected with TNF-R1-CFP/GFP (pECFP-TNF-R1 or pEGFP-TNF-R1) or TNF-R2-CFP/GFP (pECFP-TNF-R2 or pEGFP-TNF-R2) expression plasmids using Effectene transfection reagent (Qiagen AG). 5-10 ng of the expression plasmids were mixed in EC buffer with noncoding plasmids to a total amount of 750 ng. 6 µl enhancer was added and the mixture was incubated for 5 min at room temperature. Then 7,5 µl Effectene reagent was added followed by an incubation for 10 min at room temperature and the addition of 600 µl cell culture medium. The transfection mix was applied on the

cells that were washed with phosphate buffered saline (PBS) and cultured in 1.6 ml cell culture medium and incubated overnight at 37 °C in an incubator under 5% CO_2 atmosphere. The next day medium was changed to a phenol-red-free culture medium and cells were applied to FCS experiments. Prior to the measurements, cells were rinsed several times with PBS.

4.3.2 Membrane treatment

Membranes of wt HeLa and HeLa80 cell lines were stained with rhodamine6G marked phospholipids. Prior to the experiments 20 µl of a solution containing 720 ng/ml rhodamine6G labelled phosphatidylethanolamine (Rh-PE, Avanti Polar Lipids) and 0.09% 1,2 diheptanoyl-*sn*-phosphatidylcholine (DHPC, Avanti Polar Lipids) were mixed with 2 ml PBS buffer and added to the adhered cells in the microwell dish. The cells were then incubated for 30-40 min at 37 °C in an incubator under 5% CO_2 atmosphere and washed afterwards several times with PBS buffer.

Labelling of lipid rafts (see 4.1.2) was done with cholera toxin subunit B (CT-B) conjugated with AlexaFluor647 (Molecular Probes). 2 µl of a 1 mg/ml CT-B solution was mixed with 2 ml PBS buffer and added to the adhered cells in the microwell dish. After 5 min of incubation at room temperature the labelled cells could be observed under the confocal microscope.

For the cholesterol depletion experiments the cells were treated with 2 ml of a 1 mM methyl-β-cyclodextrin (MβCD) (Sigma-Aldrich) solution and incubated for at least 30 min at room temperature. Cells were then washed several times with PBS buffer.

Depolymerization of actin filaments in HeLa cells were induced by treatment of the cells with cytochalasin D (cytD) (Sigma-Aldrich). CytD was added to the

sample buffer to a total concentration of 0.6-0.8 mg/ml and the cells were incubated for 40-60 min at 37 °C.

CHAPTER 5

Fluorescence Correlation Spectroscopy (FCS)

FCS has developed into a widely used and very successful spectroscopic technique for detecting and quantifying small concentrations of fluorescing molecules in solution as well as for obtaining information about molecular parameters such as diffusion coefficients, transitions rates, or chemical reaction kinetics.

For measuring diffusion coefficients the molecules are excited in a very small detection volume (≈1 femtoliter) with a laser beam focused through a microscope objective and the emitted fluorescence is detected through the same optics. Excitation and emission wavelengths are separated by dichroic mirrors

and optical filters with this technique. Very small concentrations (< 1 picomolar) of fluorescent particles can be detected because individual fluorescent particles will give clearly distinguishable fluorescence bursts of an intensity above the background arising from detector noise. The amplitudes and characteristic time scales of the measured fluorescence intensity fluctuations are directly connected to macroscopic properties such as particle concentration and diffusion constants.

5.1 Theory of FCS

The primary data obtained in an FCS measurement is the time-dependent fluorescence intensity *F(t)*, which is proportional to the number of particles in the observation volume at time *t*. The autocorrelation function (ACF) of the *F(t)* contains all relevant information relating to the diffusion of the fluorophores. The normalized ACF $g^{(2)}(\tau)$ is defined as

$$g^{(2)}(\tau) = \frac{\langle F(t)F(t+\tau)\rangle}{\langle F(t)\rangle^2} \Leftrightarrow g^{(2)}(\tau) - 1 = \frac{\langle \delta F(t)\delta F(t+\tau)\rangle}{\langle F(t)\rangle^2} = G(\tau)$$

where $F(t)$ and $F(t+\tau)$ are the fluorescence at the time *t* and at an interval τ later, $\delta F(t)$ and $\delta F(t+\tau)$ are the fluctuations around the mean value and the brackets denote the time average.

The ACF for free three-dimensional diffusion in a volume element of Gaussian shape is described as [151]

$$G(\tau) = \frac{1}{N} \frac{1}{\left(1 + \frac{4D\tau}{\omega^2}\right)} \frac{1}{\sqrt{1 + \frac{4D\tau}{z^2}}} \tag{5.1}$$

or

$$G(\tau) = \frac{1}{N} \frac{1}{\left(1 + \frac{\tau}{\tau_D}\right)} \frac{1}{\sqrt{1 + K^2 \frac{\tau}{\tau_D}}} \tag{5.2}$$

with the diffusion time

$$\tau_D = \frac{\omega^2}{4D}, \tag{5.3}$$

where D is the diffusion coefficient, $K = \omega / z$ is the structure factor and N is the number of fluorescing molecules in the focal volume. The values ω and z are the lateral and axial radii of the Gaussian intensity profile of the focus at which the initial intensities have decayed to their $1/e^2$ - values. The expression for τ_D given in eqn. (5.3) is only valid for one-photon excitation (1PE) of the fluorophore. A simulated ACF is shown in Fig. 5.1.

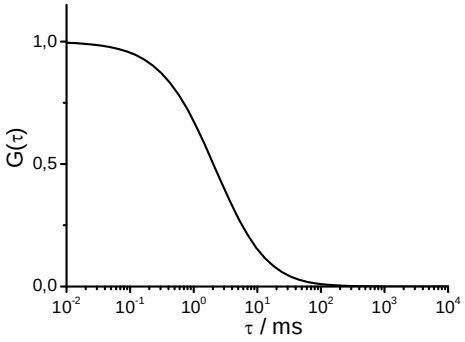

Figure 5.1. Simulation of the ACF given in eqn. (5.1). Parameters used: $N = 1$, $\omega = 300$ nm, $D = 1 \times 10^{-7}$ cm^2/s.

For a two dimensional (2D) diffusion processes ($z >> \omega$), e.g. diffusion in the cell membrane or in thin films, eqn. (5.1) can be simplified to

$$G(\tau) = \frac{1}{N} \frac{1}{\left(1 + \frac{\tau}{\tau_D}\right)}. \qquad (5.4)$$

In this special case τ_D denotes the time at which the function $G(\tau)$ has decayed to the half of its initial value.

In a mixture of molecules with different diffusion coefficients the ACF is the sum of the contributions of individual species. The general form of $G(\tau)$ for a mixture of *m* different fluorescent species with diffusion times $\tau_{D,i}$ is then given

$$G(\tau) = \frac{1}{N} \sum_{i=1}^{m} \rho_i g_i(\tau) \qquad (5.5)$$

with

$$g_i(\tau) = \frac{1}{\left(1+\frac{\tau}{\tau_{D,i}}\right)} \frac{1}{\sqrt{1+K^2\frac{\tau}{\tau_{D,i}}}}$$

The ρ_i are relative amplitudes corresponding to molecules with distinct diffusion coefficients.

In an FCS application the excitation power has to be chosen carefully to prevent the fluorophores from photobleaching. The unwanted effect of photobleaching results in a decrease of the apparent dwell time of the fluorophores in the focal volume and therefore to an increase of the computed diffusion coefficient. Other artifacts can be caused by photobleaching and continuous depletion of fluorophores leading to a loss of signal, in the case of biological samples, e.g. due to denaturation of proteins or cell damage.

5.1.1 Two photon excitation (2PE)

Two photon excitation (2PE) requires the absorption of two photons of a wavelength which is twice the wavelength needed for a one photon excitation (1PE) process (Fig. 5.2). In a 2PE process the absorption has to take place almost simultaneously, i.e. within a time interval of about 1fs, and within the absorption cross section of the molecule.
This requires a high photon flux which is usually obtained by pulsed lasers and a tight focusing of the excitation light by high aperture objectives.

The absorption probability for two photons is proportional to the mean square of the intensity which results in an inherent spatial discrimination of excitation. That means that only in a small volume around the focal spot the photon flux density is sufficient for a 2PE processes.

Figure 5.2. Comparison between one- and two photon absorption processes.

In contrast to the conventional 1PE confocal microscopy (chapter 4.1) this inherent spatial discrimination allows to work without a pinhole in the image plane in the confocal set-up.

The ACF for diffusing molecules excited by two photons remains the same as given in equation 5.2 and 5.4, respectively. The only differences in the case of 2PE is a value for the diffusion time τ_D which now is given by

$$\tau_D = \frac{\omega^2}{8D}.$$

The difference in the conventional 1PE value of $\tau_D = \omega^2/4D$ results from the introduction of the convolution factor as a squared instead of a simple Gaussian-profile.

Investigation of turbid samples like cells or deep layers in tissues benefit from the inherent spatial discrimination of 2PE. Because unlike in the case of 1PE confocal microscopy where all molecules in the beam path, not only in the focal

region, are excited, the fluorescence in the case of 2PE comes only from the focal volume which results in an improvement of the signal quality. A drawback of 2PE is that it is hardly possible to predict the absorption maximum of a fluorophore for a 2PE process whereas the emission spectra remain basically the same. The absorption spectra for 2PE are often blue-shifted and broader compared with the spectra for 1PE. This spectral shift might be expected to enhance the possibility of nonspecific excitation of the autofluorescent background.

5.2 Determination of focal volume

One of the crucial parameters in FCS measurements is the size of the focal volume, which determines the mean dwell time of the fluorophores and therefore their diffusion time, too. In this work the lateral and axial $1/e^2$-radii were determined by measuring a sample of fluorescent polystyrene beads (FluoSpheres F-8784, Molecular Probes, ∅ 20 nm) immobilized in poly(vinyl alcohol). A lateral and axial intensity profile of a single fluorescent bead excited with 488 nm is shown in Fig.5.3 (A) and (B), respectively. The $1/e^2$-radii ω and z were calculated by fitting these curves with a Gaussian-profile.This method was used to determine the radii of the excitation focus for the 1PE and 2PE experiments.

Another method would be to measure the ACF of dye molecules in solution with a known diffusion constant, e.g. rhodamine in water or ethylene glycol. The values for ω and z are then computed by a routine which fits eqn. 5.1 to the measured ACF.

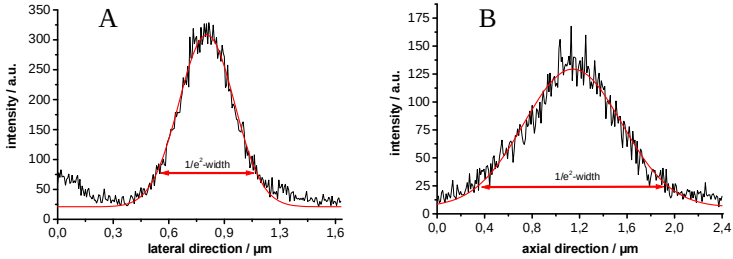

Figure 5.3. (**A**) lateral and (**B**) axial intensity profile of a single fluorescent bead (∅ 20 nm) excited with an excitation wavelength of 488 nm and fitted with a Gaussian profile (red curves). The calculated values are ω = (292 ± 4) nm and z = (803 ± 8) nm for the lateral and axial $1/e^2$-radius, respectively.

5.3 FCS in living cell

In this work most measurements were done in living cells. In plasma membranes and inside the cytoplasm of a living cell the model of Brownian diffusion cannot be applied to diffusing particles, because the movement of a particle is in many cases confined and the motility shows strong local changes [152;153]. Such deviations exist due to restrictions of the particles motility within cellular compartments or lipid microdomains in membranes, but also due to interactions between other molecules or cellular structures. To describe the phenomenon of non-Brownian diffusion, also called anomalous diffusion, the following replacement in the eqns. (5.2) and (5.4) has to be made

$$\frac{\tau}{\tau_D} \rightarrow \left(\frac{\tau}{\tau_{anom}} \right)^{\alpha} \tag{5.6}$$

with α <1 [154]. In this case a diffusion constant, as for Brownian diffusion, is not defined.

Another type of non-Brownian particle motion in living cell is the active transport, e.g. a protein driven movement of particles along filamentous structures. The ACF for the case of active transport with velocity v_i is given by [4]

$$G(\tau) = \frac{1}{N} e^{-\left(\frac{\tau \cdot v_i}{\omega}\right)^2} \tag{5.7}$$

where ω is again the lateral radius of the focal volume.

Simulated ACFs for the different transport and diffusion processes described above are shown in Fig. 5.4. It is to some extend possible to distinguish the different processes by the shapes of their ACFs. Compared with the 3D or 2D diffusion, the function for the active transport decays more abruptly, whereas the function for anomalous diffusion exhibits a more gradual decay.

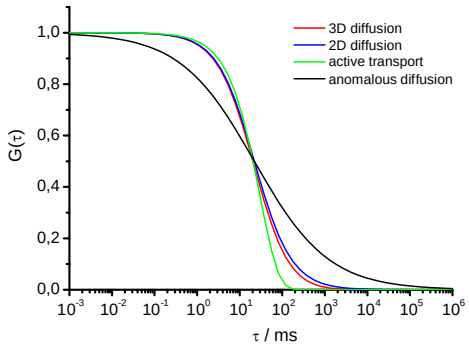

Figure 5.4. Simulated ACFs for different kinds of particle motion. Parameters used for these plots: N = 1, D = = 10^{-8} cm^2/s, ω = 300 nm, z = 1 µm v_i = 5 µm/s and α = 0.5.

During the measurements done in this work, all four type of diffusion processes were observed.
A review about the theoretical concepts of FCS and the different diffusion processes can be found in [4] and [147].

5.3.1 FCS on plasma membranes

For studies on plasma membranes of living cells an extension of the theory presented in chapter 5.1 has to be made in order to take into account the topology of the cell membrane. For this reason the diffusion behavior of gap junction hemichannels fused with CFP in the plasma membrane of HeLa cell was investigated. Gap junctions are membrane structures that consist of clusters of cell-cell channels, which mediate fast exchange of low molecular weight molecules (see chapter 3.3).
As shown in the theory section the diffusion constant should be strongly dependent on the tilting angle between optical axis and membrane. Unfortunately, it is not possible to determine the tilting angle for each FCS measurement directly. Hence, we choose a statistical approach to extract the real diffusion constant from measuring the apparent diffusion constant (2D model, eqn. (5.4)) at positions on the cell surface corresponding to the extreme positions of the tilting angle.
For investigations of 2D diffusion processes taking place in a plane which is not orthogonal to the optical axis of the focus but on a tilted or curved surface it is necessary to modify the 2D model which is given in eqn. (5.4). The necessity of this correction is illustrated in Fig. 5.5.

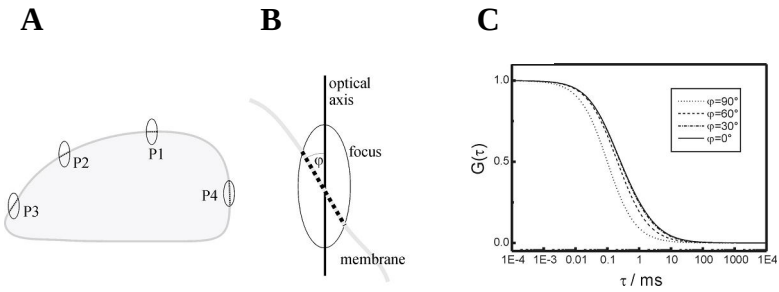

Figure 5.5. (**A**)The cross-section between focus and cell membrane depends on the position of the focus. (**B**) Off-axis angle φ between membrane and optical axis. (**C**) Dependence of the ACF on the off-axis angle. Simulated curves with a diffusion constant D = 1×10^{-9} cm^2/s and varying off-axis angles $\varphi = 0^o, 30^o, 60^o, 90^o$ corresponding to the positions P1 to P4 in (A), respectively.

The ellipses P1 to P4 in Fig. 5.5 A represent laser foci at different positions of the plasma membrane. It is obvious that only in the case of a membrane which runs orthogonal to the optical axis (P1) eqn. (5.4) is applicable. At any other angle between the optical axis and membrane plane (P2-P4) the cross-section is larger than for the orthogonal case. This results in an overestimation of the actual diffusion time of the molecules through the focus.

To calculate the ACF for positions different from P1, the membrane within the focus is approximated as a flat surface. The cross-section of a 3D Gaussian profile with a plain surface is simply a 2D Gaussian profile of width $r_1 = \omega$ for one axis and for the other r_2 depending on the tilting angle α (see Fig. 5.5 B) and the structure factor of the excitation volume K

$$r_2 = \omega\sqrt{K\cos^2\varphi + \sin^2\varphi}\ . \qquad (5.8)$$

This yields a new 2D ACF

$$G(\tau) = \frac{1}{N} \frac{1}{\sqrt{1+\frac{4D}{\omega^2}\tau}} \frac{1}{\sqrt{1+\frac{4D}{r_2^2}\tau}} . \qquad (5.9)$$

A series of simulated ACFs for different off-axis angle φ = 90°, 60°, 30° and 0° is shown in Fig. 5.5 C to demonstrate the dependence of eqn. (5.9) on φ. Fitting these curves with the standard 2D model (eqn. (5.4)) results in diffusion constants which are 53% reduced in case of a tilt angle of 60°, by 63% in the case of a tilt angle of 30°, and by 65% in case of 0°, i.e. the smaller the tilt angle, the smaller the apparent diffusion constant.

Fig. 5.6 shows a representative example from a total of 145 measured ACFs of HeLa Cx46-ECFP transfectants using two-photon excitation at 820 nm. Time traces (Fig. 5.6 A) typically show a high signal to noise (S/N) ratio up to 10:1. Correspondingly, the ACFs also have excellent S/N ratios, which are comparably high for studies in living cells. To obtain a first overview of the diffusion constants of hemichannels the measured ACFs were fitted using the simple 2D model with one component (see eqn. (5.4)). Of the 145 measurements, 78% of the measured ACFs show a good fit, 22% a poor fit. The values of the diffusion constants derived from these fits show a relatively wide distribution ranging from 1×10^{-9} cm^2/s to 3×10^{-8} cm^2/s.

To achieve a more representative value for the diffusion constant of gap-junction hemichannels, we subdivided the ACF measured at different positions into three principal positions, namely, top, middle, and bottom of the cell.

Fig. 5.7 (A-C) shows confocal images of different locations within the cell that correspond to the three principal geometries: Fig. 5.7 A shows a confocal section at the top of the cell, which corresponds to the focus possition P1 (Fig. 5.5 A). Fig. 5.7 B shows the situation at a lateral position of the plasma membrane at about half distance from the top to the substrate, which corresponds to focal possitions P2-P4 (Fig. 5.5 A). At this position the cross-section between focus

and membrane is oriented approximately parallel to the optical axis (the ellipse P4 in Fig. 5.5 A). Fig. 5.7 C was from of the bottom of the cell close to the substrate with the cross section oriented normal to the main axis of the focal ellipsoid. At each of these three principal positions we measured 40–50 different correlation functions.

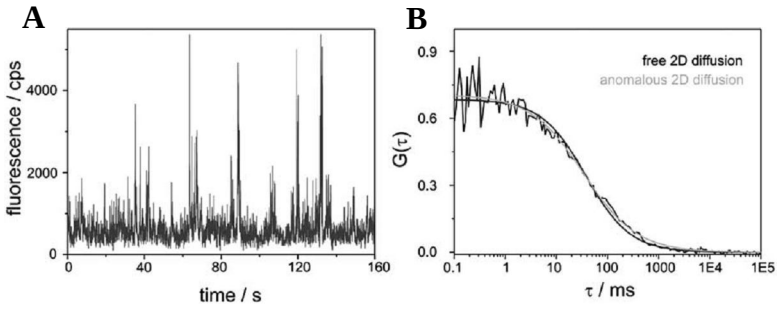

Figure 5.6. (**A**) Time trace of the fluorescence intensity of ECFP-labeled connexons diffusing through a confocal area in the plasma membrane of living HeLa cells. Every spike represents transit of a single connexon through the focal volume. (**B**) ACF of the trace in (**A**) fitted by the 2D diffusion model (solid line) and the anomalous diffusion model (dashed line).

The diffusion constants obtained by fitting with the 2D model are shown in the histograms in Fig. 5.7 D (top), 5.7 E (middle), and 5.7 G (bottom) respectively. The fastest diffusion was observed in the top region of the cells with an average diffusion constant of $\overline{D} = 7.7 \times 10^{-9}$ cm^2/s. In contrast, the distribution of the *D*-values measured in the middle of the cells has the smallest mean value of $\overline{D} = 3.5 \times 10^{-9}$ cm^2/s, corresponding to the slowest apparent diffusion. The distribution measured at the bottom of the cell lies in between the distributions measured at the bottom and in the middle of the cells, containing a mean value of $\overline{D} = 5.4 \times 10^{-9}$ cm^2/s. However, the histogram clearly shows a bimodal distribution of the apparent diffusion constants.

The data for the middle position (Fig. 5.7 (B, E)) was refitted using eqn. (5.9) assuming a tilting angle of 0°. Fig. 5.7 F shows the histogram of diffusion coefficients with a mean value of $\overline{D} = 9.5 \times 10^{-9}$ cm^2/s. This value is much closer to the mean values obtained for the top and bottom positions of the cell.

On the other hand the poor fits of the 2D model indicate that the diffusion of hemichannels in living cells is affected by the membrane environment. Fig. 5.7 (H-J) show again all the data measured at the three principal positions now fitted with an anomalous 2D diffusion model (eqn. (5.6)) and again Fig. 5.7 I shows the data of the middle position fitted with the largest possible focus, i.e. we used eqn. (5.9) with an anomalous diffusion exponent and tilting angle 0°. The histograms of the distributions of the diffusion coefficients look very similar to the D-values obtained with the 2D diffusion model. The mean values of $\overline{D}$ result to $\overline{D} = 7.4 \times 10^{-9}$ cm^2/s (top), $\overline{D} = 8.7 \times 10^{-9}$ cm^2/s (middle), and $\overline{D} = 4.2 \times 10^{-9}$ cm^2/s (bottom).

The solid line in Fig. 5.7 H represents a fit of the distribution assuming two Gaussian components. The narrow Gaussian component has its peak at $\overline{D} = 10.4 \times 10^{-9}$ cm^2/s. We attribute the diffusion coefficients covered by this Gaussian component to positions of the cell surface where the membrane is normal to the optical axis and the focal spot has a circular cross-section (tilting angle 90°). The other diffusion coefficients originate from membrane areas with smaller tilting angles and therefore larger cross-sections.

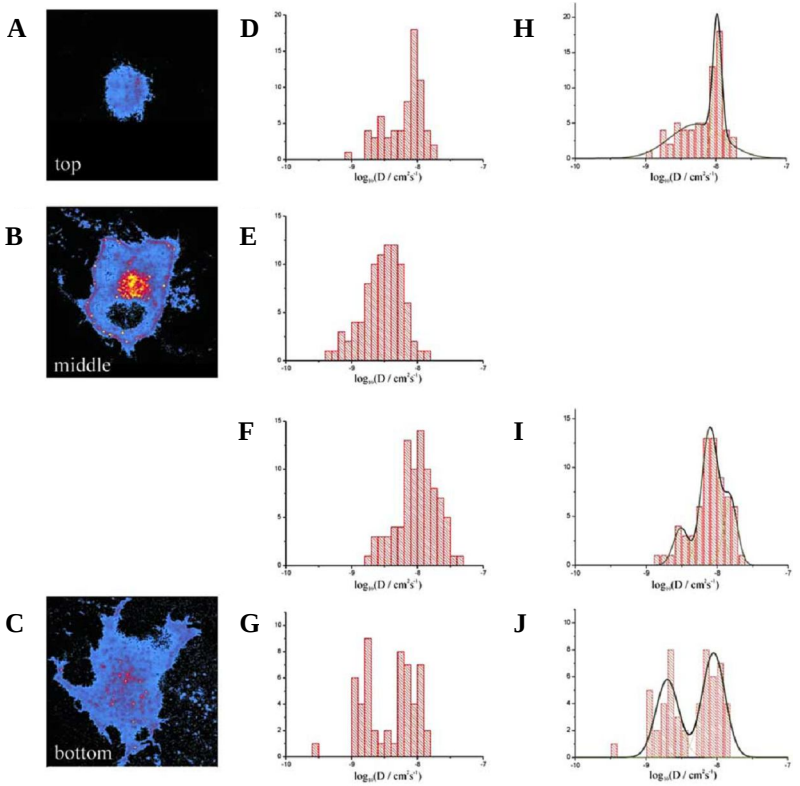

Figure 5.7. (**A-C**) Confocal images of a HeLa cell expressing ECFP-labeled connexons. The confocal sections through the cell represent three principal positions where the diffusion coefficients of connexons were measured. (**D-G**) Histograms of diffusion coefficients of connexons measured on top (**D**), middle (**E**), and bottom (**G**) position within the plasma membrane using the 2D diffusion model. A tilt angle $\varphi = 0°$ (see text) was assumed in histogram (**F**). (**H-J**) Same data as in (**D-G**) fitted with the anomalous diffusion model. Again, for histogram (**I**) a tilting angle $\varphi = 0°$ was assumed.

CHAPTER 6

Experimental Results

In this chapter the results of FCS measurements of fluorescence labelled TNF-R1/2 proteins in plasma membranes as well as fluorescence labelled TRAF2 protein in the cytoplasm of living cells will be presented. The diffusion behaviour of TNF-R1/2, fused to EGFP and ECFP, in membranes of different cell lines, wtHeLa, HeLa80 and immortalized murine fibroblasts (MF TNF-R1/TNF-R2 (-/-; -/-)), before and after stimulation with cysTNF ligand was investigated with one-photon (1PE) and two-photon (2PE) excitation. To get further insight in the interaction of TNF-R proteins with their nearest surrounding the cells were treated with different substances like methyl-β-cyclodextrin (MβCD), cholera toxin subunit B (CT-B) and cytochalasin D (cytD) to alter certain cell properties. Further investigations were done on the diffusion

behaviour of TRAF2 protein labelled with EGFP in the cytoplasm of wtHeLa and HeLa80 (HeLa cell line stably expressing TNF-R2) cell lines before and after stimulation of the TNF-R2 receptor protein with CysHisTNF D143N/A145R (cysTNF) a TNF-R2-selective mutein assuring the full activation of TNF-R2.
All measurements presented in this chapter were performed at room temperature with the home-built confocal set-up described in chapter 4.

In an FCS experiment it is important on the one hand to use excitation powers high enough to achieve a good S/R ratio but on the other hand the fluorophores should not bleach while diffusing through the focal volume. The unwanted effects of bleaching were already described in chapter 5.1. Suitable excitation powers were determined by measuring the ACFs for EGFP in solution at different excitation powers. Fig. 6.1 shows the result of this measurement. It turned out that only for an excitation power levels P = 20 – 120 μW the diffusion times correspond to a diffusion coefficient of $(3 \pm 1) \times 10^{-7}$ cm^2/s which is in good agreement with the literature values for EGFP in solution of $(5 \pm 2) \times 10^{-7}$ cm^2/s [4] and $3 - 8 \times 10^{-7}$ cm^2/s [155]. For a power level of about 120 μW the curves exhibited also maximal S/R ratios. With increasing excitation power (P > 230 μW) the diffusion time for EGFP began to decrease significantly, indicating the onset of bleaching processes in the focus.
The cells used for the investigation of EGFP labelled proteins (EGFP-TNF-R2/1, EGFP-TRAF2) were chosen from confocal images of the sample taken prior to each measurement. Such a confocal image of a HeLa cell sample is shown in Fig. 6.2. For FCS measurements only cells whose membranes exhibited low or medium brightness were chosen for reasons of a high ACF contrast and a good S/R. The sample was then moved using the scanner until the membrane of the selected cell came into focus.

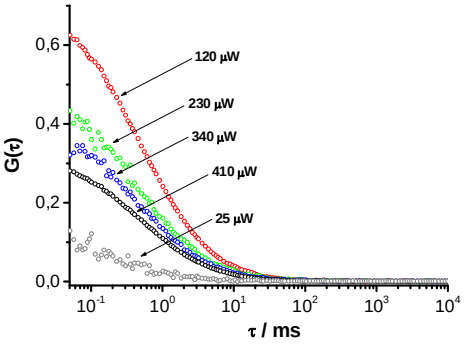

Figure 6.1. ACFs for EGFP in solution measured at different excitation power levels. The curve measured at P = 120 µW (red circles) exhibits the correct diffusion time for EGFP and the maximum S/R ratio, whereas the curves measured at higher power levels show significantly shorter apparent diffusion times and lower S/R ratios.

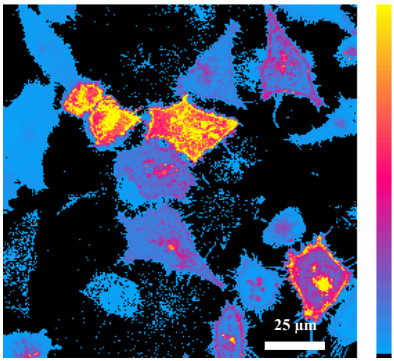

Figure 6.2. Miscolored confocal image of wtHeLa cells expressing EGFP labelled TNF-R2. The color bar on the right indicates the fluorescence intensities: from low (black) to high (yellow).

For calculating the diffusion coefficient or the diffusion time, the ACFs were fitted with the theoretical ACF given by eqns. (5.1) and (5.4). To reach a statistical significance of the diffusion coefficients all FCS measurements were done on several cells of a sample and at different positions on their membranes.

6.1 TNF-R2 in cell membranes

6.1.1 TNF-R2 in the cell line HeLa80

Lateral diffusion coefficients of TNF-R2 in HeLa80 cell membranes prior to stimulation with the cytokine TNF were measured at room temperature with 1PE and 2PE. In case of the 1PE measurements of EGFP-labelled TNF-R2 the chromophore was excited at 488 nm (50-120 µW, measured before the beam splitter) and a 50 µm pinhole was used in the confocal set-up. For the equivalent 2PE measurements of CFP labelled TNF-R2 the excitation wavelength was changed to 820 nm (6-10 mW, measured before beam splitter) and no pinhole was used. The obtained 1PE and 2PE autocorrelation functions (ACFs) were nearly identical.

A typical ACF measured with 1PE for the diffusion of the EGFP-labelled protein TNF-R2 is shown in Fig. 6.3.

Corresponding fluorescence time traces for single labelled TNF-R2 proteins, before and after stimulation with cysTNF ligand, are present in Fig. 6.4.

Fig. 6.5 shows the distribution of diffusion coefficients before stimulation, taken from 46 experiments (red bars). The mean value for the diffusion coefficient of EGFP-TNF-R2 in cell membranes is $\overline{D} = (3.6 \pm 0.5) \times 10^{-9}\ \mathrm{cm}^2/\mathrm{s}$.

After observation of the diffusion of unstimulated TNF-R2, cysTNF ligand was added to the buffer, as described in chapter 4.3.1, to stimulate the receptor. The

effect of the ligand on the diffusion behaviour of EGFP-TNF-R2 is shown in Fig. 6.6 where ACFs recorded at different times after simulation are displayed .

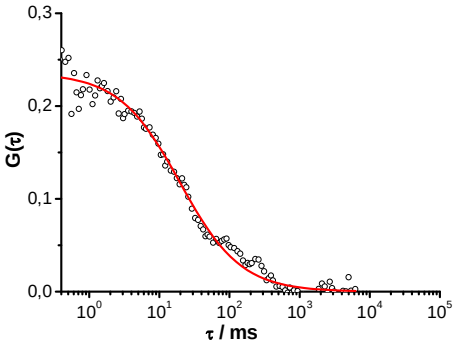

Figure 6.3. A typical ACF for the diffusion of EGFP labelled transmembrane protein EGFP-TNF-R2. EGFP was excited with laser light at 488 nm and a power of typically 100 µW.

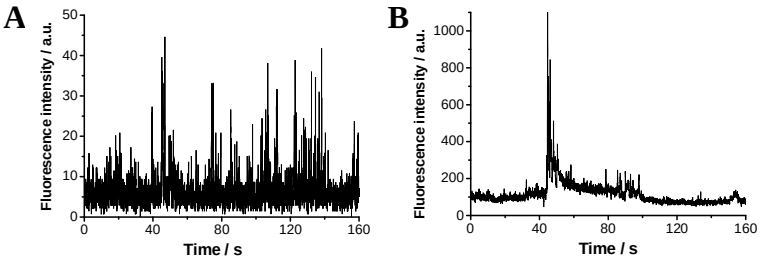

Figure 6.4. Fluorescence time traces for diffusing EGFP-TNF-R2 proteins (**A)** before and (**B)** after stimulation with the cysTNF ligand.

An increase in diffusion time, corresponding to a decrease in diffusion coefficient, was observed already a few minutes after stimulation with cysTNF ligand (black circles) and after 50 minutes (grey circles) the diffusion time

reached the upper resolution limit of the hardware correlator. This time evolution of the diffusion coefficient after stimulation measured in the membrane of a single HeLa80 cell is shown in Fig. 6.7.

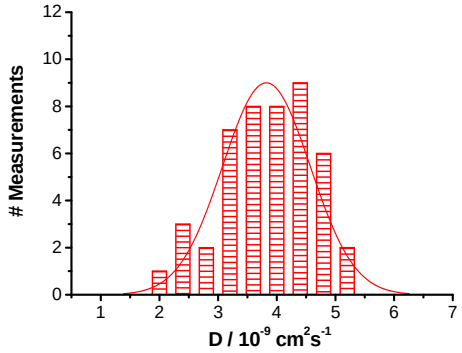

Figure 6.5. Distribution of diffusion coefficients taken from 46 experiments for EGFP-TNF-R2 before stimulation with cysTNF ligand. Mean value: $\overline{D} = (3.6 \pm 0.5) \times 10^{-9}\ \mathrm{cm}^2/\mathrm{s}$.

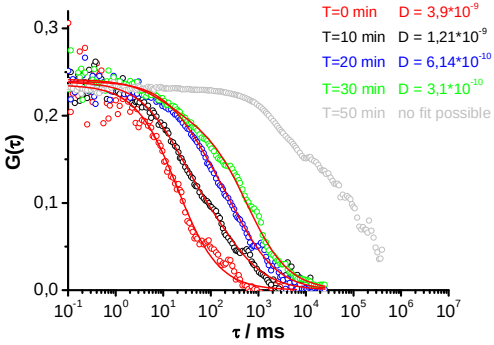

Figure 6.6. Behaviour of the ACFs of diffusing TNF-R2 in HeLa80 cells measured at different times after stimulation with cysTNF ligand. The functions were fitted (red curves) with the 2D model given in eqn. (5.4).

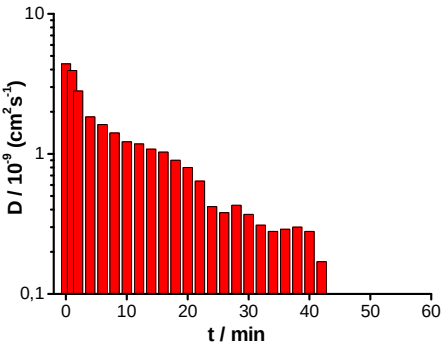

Figure 6.7. Time evolution of the diffusion coefficient after stimulation with cysTNF (stimulation at t=0) measured in a membrane of a single HeLa80 cell. For times $t \geq 45$ min the upper resolution limit of the hardware correlator was reached.

Such drastic changes in the diffusion behaviour can be explained only if dramatic changes in mass or membrane viscosity occur (eqn. (6.1)). There are two effects which could cause this kind of behaviour. The first effect could be that TNF ligand itself influences the membrane viscosity. The second is a possible aggregation of TNF-R2 induced by the stimulation with cysTNF. Both possibilities were examined in the following experiments.

For measurements of probable changes in membrane viscosity due to the presence of TNF ligand, HeLa80 cell membranes were stained with rhodamine labelled phospholipids (Rh-PE). The diffusion coefficient of the Rh-PE was then measured before and after the addition of cysTNF ligand. Typical ACFs, before and after the addition of the ligand, are shown in Fig. 6.8. It is obvious from this figure that the diffusion coefficient of Rh-PE did not change after TNF ligand was added, which indicates that cysTNF did not influence the membrane viscosity.

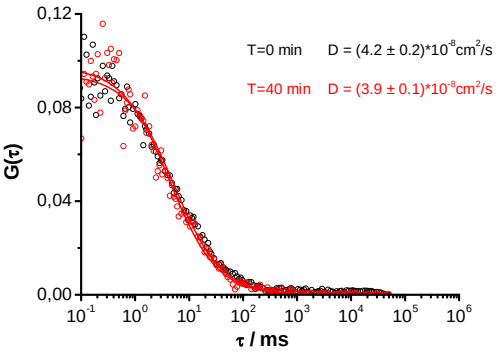

Figure 6.8. Typical ACFs of Rh-PE diffusion in the plasma membrane of a HeLa80 cell before (black circles) and 40 min after (red cicrcles) stimulation with cysTNF.

To examine the second possibility, namely the aggregation of TNF-R2, the protein radius corresponding to a 10-fold decrease of the diffusion coefficient should be estimated using the Saffman-Delbrück-model [156;157]. This model describes the motility of a cylindric particle with radius R embedded in a 2-dimensional viscous sheet with height h and viscosity η. This sheet is surrounded on both sides by an aqueous medium with the viscosity η_w. For this kind of geometry the diffusion coefficient D for the particle is given by

$$D = \frac{k \cdot T}{4\pi \cdot \eta \cdot h}\left[\ln\left(\frac{\eta \cdot h}{\eta_w \cdot R}\right) - \gamma\right] \qquad (6.1)$$

where γ is Euler`s constant (γ = 0.5772). Strictly speaking, the Saffman-Delbrück-model is not applicable for the TNF-R2 protein because of the receptors large extracellular and intracellular domains which protrude into the

surrounding aqueous medium. However, in this work the Saffman-Delbrück-model is used just to get a rough estimation of the aggregate size.

The dependence of D on the particle radius R is shown in Fig. 6.9, where other parameters were kept constant: T = 300 K, η = 10 P, η_w = 0.01 P (1 P = 1 Poise = 0.1 Nsm^{-2}) and h = 5 nm. The value taken for η_w is the viscosity of water at room temperature and η = 10 P is a reasonable value for the viscosity of natural membrane far above its transition temperature [158]. With this choice of parameters and an estimated radius R = 3 nm for the membrane spanning domain of the receptor (see chapter 3.1.2, Fig. 3.4) the result of the Saffman-Dellbrück-equation (6.1) approximately matches the measured mean value for D of the unstimulated receptor.

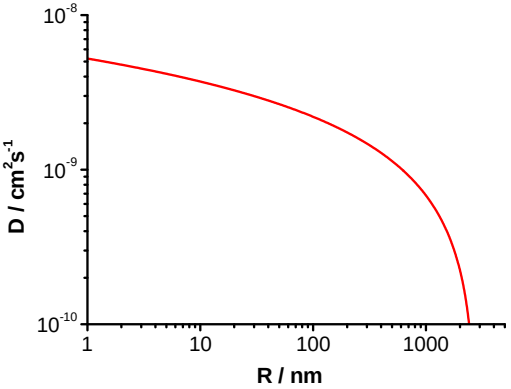

Figure 6.9. Simulation of the Saffman-Delbrück-equation (6.1) as a function of the particle radius R. Values for the other parameters: see text.

This simulation also showed that for a decrease of the diffusion coefficient from 4×10^{-9} cm^2/s to 4×10^{-10} cm^2/s the radius of the diffusing particle must have grown by a factor of approximately 250. Such a large particle would consist of about

7000 proteins. However, an increase in fluorescence corresponding to an aggregate of several thousand EGFP labelled proteins was not detected in the experiments (see Fig. 6.4 (B)).

To exclude artefacts from using overexpressed HeLa80 cells, these measurement were repeated with wtHeLa cell line because of a low concentration of TNF-R2 in the cell membranes.

6.1.2 TNF-R2 in wtHeLa cell

Measurements in wtHeLa cells were performed under the same conditions as described for the HeLa80 cell line. In contrast to the measurements on HeLa80 cells the ACFs for EGFP-TNF-R2 diffusion in wtHeLa membranes mostly showed a two component behaviour. A typical ACF for EGFP-TNF-R2 diffusion in wtHeLa cell membrane before stimulation is presented in Fig. 6.10.

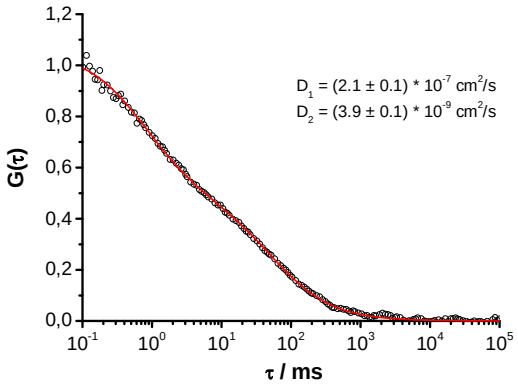

Figure 6.10. A typical two-component ACF for TNF-R2 diffusion in wtHeLa cell membrane before stimulation.

The ACFs were fitted with a two-component 2D model (see chapter 5.1) and it turned out that the diffusion coefficient corresponding to the fast component were constant (~2×10^{-7} cm^2/s) in almost all experiments (with and without cysTNF ligand). The diffusion coefficient corresponding to the slow component (~10^{-9} cm^2/s) was assigned to the diffusion of EGFP-TNF-R2 in the plasma membrane whereas the origin of the fast component is still vague. Because of the numerical value of the diffusion coefficient it could be assigned to freely diffusing EGFP in the cytoplasm or buffer.

Fig. 6.11 summarizes the measurements for EGFP-TNF-R2 in wtHeLa cells. For the unstimulated receptor the distribution has a mean value of $\overline{D} = (3.2 \pm 0.5)\times10^{-9}$ cm^2/s which is comparable to the mean value $\overline{D} = (3.6 \pm 0.5)\times10^{-9}$ cm^2/s measured for the receptor diffusion in HeLa80 cells.

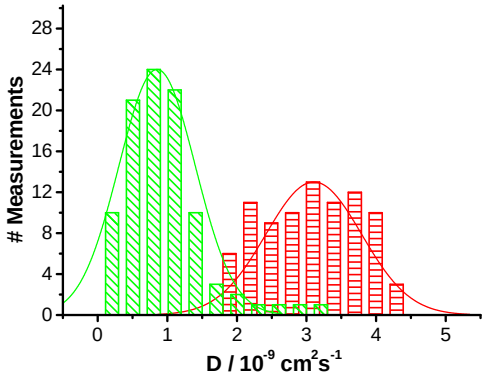

Figure 6.11. Distribution of diffusion coefficients taken from 181 experiments for EGFP-TNF-R2 in wtHeLa cell before (red bars) and within 40 minutes after stimulation (green bars) with cysTNF ligand. Mean value: a) before stimulation $\overline{D} = (3.2 \pm 0.5)\times10^{-9}$ cm^2/s, b) after stimulation $\overline{D} = (0.8 \pm 0.6)\times10^{-9}$ cm^2/s .

After adding cysTNF ligand to the sample buffer the diffusion behaviour started to change. 30 minutes after the diffusion time (slow component) dropped by nearly one order of magnitude, corresponding to an decrease of the diffusion coefficient by one order of magnitude, and recovered 20 minutes later to its initial value.

Table 6.1. Diffusion coefficients for EGFP-TNF-R2 in wtHeLa cell at different times T after stimulation.

T / min	$\mathbf{D_1}$ / cm^2/s	$\mathbf{D_2}$ / cm^2/s
0	$(2.1 \pm 0.01) \times 10^{-7}$	$(3.2 \pm 0.2) \times 10^{-9}$
25	$(2.2 \pm 0.04) \times 10^{-7}$	$(5.2 \pm 0.4) \times 10^{-10}$
45	$(2.1 \pm 0.02) \times 10^{-7}$	$(3.6 \pm 0.3) \times 10^{-9}$

The development of the ACFs and the diffusion coefficients are shown in Fig. 6.12 and 6.13, respectively.

Fig. 6.13 was created with data measured in a single cell at a fixed position in the plasma membrane. Calculated diffusion coefficients D_1 and D_2 for the ACFs shown in Fig. 6.12 are given in Table 6.1.

A possible explanation for the recovery of the diffusion coefficient starting 30 minutes after stimulation could be the internalisation of TNF-R2 after interaction with cysTNF (unpuplished data, manuscript is in preparation). Internalisation can lead to a depletion of stimulated receptors and only unstimulated TNF-R2 molecules remain in the plasma membrane.

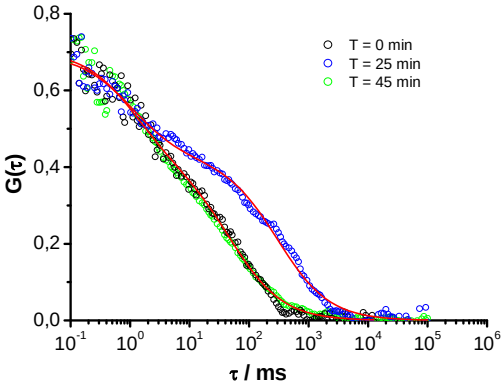

Figure 6.12. Behaviour of the ACFs of diffusing TNF-R2 in the membrane of a single wtHeLa cell measured at different times T after stimulation with cysTNF ligand. The functions were fitted with two-component 2D model (red curves).

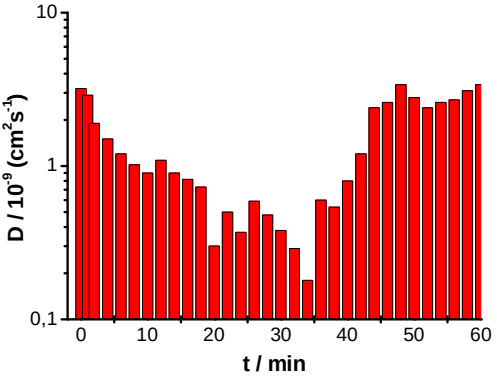

Figure 6.13. Time evolution of the diffusion coefficient after stimulation with cysTNF ligand (stimulation at t = 0) measured on a plasma membrane of a single wtHeLa cell at a fixed position in the plasma membrane.

This internalisation process was examined in the group of Prof. P. Scheurich (Institute for Cell Biology and Immunology) by observing the behaviour of TNF-R2 conjugated with fluorescent antibodies in stained HeLa cell membranes. A series of confocal images showing the internalisation process is shown in Fig. 6.14.

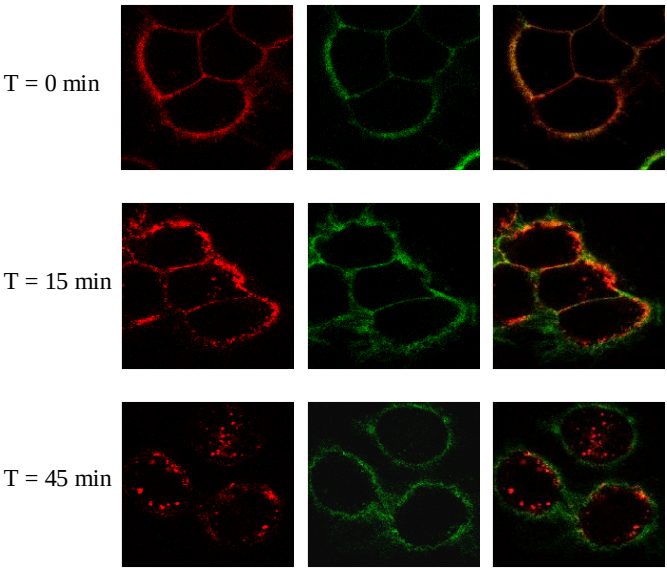

Figure 6.14. Confocal images of TNF-R2 conjugated with 80M2-AlexaFluor546 antibodies (red marker) in HeLa cell membrane marked with fluorescein labelled anti-human-leucocyte- antigen-antibody (green marker) before (T = 0 min) and after (T = 15, 45 min) stimulation with cysTNF. Left column: AlexaFluor546 fluorescence; middle column: fluorescein fluorescence; right column: sum image. (Courtesy of Susanne Bryde)

The internalisation of receptors is a plausible reason for the observed increase of diffusion coefficients after stimulation since it removes all stimulated and slowly diffusing receptors from the membrane. All unstimulated receptors left in the

membrane should be stimulated by TNF which is still present in the medium resulting in an a new decrease of the diffusion coefficient (see chapter 7). But such a behaviour was not observed and it also remains unclear why the diffusion coefficients drop after stimulation.

6.1.3 TNF-R2 in murine fibroblast cell line

As mentioned previously, TNF-R2 is present in the plasma membrane of wtHeLa cells even before transfection with a TNF-R2 vector. The presence of unlabelled receptors after transfection may cause some difficulties in observing aggregation processes by recording the fluorescence time traces.
The murine fibroblast (MF TNF-R1/TNF-R2 (-/-; -/-)) cell line generated from a TNF-R1/TNF-R2 double knock out mice (MF TNF-R1/TNF-R2 (-/-; -/-)) was used for its lack of TNF-R2 in the cell membrane until transfection with the pEGFP-TNF-R2 expression plasmids so that after transfection only EGFP labelled TNF-R2 was present in the membrane. By using the MF TNF-R1/TNF-R2 (-/-; -/-) cell line receptor aggregation should be observable in the fluorescence time traces. A drawback of working with the MF TNF-R1/TNF-R2 (-/-; -/-) cell line is the high cell autofluorescence and the low transfection efficiency. Therefore, in all experiments with MF TNF-R1/TNF-R2 (-/-; -/-) cells different amounts of the EGFP-TNF-R2 transfection vector were used as well as different optical filters and excitation powers to minimize the auto-fluorescence background.

The observed diffusion behaviour of EGFP-TNF-R2 in MF TNF-R1/TNF-R2 (-/-; -/-) cell membranes was similar to the diffusion behaviour measured on wt HeLa cells. Approximately 30 minutes after stimulation of TNF-R2 the diffusion coefficient decreased by nearly one order of magnitude but recovered within the

next 30 minutes to its initial value. Fig. 6.15 summarizes the measurements showing the distribution of diffusion coefficients measured before and within 40 minutes after stimulation with cysTNF ligand.

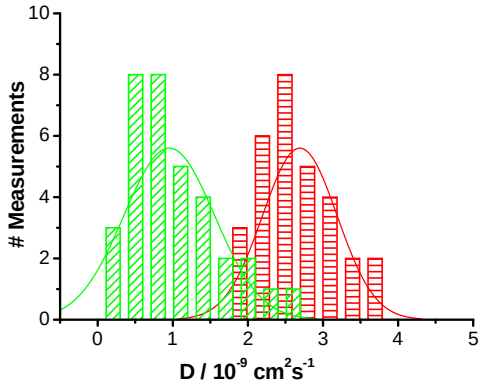

Figure 6.15. Distribution of diffusion coefficients, taken from 64 experiments for EGFP- TNF-R2, in MF TNF-R1/TNF-R2 (-/-; -/-) cell membranes, before (red bars) and within 40 minutes after stimulation (green bars) with cysTNF ligand. Mean value: a) before stimulation $\overline{D} = (2.9 \pm 0.5) \times 10^{-9}$ cm^2/s, and (b) after stimulation $\overline{D} = (0.9 \pm 0.6) \times 10^{-9}$ cm^2/s.

The mean value for the diffusion coefficient before stimulation is $\overline{D} = (2.9 \pm 0.5) \times 10^{-9}$ cm^2/s, which is comparable to the values obtained for the diffusion in the HeLa80 and wtHeLa cell lines. The mean value for the stimulated receptors would correspond to the diffusion of an aggregate of about 5000 proteins (see chapter 6.1.1), but a corresponding increase in fluorescence intensity was again not detected. As shown in Fig. 6.16. (B) the increase in fluorescence intensity after stimulation only corresponds to an aggregate including 3-4 fluorophores.

The results of the experiments which have been presented in 6.1.1, 6.1.2 and 6.1.3 show that a ligand induced aggregation of TNF-R2 could be excluded. To

find an explanation for the diffusion behaviour of TNF-R2 after stimulation the interaction of TNF-R2 with membrane micro domains (rafts) and the cytoskeleton (actin filaments) were investigated in wtHeLa cell lines.

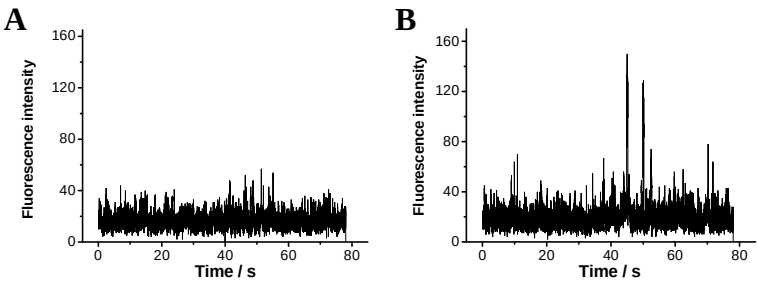

Figure 6.16. Fluorescence time traces of EGFP-TNF-R2 proteins in MF TNF-R1/TNF-R2 (-/-; -/-) cell membranes, (**A**) before and (**B**) after stimulation with TNF ligand.

6.1.4 2-Methylcyclodextrin (MβCD) treatment of wtHeLa

Treatment of biological membranes with 2-Methylcyclodextrin (MβCD) (see chapter 4.3.2) leads to a depletion of cholesterol in cholesterol rich micro domains, so called rafts. This depletion is supposed to change the diffusion behaviour of TNF-R2 in the case of an interaction with rafts.

All measurements were performed under the same conditions, as described above. The wtHeLa cells were treated with MβCD before and after stimulation with 100 ng/ml cysTNF. After treatment with MβCD the cells were incubated for 30 minutes before the measurements were continued.

The results for the unstimulated TNF-TR2 receptor showed that treatment with MβCD did not alter the diffusion behaviour. The distributions and the mean diffusion coefficients for the treated and the untreated cells were nearly unchanged as shown in Fig. 6.17.

After stimulation of EGFP-TNF-R2 and treatment with MβCD the receptor showed a diffusion behaviour analogue to that observed for the stimulated receptor in wtHeLa cell without MβCD treatment (see chapter 6.1.2). This similarity is exemplified by comparing the distributions in Fig. 6.18 with that in Fig. 6.11.

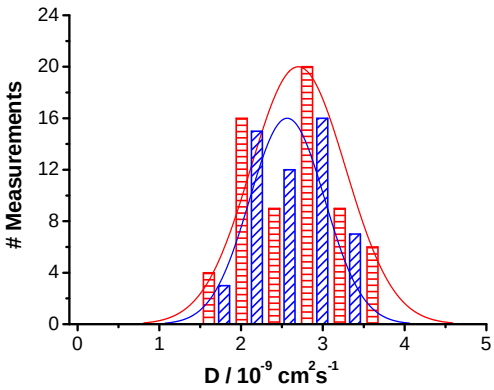

Figure 6.17. Distribution of diffusion coefficients taken from 117 experiments for EGFP-TNF-R2, in the plasma membrane of wtHeLa, before (red bars) and after (blue bars) treatment with MβCD. Mean values: a) before treatment $\overline{D} = (2.7 \pm 0.6) \times 10^{-9}$ cm^2/s, b) after treatment $\overline{D} = (2.6 \pm 0.7) \times 10^{-9}$ cm^2/s.

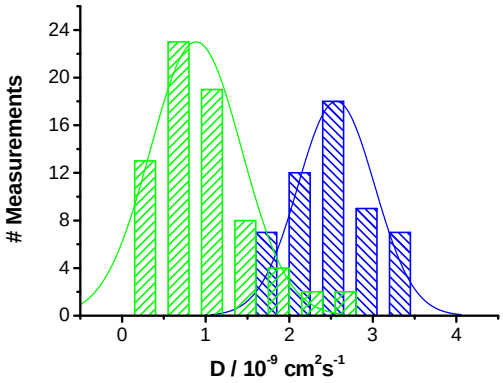

Figure 6.18. Distribution of diffusion coefficients taken from 124 experiments for EGFP-TNF-R2, in MβCD treated plasma membrane of wtHeLa cells before (blue bars) and within 40 min. after stimulation with the ligand cysTNF (green bars). Mean values: a) before stimulation $\overline{D} = (2.6 \pm 0.7) \times 10^{-9}$ cm^2/s, b) after stimulation $\overline{D} = (0.9 \pm 0.6) \times 10^{-9}$ cm^2/s.

The mean value for the diffusion coefficient of EGFP-TNF-R2 in MβCD treated membranes is $\overline{D} = (2.6 \pm 0.7) \times 10^{-9}\,\mathrm{cm}^2/\mathrm{s}$, and after stimulation of TNF-R2 $\overline{D} = (0.9 \pm 0.6) \times 10^{-9}\,\mathrm{cm}^2/\mathrm{s}$. These values match the diffusion coefficients measured in wtHeLa without MβCD treatment. Thus, treatment with MβCD has no effect on the diffusion behaviour of receptors neither before nor after stimulation. This suggests that the receptor is not embedded in cholesterol rich micro domains before and after stimulation.

6.1.5 Cytochalasin D treatment of wtHeLa

As mentioned previously, a possible reason for the decreasing diffusion coefficient after stimulation is an interaction between the receptors cytoplasmic

domain and the cytoskeleton. To examine this, wtHeLa cells were treated with Cytochalasin D (cytD) (chapter 4.3.2) which depolymerises the actin filaments in the cells. In case of an interaction of the stimulated receptor with actin filaments the treatment with cytD should result in similar diffusion coefficients for the stimulated and unstimulated receptor.

The series of confocal images in Fig. 6.19 depicts the influence of various cytD concentra-tions on the cytoskeleton of wtHeLa cells. The images were taken two hours after a treatment with cytD. Red patches in the confocal images (B), (C) and (D) indicate the depolymerisation process. At concentrations of 156 µg/ml (B) and 625 µg/ml (C) the cells shapes appear still unaltered whereas at 1.25 mg/ml (D) cells already collapsed referring to dying cells.

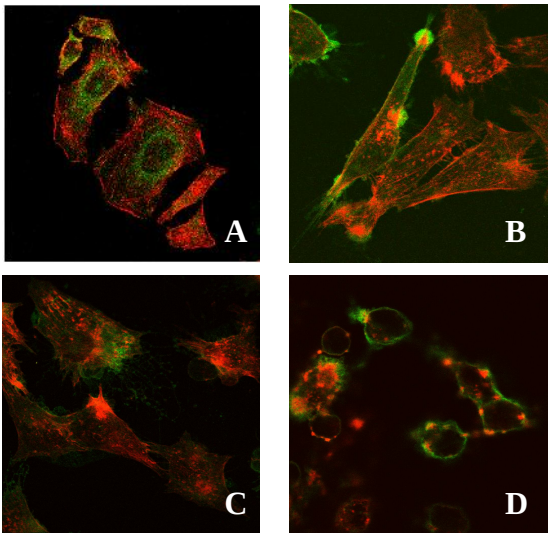

Figure 6.19. Confocal images of wtHeLa cells before (**A**) and after (**B**, **C**, **D**) treatment with different concentration of cytD: (**B**) 156 µg/ml, (**C**) 625 µg/ml, (D) 1.25 mg/ml. The cell membrane was stained with anti-human-leucocyte-antigen-antibody conjugated with fluorescein (green colour) and the actin filaments with rhodamine labelled phalloidine (red colour). (Courtesy of Susanne Bryde, Institute for Cell Biology and Immunology).

For the FCS measurement cytD was added to the sample buffer to a total concentration of 800 µg/ml. After an incubation time of 40-60 minutes the diffusion coefficients of EGFP-TNF-R2 were determined.

After stimulation with cysTNF the diffusion coefficients were decreasing in a similar extent as described for the untreated wtHeLa cells in chapter 6.1.2. The mean value of the diffusion coefficient dropped from its initial value $\overline{D} = (2.3 \pm 0.4) \times 10^{-9}$ cm^2/s within 40 minutes after stimulation to $\overline{D} = (1.0 \pm 0.4) \times 10^{-9}$ cm^2/s as shown in Fig. 6.20 but no recovery was observed.

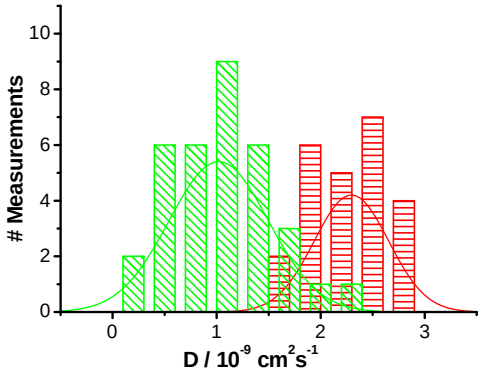

Figure 6.20. Distribution of diffusion coefficient of EGFP-TNF-R2 in cytD treated wtHeLa cells before (red bars) and within 40 min. after (green bars) stimulation with cysTNF ligand. Mean values: a) before stimulation $\overline{D} = (2.3 \pm 0.4) \times 10^{-9}$ cm^2/s, b) after stimulation $\overline{D} = (1.0 \pm 0.4) \times 10^{-9}$ cm^2/s.

This behaviour could be attributed to the loss of actin filaments in the cytoskeleton. But it would be also possible that the beginning degradation of the cell related the loss of its actin filaments influences the diffusion behaviour.

6.1.6 TNF-R2Δcyt and TNF-R2Δcyt14aa in wtHeLa cells

To exclude any interaction between TNF-R2 and the cytoskeleton or other interaction of the cytoplasmic part of TNF-R2 two constructs of EGFP-TNF-R2, lacking part or the complete C-terminal cytoplasmic domain, were used in control experiments. The first construct EGFP-TNF-R2Δcyt14aa still contains 14 amino acids of its cytoplasmic domain, whereas the second construct EGFP-TNF-R2Δcyt lacked its cytoplasmic domain completely.

Measurements of both proteins were done under the same conditions as for wtTNF-R2 in wtHeLa cells. The ACFs of both mutants exhibited two components just as the ACFs measured with the wild type protein (see chapter 6.1.2). Typical two component ACFs measured on unstimulated TNF-R2Δcyt and TNF-R2Δcyt14aa as well as EGFP-TNF-R2 are shown in Fig. 6.21. The calulated diffusion coefficients are given in Table 3.

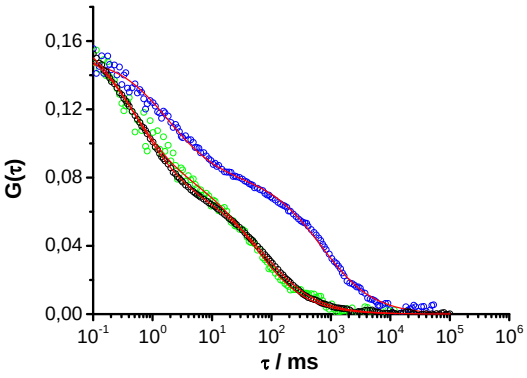

Figure 6.21. Typical two component ACFs for EGFP-TNF-R2Δcyt14aa (black circles), EGFP-TNF-R2Δcyt (blue circles) and EGFP-TNF-R2 (green circles) diffusion in wtHeLa cell membranes before stimulation. The calulated diffusion coefficients are given in Table 3.

Table 3. Diffusion coefficients for different TNF-R2 receptors.

Protein	$\mathbf{D_1}$ / cm^2/s	$\mathbf{D_2}$ / cm^2/s
EGFP-TNF-R2Δcyt14aa	$(3.1 \pm 0.1) \times 10^{-7}$	$(3.4 \pm 0.4) \times 10^{-9}$
EGFP-TNF-R2Δcyt	$(2.1 \pm 0.1) \times 10^{-7}$	$(3.1 \pm 0.1) \times 10^{-10}$
EGFP-TNF-R2	$(2.9 \pm 0.1) \times 10^{-7}$	$(3.9 \pm 0.1) \times 10^{-9}$

EGFP-TNF-R2Δcyt14aa

The diffusion behaviour for unstimulated EGFP-TNF-R2Δcyt14aa in wtHeLa membranes was identical to the behaviour of unstimulated EGFP-TNF-R2 in the same cell line (see chapter 6.1.2). Within approximately 40 minutes after stimulation with cysTNF the diffusion coefficient was dropping comparable to the behaviour of the wild type protein in wtHeLa cells. The distribution of diffusion coefficients for EGFP-TNF-R2Δcyt14aa measured before and within 40 minutes after stimulation are shown in Fig. 6.22. Corresponding fluorescence time traces are shown in Fig. 6.23. These traces indicate that the drop of the diffusion coefficient can not only be attributed to receptor aggregation because the estimated size off these aggregates (see chapter 6.1.1) did not correspond to the observed changes in fluorescence intensity.

After this decline the diffusion behaviour changed compared with the wild type protein. Whereas the diffusion coefficient for the wild type proteins reached its initial value after about 50 minutes, the diffusion coefficient for the mutant protein started fluctuating between 0.1×10^{-9} cm^2/s and a value close to its initial value. This behaviour measured on a single cell is depicted in Fig. 6.24.

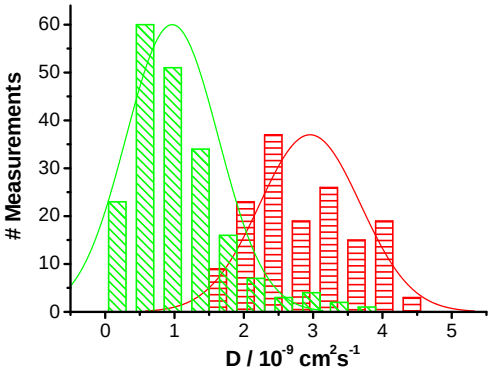

Figure 6.22. Distribution of diffusion coefficients taken from 359 experiments for EGFP-TNF-R2Δcyt14aa in wtHeLa cells before (red bars) and within 40 minutes after (green bars) treatment with MβCD and cysTNF ligand. Mean values: a) before stimulation $\overline{D} = (2.9 \pm 0.9) \times 10^{-9}$ cm^2/s, b) after stimulation $\overline{D} = (0.9 \pm 0.6) \times 10^{-9}$ cm^2/s.

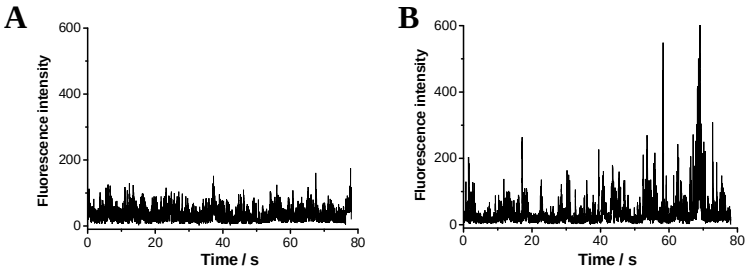

Figure 6.23. Fluorescence time traces of EGFP-TNF-R2Δcyt14aa before (**A**) and 20 minutes after (B) stimulation with cysTNF ligand.

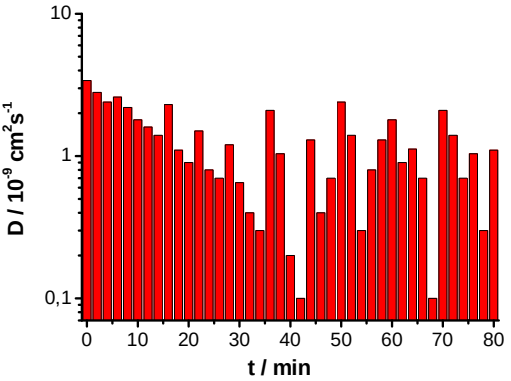

Figure 6.24. Time evolution of the diffusion coefficient *D* of EGFP-TNF-R2Δcyt14aa after stimulation with cysTNF (stimulation at t = 0) measured in a membrane of a single wtHeLa cell.

EGFP-TNF-R2Δcyt

A completely different behaviour was observed for the other mutant receptor EGFP-TNF-R2Δcyt. Unstimulated EGFP-TNF-R2Δcyt possessed a comparatively low diffusion coefficient with a mean value of $\overline{D} = (0.5 \pm 0.3) \times 10^{-9}$ cm^2/s as shown in Fig. 6.25 (A). After the appliance of MβCD, as described in chapter 4.3.2, the diffusion coefficient started to increase by nearly one order of magnitude within about 130 minutes. 2½ hours after MβCD treatment cysTNF was added to the sample to stimulate the receptor. The stimulation led to a decrease of the diffusion coefficient followed by a fluctuating behaviour after one hour. The fluctuations showed the same extent as the fluctuations observed for the EGFP-TNF-R2Δcyt14aa mutant and had a mean value of $\overline{D} = (0.9 \pm 0.4) \times 10^{-9}$ cm^2/s (see Fig. 6.25 (B)). The time

evolution before and after stimulation observed on a single wtHeLa cell is shown in Fig. 6.26.

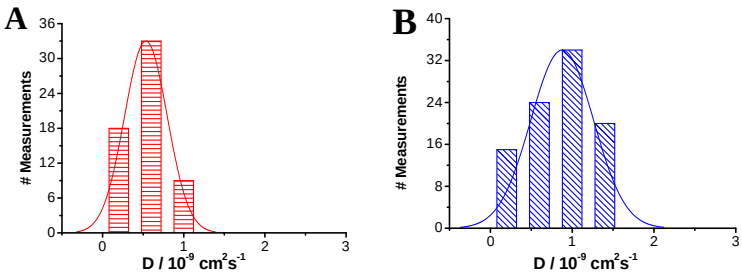

Figure 6.25. (**A**) Distribution of diffusion coefficients taken from 60 experiments for EGFP-TNF-R2Δcyt in wtHeLa cells before stimulation. Mean value: $\overline{D} = (0.5 \pm 0.3) \times 10^{-9}$ cm^2/s. (**B**) Distribution of diffusion coefficients taken from 93 experiments for EGFP-TNF-R2Δcyt in wtHeLa cells after treatment with MβCD and cysTNF ligand. Mean value: $\overline{D} = (0.9 \pm 0.4) \times 10^{-9}$ cm^2/s.

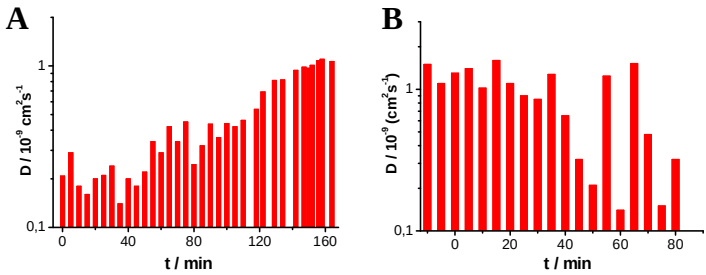

Figure 6.26. (**A**) Time evolution of the diffusion coefficient of EGFP-TNF-R2Δcyt after treatment with MβCD and incubation about 30 minutes, measured in a membrane of a single wtHeLa cell. (**B**) Time evolution of the diffusion coefficient of EGFP-TNF-R2Δcyt after treatment with MβCD and cysTNF (stimulation at t=0) measured in the plasma membrane of a single wtHeLa cell.

These data showed that only EGFP-TNF-R2Δcyt responded to a membrane treatment with MβCD, that suggests that only this particular construct is embedded in cholesterol rich domains. The C-terminal cytoplasmic domain of TNF-R2 contains the amino acid sequence Lys-Lys-Lys-Pro which is believed to be phospholipophilic. The construct EGFP-TNF-R2Δcyt14aa still bears this particular sequence in its residual cytoplasmic domain whereas EGFP-TNF-R2Δcyt does not. Hypothetically the lack of these four amino acids might enable the receptor EGFP-TNF-R2Δcyt to interact with cholesterol rich domains (rafts) in the plasma membrane. So this response to the MβCD treatment should be considered as a consequence due to the lack of the phospholipophilic amino acid sequence Lys-Lys-Lys-Pro.

6.2 The dynamic of TNF-R1 in the plasma membrane

6.2.1 TNF-R1 in wtHeLa cell

It was mentioned earlier that the death domains (DDs) of TNF-R1 tend to auto-aggregate. This leads to the induction of apoptosis upon over-expression of this receptor (chapter 3). Therefore, for the investigation of TNF-R1 the wtHeLa cell line was chosen with low concentration of exogenous EGFP-TNF-R1 expression. All measurements with the EGFP-TNF-R1 were done under the same conditions as described in chapter 4. The results for the unstimulated receptor are summarized in Fig. 6.27 (A).

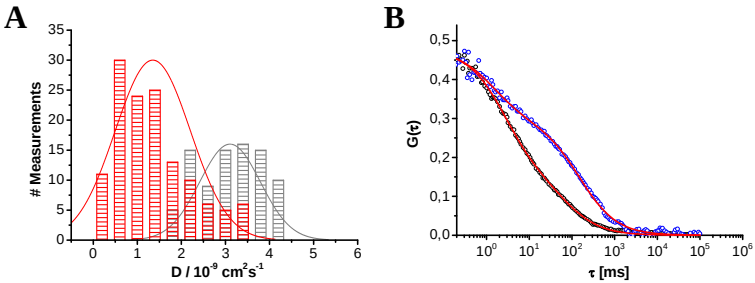

Figure 6.27. (**A**) Distribution of diffusion coefficients taken from 85 experiments for EGFP-TNF-R2 in wtHeLa cell (grey bars) and from 130 experiments for EGFP-TNF-R1 in wtHeLa (red bars), both before stimulation. Mean value: a) before stimulation for EGFP-TNF-R2 $\overline{D} = (3.2 \pm 0.5) \times 10^{-9}$ cm^2/s, b) before stimulation for EGFP-TNF-R1 $\overline{D} = (1.2 \pm 0.8) \times 10^{-9}$ cm^2/s . (**B**) Two typical two-component ACFs for unstimulated EGFP-TNF-R1 diffusion in wtHeLa plasma membranes. Red curves represent two-exponential fit function.

The observed diffusion coefficients of unstimulated TNF-R1 differed from the behaviour observed for TNF-R2 (Fig. 6.27 (A) red and grey bars, respectively). While the diffusion coefficients of TNF-R2 were in a range between 1.8×10^{-9} and 3.8×10^{-9} cm^2/s, the diffusion coefficients for TNF-R1 were found in a range between 2×10^{-10} and 3.6×10^{-9} cm^2/s with a mean value of $\overline{D} = (1.2 \pm 0.8) \times 10^{-9}$ cm^2/s. Two ACFs in Fig 6.27 (B) measured on a single cell exemplify the broad range in which the diffusion coefficients have been found.

After treatment with MβCD the diffusion coefficient of TNF-R1 increased. Within an incubation time of 40 minutes the mean value of the diffusion coefficient distribution increased until $\overline{D} = (1.6 \pm 0.8) \times 10^{-9}$ cm^2/s. Two hours after MβCD treatment soluble TNF (sTNF) was then added to the sample to stimulate the receptor. The stimulation did not change the diffusion behaviour and only the ongoing effect of MβCD was observed. The diffusion coefficient

distributions of EGFP-TNF-R1, taken from 221 experiments, before and after MβCD treatment and stimulation, respectively, are shown in Fig. 6.28.

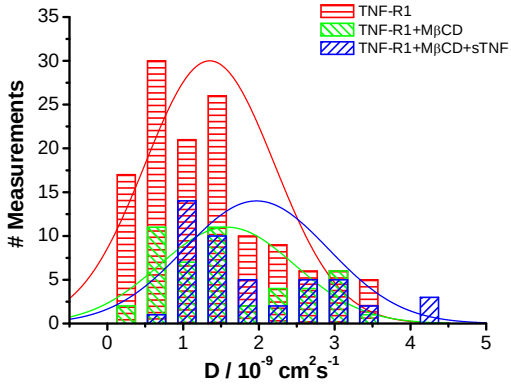

Figure 6.28. Distribution of diffusion coefficients taken from 221 experiments for EGFP-TNF-R1 in wtHeLa cells (red bars), 40 minutes after treatment with MβCD (green bars) and 120 min with MβCD and 40 min with sTNF ligand treatment (blue bars). Mean value: a) before stimulation $\overline{D} = (1.1 \pm 0.9) \times 10^{-9}$ cm^2/s, b) after treatment with MβCD $\overline{D} = (1.6 \pm 0.8) \times 10^{-9}$ cm^2/s, c) after treatment with MβCD and sTNF $\overline{D} = (2.0 \pm 0.9) \times 10^{-9}$ cm^2/s.

This experiment showed that the diffusion behaviour of TNF-R1 responds to an MβCD treatment which indicates that the TNF-R1 receptors are embedded in cholesterol-rich domains of the plasma membrane.

This result could be approved by a 2PE experiment where the cells were treated with cholera toxin subunit B (CT-B) labelled with AlexaFluor 647. CT-B specifically binds to the glycosphingolipids (GSL) which are constituents of lipid rafts (see 3.1.2). This treatment leads to a labelling of rafts in the cell membranes with AlexaFluor 647 CT-B as shown in the confocal images in Fig. 6.29. Both fluorophores, EGFP and AlexaFluor 647 were excited at 850 nm and their fluorescence were separated by a dichroic mirror (chapter 4, Fig. 4.5).

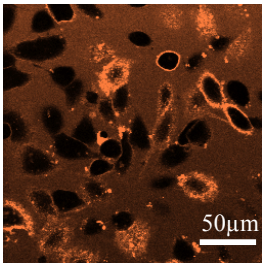

Figure 6.29. Confocal image of a wtHeLa cell sample treated with AlexaFlour 647 labelled cholera toxin subunit B (CT-B). The cells appear as dark objects against the fluorescing background of the CT-B solution. Cell membranes which are marked with labelled CT-B are indicated by their partially or completely fluorescing outlines.

Two typical ACFs for the diffusion of TNF-R1 and CT-B are presented in Fig. 6.30. Nearly all ACFs of CT-B were comparable with the ACFs obtained for the diffusion of unstimulated TNF-R1. This observation is reflected in the mean diffusion coefficient for CT-B of $\overline{D} = (0.8 \pm 0.6) \times 10^{-9}\ cm^2/s$ which is comparable to the mean value obtained for TNF-R1.

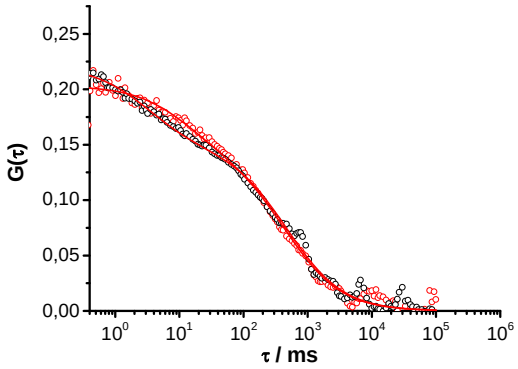

Figure 6.30 Typical ACFs for EGFP-TNF-R1 (black circles) and AlexaFluor 647-CT-B (red circles) diffusion in wtHeLa cell membranes before stimulation.

6.2.2 TNF-R1Δcyt in wtHeLa cell

To rule out any interaction between TNF-R1 and the intracellular network a mutant of EGFP-TNF-R1 lacking its complete cytoplasmic domain (EGFP-TNF-R1Δcyt) were used.

The mean diffusion coefficient $\overline{D} = (1.2 \pm 0.9) \times 10^{-9}$ cm^2/s of unstimulated EGFP-TNF-R1Δcyt was comparable to the value measured for EGFP-TNF-R1 in wtHeLa membranes and the width of the distribution of diffusion coefficients taken from 75 experiments (see Fig. 6.27) was similar, too. After addition of MβCD the cells were incubated for one hour and then stimulated with sTNF. Data were collected within 3 hours after stimulation.

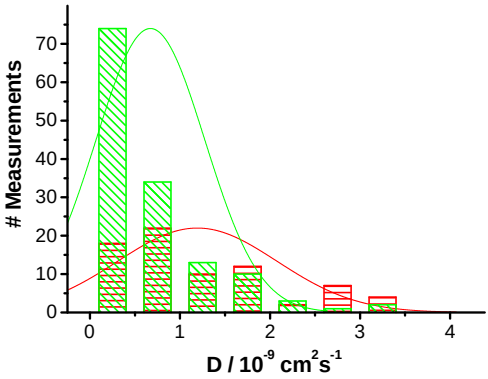

Figure 6.31 Distribution of diffusion coefficients taken from 212 experiments for EGFP-TNF-R1Δcyt in wtHeLa cells (red bars), 60 minutes after treatment with MβCD and sTNF ligand (green bars). Mean value: a) before stimulation $\overline{D} = (1.2 \pm 0.9) \times 10^{-9}$ cm^2/s, b) after treatment $\overline{D} = (0.7 \pm 0.8) \times 10^{-9}$ cm^2/s.

This treatment induced a decrease of the diffusion coefficients as shown in Fig. 6.31. The mean value of the diffusion coefficient distribution dropped from $\overline{D} = (1.2 \pm 0.9) \times 10^{-9}$ cm^2/s to $\overline{D} = (0.7 \pm 0.8) \times 10^{-9}$ cm^2/s.

6.3 TRAF2 protein in wtHeLa cells

It is known that the stimulation the TNF-R2 with cysTNF leads to the recruitment of TRAF2 protein to the TRAF-binding site of TNF-R2 cytosolic domain (chapter 3).

The diffusion behaviour of EGFP-TRAF2 protein was measured under the same conditions as described for TNF-R2 in chapter 6.1. The diffusion coefficient for EGFP-TRAF2 was determined inside the cell and close to the cell membrane before and after stimulation of the (not labelled) receptor TNF-R2.

Typical ACFs for the diffusion of EGFP-TRAF2 inside the cell and close to the membrane are shown in Fig. 6.32 (A). Close to the membrane EGFP-TRAF2 possessed an evidently lower diffusion coefficient than inside the cell. The distributions of diffusion coefficients, taken from 72 experiments, are shown in Fig. 6.32 (B). The mean values of these distributions are $\overline{D} = (2.6 \pm 0.2) \times 10^{-7}$ cm^2/s for diffusion inside the cell and $\overline{D} = (0.3 \pm 0.2) \times 10^{-7}$ cm^2/s for diffusion close to the membrane, respectively. Obviously, the TRAF2 protein tends to interact with the plasma membrane.

After stimulating the TNF-R2 receptor with cysTNF the diffusion of TRAF2 close to the membrane was investigated. A few minutes after cysTNF was added an increase of the diffusion time, corresponding to a decrease of the diffusion coefficient about one order of magnitude, was observed. 40 minutes after stimulation even diffusion coefficients in the range of 10^{-9} cm^2/s were measured.

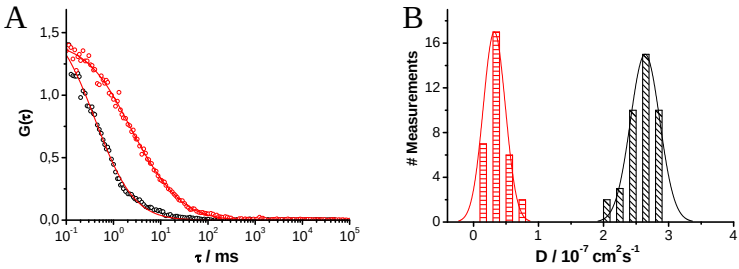

Figure 6.32. (**A**) A typical ACFs for the diffusion of EGFP-TRAF2 inside the cell (black circles) and close to the membrane (red circles) of wtHeLa cell. (**B**) Distribution of diffusion coefficients taken from 72 experiments for EGFP-TRAF2 inside (black bars) and close to the membrane (red bars) of wtHeLa cells. Mean value: inside of the cell $\overline{D} = (2.6 \pm 0.2) \times 10^{-7}$ cm^2/s and close to the membrane $\overline{D} = (0.3 \pm 0.2) \times 10^{-7}$ cm^2/s.

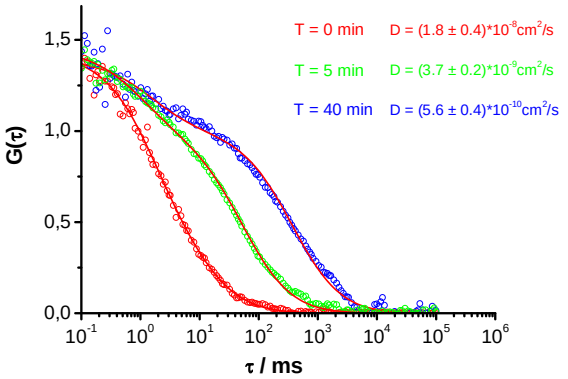

Figure 6.33. Behaviour of the ACFs of diffusing EGFP-TRAF2 protein close to the plasma membrane measured at different times after stimulation of TNF-R. The functions were fitted (red curves) with the 2D model given in eqn. (5.4).

The ACFs in Fig. 6.33 and the distribution of diffusion coefficients in Fig. 6.34 show this difference between the stimulated and unstimulated case. The measured mean values for the unstimulated and the stimulated cells are $\overline{D} = (0.3 \pm 0.1) \times 10^{-7}$ cm^2/s and $\overline{D} = (0.03 \pm 0.02) \times 10^{-7}$ cm^2/s, respectively.

As expected, the diffusion behaviour of TRAF2 close to the membrane in stimulated cells was similar to the behaviour of TNF-R2 after stimulation with (see chapter 6.1.2). This is a consequence of TRAF2 recruitment by the stimulated TNF-R2 receptor (see chapter 3.1).

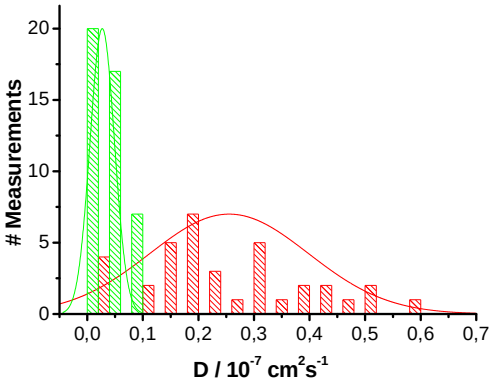

Figure 6.34. Distribution of diffusion coefficients taken from 80 experiments for EGFP-TRAF2 in wtHeLa cells before (red bars) and after (green bars) stimulation of the TNF-R2 receptor with cysTNF. Mean values: a) before stimulation $\overline{D} = (0.3 \pm 0.1) \times 10^{-7}$ cm^2/s, b) after stimulation $\overline{D} = (0.03 \pm 0.02) \times 10^{-7}$ cm^2/s.

CHAPTER 7

Discussion and Outlook

At the starting point of this thesis only a few results of FCS on living cells have been published. A large community of researches even has believed that FCS on cells would not be possible. The results of this work clearly showed, that FCS within living cells and on plasma membranes is practicable with both 1PE and 2PE, even with low S/R ratios due to autofluorescence of the cell or a poor quantum yield of the used fluorophores. FCS within living cells provides an opportunity to investigate the mobility of a large number of proteins and their interactions inside the cytoplasm and within membranes. The dynamic range of the observed diffusion coefficients was widespread from 10^{-7} - 10^{-10} cm^2/s for protein diffusion in cell cytoplasm and membrane bound proteins, respectively.

It was found that the geometry of the membrane versus the focal volume is crucial for the correct determination of the diffusion coefficient. A deviation

from the assumption of a circular cross-section between focus and membrane leads to smaller diffusion constants. For example, at the bottom of the cell the plasma membrane is supposed to be parallel to the glass substrate and perpendicular to the optical axis. Here a circular cross section with the focal spot is a good approximation and hence, the standard model for 2D diffusion should give accurate results for the diffusion constants. The ACFs of TNF-R1 and -R2 diffusion in the plasma membrane strongly suggests a two-component behaviour. Hence, curves were fitted with a two-component model assuming 2D diffusion. It turned out that the diffusion coefficient corresponding to the fast component were constant (~2×10^{-7} cm^2/s) in all experiments.

7.1 TNF-R2

In the last chapter it was shown that in all investigated cell lines, wtHeLa, HeLa80 and MF, stimulation of the TNF-R2 receptor with cysTNF ligand led to a decrease of its diffusion coefficient within 40 minutes after stimulation. Although the distribution of D-values is relatively broad in both cases, a significant shift of the distribution from a mean value of $\overline{D} = 3.2 \times 10^{-9}$ cm^2/s to $\overline{D} = 0.8 \times 10^{-9}$ cm^2/s could be observed. This effect could not be caused solely by aggregation of labelled receptors because the estimated size of such slow diffusing aggregates would correspond to 10^4 receptors and such a large number of molecules are not in accord with the measured intensity time traces. In the case of the HeLa80 cell line the expected appearance of long and intense bursts in the time traces, caused by large fluorescing aggregates, could be hindered by the presence of huge amounts of unlabelled receptors (see chapter 2.3.1). But the same results were obtained for the cell lines wtHeLa and MF which express unlabelled TNF-R2 only in small amounts or not at all. Another explanation for

the measured drop of the diffusion coefficients for TNF-R2 in this work could be a change in membrane viscosity induced by receptor stimulation. However, the experiments with rhodamine labelled lipids in the cell membranes of HeLa80 and wtHeLa cells could not verify this assumption.

Similar results were obtained by FRAP [40] and FCS [38] experiments on the mobility of the b2-AR receptor in A549 cells (see chapter 2.1).

To investigate the role of cholesterol rich microdomaines (see chapter 2.2) in the diffusion behaviour of TNF-R2, the membranes of wtHeLa cells were treated with MβCD in order to deplete cholesterol. Our data showed, that the induced depletion did not change the diffusion behaviour of TNF-R2 neither before nor after stimulation. Thus, it can be concluded that the TNF-R2 receptor is neither before nor after stimulation embedded in rafts. This conclusion was done in virtue of many other works (see chapter 2.1).

In order to check for interactions of the TNF-R2 receptor with actin filaments from the membrane skeleton wtHeLa cells were treated with cytD. The results of these experiments were quite ambiguous. Due to the huge amount of cytD the observed drop of the diffusion coefficient after stimulation could be attributed to either the loss of actin filaments in the membrane skeleton due to cytD or to the beginning degradation of the whole cell. In order to exclude any interaction of the receptor with the cytoskeleton the diffusion behaviour of two TNF-R2 mutants, EGFP-TNF-R2Δcyt14aa and EGFP-TNF-R2Δcyt, which possess mutations in their cytoplasmic domains, were examined. The data showed that only EGFP-TNF-R2Δcyt, which lacks its complete cytoplasmic domain, responded to the MβCD treatment by an increase of the measured diffusion coefficients. However, this response should be considered as an artefact due to the lack of the phospholipophilic Lys-Lys-Lys-Pro amino acid sequence which is included in the cytoplasmic domain.

Based on the results of our experiments it is not possible to conclude why the diffusion of the receptors slowed down after stimulation with cysTNF whereas

the subsequent recovery of the diffusion coefficients, as observed in wtHeLa and MF cells, can be explained. In the case of the wtHeLa cell line the recovery can be explained by the internalisation of stimulated receptors. Even though one would expect a second decrease of the diffusion coefficient after the first recovery, caused by an interaction of unbound ligands and receptors, which have not been internalised. Such behaviour was not observed. Recent studies on the function of TNF-R2 receptor suggest that TNF-R2 has the ability to form dimers by linking two receptors with disulfid bonds at its transmembrane domaine. It could be imagined that two pooles of TNF-R2 exist on the cell surface: one that does not form homodimers by dislulfid bridges and another one that forms dimmers by intermolecular disulfide bonds. If only the latter is able to bind to CysTNF and internalise, then one could speculate that after stimulation receptors of the other kind remain on the cell membrane since they are not activatable. The observed broad distribution of diffusion coefficients and the weak mass dependence of D ($D^{-1} \sim \sqrt[3]{m}$) would result in a similar diffusion behaviour for TNF-R2 dimmers compared with monomeric TNF-R2.

The process of internalisation may also be responsible for the observed drop of the diffusion coefficient after stimulation. Internalisation occurs by multiple mechanisms and is not yet known which mechanism is responsible for the internalisation of TNF-R2 and TNF-R1. There are at least three basic mechanisms which lead to internalisation of integral membrane proteins: endocytosis dependent on the protein clathrin, endocytosis that requires caveolin, and the clathrin- and caveolin-independent endocytosis [159]. In the early stage of internalisation flask-shaped invaginations are formed in the plasma membrane. In the case of protein-dependent endocytosis the outer surface of the invagination has a scaffolding of specialised proteins, caveolin, clathrin or dynamin, stabilizing the caveolae, which is depicted in Fig.7.1. These caveolae are pinched off from the membrane forming the endocytotic vesicles.

The accumulation of scaffolding proteins may cause a decrease of membrane viscosity in the invaginations leading to a reduced motility of the receptors which are localized in the invaginations prior to their internalisation. P.Tomsen and co. determined the diffusion coef-ficient for the mobile fraction of caveolin by FRAP from 1×10^{-10} cm^2/s to 0.3×10^{-10} cm^2/s [41]. Caveolin is a dimeric protein that binds cholesterol and conferred the shape and structural organization of caveolae, insert as a loop into the inner leaflet of the plasma membrane, and self-associates to form a caveolin coat on the surface of the plasma invaginations [159].

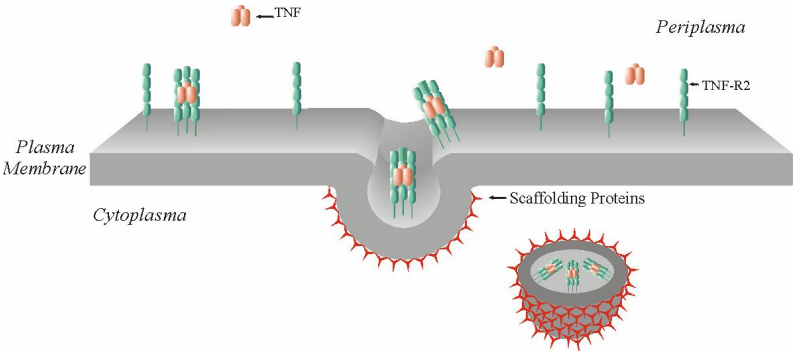

Figure 7.1. Schematic representation of the internalisation process exemplified for TNF-R2. Possible scaffolding proteins: clathrin, caveolin or dynamin.

Another reason for the observed diffusion behaviour of the stimulated TNF-R2 receptor could be the effect of membrane compartmentalisation as described in chapter 2.2.

Because of the small size of the compartments and the short residence time, the diffusion within these structures might not be observable by FCS. The diffusion coefficient for unstimulated TNF-R2 is comparable with the diffusion coefficient

of other receptors within the larger compartments. But due to the fact that mutants lacking the cytoplasmic domain behave identical to native receptors we can rule out that direct interactions between the signalling complex and actin skeleton is the reason for the decrease of the diffusion coefficient. Thus membrane compartments could be responsible for the observed diffusion times of unstimulated TNF-R2 but most probably not for the dramatically decrease of diffusion coefficient after stimulation.

7.2 TNF-R1

Our data showed that the diffusion behaviour of the unstimulated receptor TNF-R1 in wtHeLa cells was completely different than the behaviour observed for TNF-R2. The TNF-R1 receptor showed a comparatively broad distribution of diffusion coefficients spanning from 2×10^{-10} to 3×10^{-9} cm^2/s. The mean value of this distribution was approximately three times smaller compared with the mean value found for the diffusion of the TNF-R2 receptor in the same cell line. In contrast to the TNF-R2 receptor TNF-R1, stimulated and unstimulated, responded to MβCD treatment of the cells by an increase in the diffusion coefficient which suggests that a large portion of the whole TNF-R1 population is embedded in cholesterol rich domains of the plasma membrane even before stimulation. These results were confirmed by another experiment which showed that the lipid raft marker CT-B, which is per se embedded in cholesterol rich domains, exhibited the same diffusion behaviour as unstimulated TNF-R1. This corresponds to the results of Ko et al [160], who reported that in the histocytic lymphoma cell line U937 the receptor TNF-R1 is predominantly localised in structures which they called caveolae-like-domains (CLD). These CLDs show the same biochemical properties as caveolae but they neither show any

morphologic membrane invaginations nor these domains contains caveolin. Due to the similar biochemical properties compared with the caveolae it can be concluded that these CLDs correspond to cholesterol rich domains on the plasma membrane. But it should also be mentioned that, there are cell lines expressing TNF-R1 that translocates in cholesterol rich domains only upon stimulation, e.g. Legler et al. reported that in the human fibrosarcoma cell line HT1080 TNF-R1 localise to lipid rafts after TNF ligand binding forming a signalling complex [161].

Similar results were obtained by Lommerse et al., who investigated H-Ras signalling in mouse fibroblast cell lines [54;56]. They found that inactive H-Ras was partially localized in lipid rafts with a size of 44 nm whereas active H-Ras was essentially absent from these structures. Active H-Ras was found to be localized in small 40-50 nm diameter cholesterol independent microdomains (see chapter 2.1).

The diffusion behaviour of the TNF-R1Δcyt mutant, which lacked its complete cytoplasmic domain, was investigated in order to exclude possible interactions with the cytoskeleton. Before stimulation and MβCD treatment the observed distribution of diffusion coefficients was comparable to the distribution for the wild-type receptor. The measurements showed that the absence of the cytoplasmic domain do not change the diffusion behaviour and, as already mentioned above, the long diffusion times probably indicates the localization of the receptor to lipid rafts. Subsequent stimulation with cysTNF and cell treatment with MβCD resulted, only in slight changes of the diffusion behaviour of TNF-R1Δcyt. These results are not in line with the results obtained by Cottin et al. [162] for the TNF-R1 receptor. They reported that in HeLa cells the DD of the TNF-R1, which is an integral part of the cytoplasmic domain, is necessary for the localization of the receptor to lipid rafts.

7.3 TRAF2 protein

The investigation of the TRAF2 diffusion behaviour in wtHeLa cells showed that diffusing TRAF2 tends to interact with the plasma membrane or the membrane skeleton meshwork which results in a 10 times lower diffusion coefficient compared to freely diffusing TRAF2 within the cytoplasm.

It is possible, that TRAF2 protein associates or co-localise with the scaffolding protein caveolin-1 (see above) at regions of enrichment subjacent to the plasma membrane as detected by confocal fluorescence microscopy. X. Feng et al. did not observe an association of caveolin-1 with TNF-R1, TRADD, or TNF-R2 [163].

After stimulation of the TNF-R2 receptor the TRAF2 diffusion coefficient measured close to the membrane decreased, as expected, due to the recruitment of TRAF2 to the TNF-R2 receptors TRAF binding site. Forty minutes after stimulation the mean value of the diffusion coefficient dropped by one order of magnitude to a value of $(5 \pm 1) \times 10^{-10}$ cm^2/s. This value is, within its error margin, comparable to the diffusion coefficient of $(8 \pm 6) \times 10^{-10}$ cm^2/s for the stimulated TNF-R2 receptor measured in the same cell line. Additionally, the observed temporal developing of the diffusion coefficient after stimulation was similar to the behaviour observed for the TNF-R2 in wtHeLa cells. Thus, the data obtained for TRAF2 diffusion are consistent with the results for the diffusion measurements of the activated TNF-R2 protein.

X.Feng at co. also showed, that cells cotransfected both with GFP-TRAF2 and TNF-R2, the subcellular localization of GFP-TRAF2 was then clearly co-localised with caveolin-1, indicating that both TRAF2 and caveolin-1 were corecruited to the TNF-R2 receptor. In the absence of TRAF2, much less interaction of TNF-R2 with caveolin-1 was detected. These findings strongly

suggest that the interaction of TNF-R2 with caveolin-1 is mediated via TRAF2. The role of TRAF2 in linking caveolin-1 to TNF-R2 was further supported by a mutational analysis of the TRAF2 binding region on the C-terminal region of TNF-R2 [163]. TNF-R2 proteins in which deletions were constructed by removing different numbers of amino acid residues from the C-terminal end of the receptor. They found, that TNF-R2(-16), which lacks 16 aa residues from its C terminus, retains the TRAF2 binding region. In contrast, TRAF2 remained evenly distributed in the cells in which TNF-R2(-37) or TNF-R2(-59) was expressed, indicating that loss of the ability of TNF-R2(-37) and TNF-R2(-59) to associate with TRAF2. They observed, that the distribution of caveolin- 1 in cells transfected with TNF-R2(-37) or TNF-R2(-59) did not show any receptor association.

In these experiments it was observed that, the presence of caveolin-1 increases TRAF2 expression levels. The authors suppose that caveolin-1 stabilises TRAF2 and helps to prolong the signalling process.

A more likely role for the association of caveolin-1 and TRAF2 is the targeting of activated TNF receptor complexes to caveolin-enriched membrane compartments such as caveoli [164].

As since, in this work was also investigated TNF-R2 mutant, EGFP-TNF-R2Δcyt14aa, which has only 14 amino acid residues from 174, we can insist that TRAF2 protein can not interact with that mutant. If true, then caviolin-1 also did not recruit to EGFP-TNF-R2Δcyt14aa as was observed by Ref a. But diffusion behaviour of EGFP-TNF-R2Δcyt14aa was similar with wtTNF-R2 (see above) what indicate that caviolin-1 is not only one scaffolding protein which responsible for TNF-R2 localization to CLD and internalisation.

The aim of further studies on this subject should be to control the amount of depleted cholesterol in the membrane, e.g. as described in the article of Vrljic et

al, and to measure the dynamic of the diffusion coefficients of the different receptors at different cholesterol concentrations [52].

Furthermore the role of the cytoplasmic domains, i.e. the membrane-skeleton, of both receptors, TNF-R1 and TNF-R2, in the process of localization to cholesterol rich domains should be investigated. Here it is necessary to perform experiments on several receptor mutants with deletions or point mutations in their cytoplasmic domains. Especially for TNF-R2 it seems interesting to have mutants with point mutations in the Lys-Lys-Lys-Pro amino acid sequence, which is supposed to be phospholipophilic, of its cytoplasmic domain. With these mutants it should be possible to get further insight into the interaction mechanisms of the cytoplasmic domains of these receptors with the different membrane domains.

References

[1] Magde D., Webb W.W., & Elson E. (1972) Thermodynamic Fluctuations in a Reacting System - Measurement by Fluorescence Correlation Spectroscopy. *Physical Review Letters*, **29,** 705-708.

[2] Ehrenberg M. & Rigler R. (1974) Rotational Brownian-Motion and Fluores-cence Intensity Fluctuations. *Chemical Physics*, **4,** 390-401.

[3] Berland K.M., So P.T.C., & Gratton E. (1995) 2-Photon Fluorescence Correla-tion Spectroscopy - Method and Application to the Intracellular Environment. *Biophysical Journal*, **68,** 694-701.

[4] Schwille P., Haupts U., Maiti S., & Webb W.W. (1999) Molecular dynamics in living cells observed by fluorescence correlation spectroscopy with one- and two-photon excitation. *Biophysical Journal*, **77,** 2251-2265.

[5] Rigler R. & Widengren J. (1990) Ultrasensitive Detection of Single Molecules as Observed by Fluorescence Correlation Spectroscopy. In *Bioscience* pp. 180-183.

[6] Diez M., Börsch M., Zimmermann B., Turina P., Dunn S.D., & Graber P. (2004) Binding of the b-subunit in the ATP Synthase from Escherichia coli. *Biochemistry*, **43,** 1054-1064.

[7] Börsch M., Turina P., Eggeling C., Fries J.R., Seidel C.A.M., Labahn A., & Graber P. (1998) Conformational changes of the H+-ATPase from Escherichia coli upon nucleotide binding detected by single molecule fluorescence. *FEBS Letters*, **437,** 251-254.

[8] Kim H.D., Nienhaus G.U., Ha T., Orr J.W., Williamson J.R., & Chu S. (2002) Mg2+-dependent conformational change of RNA studied by fluorescence correlation and FRET on immobilized single molecules. *Proceedings of the National Academy of Sciences of the United States of America*, **99,** 4284-4289.

[9] Chen Y., Wei L.N., & Muller J.D. (2003) Probing protein oligomerization in living cells with fluorescence fluctuation spectroscopy. *Proceedings of the National Academy of Sciences of the United States of America*, **100,** 15492-15497.

[10] Basche Th. (1992) *Physical Review Letters*, **69,** 1516-1519.

[11] Bernard J. (1993) *Journal of Physical Chemistry*, **98,** 850-859.

[12] Lippincott-Schwarts J., Snapp E., & Kenworthy A. (2001) Studying protein dynamics in living cells. *Nat. Rev. Mol. Cell Biol.*, **2,** 444-456.

[13] Reits E.A.J. & Neefjes J.J. (2001) From fixed to FRAP: measuring protein mobility and activity in living cells. *Nat. Cell Biol.*, **3,** E145-E147.

[14] Klonis N., Rug M., Harper I., Wickham M., Cowman A., & Tilley L. (2002) Fluorescence photobleaching analysis for the study of cellular dynamics. *Eur. Biophys. J.*, **31,** 36-51.

[15] Roy P., Rajfur Z., Pomorski P., & Jacobson K. (2002) Microscope based techniques to the study cell adhesion and migration. *Nat. Cell Biol.*, **4,** E91-E96.

[16] Axelrod D., Koppel D.E., Schlessinger J., Elson E., & Webb W.W. (1976) Mobility measurement by analysis of fluorescence photobleaching recovery kinetics. *Biophysical Journal*, **16,** 1055-1069.

[17] Elson E., Schlessinger J., Koppel D.E., Axelrod D., & Webb W.W. (2007) Measurement of lateral transport on cell surfaces. *Prog. Clin. Biol. Res.*, **9,** 137-147.

[18] Schlessinger J., Axelrod D., Koppel D.E., Webb W.W., & Elson E. (1977) Lateral transport of a lipid probe and labeled proteins on a cell membrane. *Science*, **195,** 307-309.

[19] Jacobson K., Elson E., Koppel D.E., & Webb W.W. (1982) Fluorescence photobleaching in cell biology. *Nature*, **295,** 283-284.

[20] Widengren J., Schweinberger E., Berger S., & Seidel C.A.M. (2001) Two new concepts to measure fluorescence energy transfer via fluorescence correlation spectroscopy: theory and experimental realization. *J. Phys. Chem.*, **105,** 6851-6866.

[21] Webb W.W. (2001) Fluorescence correlation spectroscopy: genesis, evolution, maturation, and prognosis. In *Fluorescence Correlation Spectroscopy. Theory and Applications* (Rigler,R. & Elson,E., eds), pp. 305-330. Springer, Berlin.

[22] Bacia K. & Schwille P. (2003) A dynamic view of cellular processes by *in vivo* fluorescence auto- and cross-correlation spectroscopy. *Methods*, **29,** 74-85.

[23] Haustein E. & Schwille P. (2003) Ultrasensitive investigation of biological systems by fluorescence correlation spectroscopy. *Methods*, **29,** 153-166.

[24] Hink M.A., Borst J.W., & Visser A.J. (2003) Fluorescence correlation spectroscopy of GFP fusion proteins in living plant cells. *Methods Enzymol.*, **361,** 93-113.

[25] Muller J.D., Chen Y., & Gratton E. (2003) Fluorescence correlation spectroscopy. *Methods Enzymol.*, **361,** 69-92.

[26] Cannon D.M.Jr., Winograd N., & Ewing A.G. (2000) Quantitative chemical analysis of single cells. *Annu. Rev. Biophys. Biomol. Struct.*, **29,** 239-263.

[27] Denk W., Strickler J.H., & Webb W.W. (1990) Two-photon laser scanning fluorescence microscopy. *Science,* **248,** 73-76.

[28] Zipfel W.R., Williams R.M., & Webb W.W. (2003) Nonlinear magic: :multiphoton microscopy in the biosciences. *Nat. Biotech.*, **21,** 1369-1377.

[29] Cubeddu R., Comelli D., D'Andrea C., Taroni P., & Valentini G. (2002) Time-resolved fluorescence imaging in biology and medicine. *J. Phys. D: Appl. Phys.*, **35,** R61-R76.

[30] Axelrod D. (2003) Total internal reflection fluorescence microscopy in cell biology. *Methods Enzymol*., **361,** 1-33.

[31] Ritchie K., Shan X.-Y., Kondo J., Iwasawa K., Fujiwara T., & Kusumi A. (2005) Detection of Non-Brownian Diffusion in the Cell

Membrane in Single Molecule Tracking. *Biophysical Journal*, **88 (3),** 2266-2277.

[32] Dietrich C., Yang B., Fujiwara T., Kusumi A., & Jacobson K. (2002) Relationship of lipid rafts to transient confinement zones detected by single particle tracking. *Biophys. J.*, **82,** 274-284.

[33] Fujiwara T., Ritchie K., Murakoshi H., Jacobson K., & Kusumi A. (2002) Phospholipids undergo hop diffusion in compartmentalized cell membrane. *J. Cell Biol.*, **157,** 1071-1081.

[34] Kahya N., Scherfeld D., Bacia K., Poolman B., & Schwille P. (2003) Probing Lipid Mobility of Raft-exhibiting Model Membranes by Fluorescence Correlation Spectroscopy. *J. Biol. Chem.*, **278,** 28109-28115.

[35] Kusumi A., Sako Y., & Yamamoto M. (1993) Confined lateral diffusion of membrane receptors as studied by single particle tracking (nanovid microscopy). Effects of calcium-induced differentiation in cultured epithelial cells. *Biophys. J.*, **65,** 2021-2040.

[36] Hao M., Mukherjee S., & Maxfield F.R. (2001) Cholesterol depletion induces large scale domain segregation in living cell membranes. *Proc. Natl. Acad. Sci. USA*, **98,** 13072-13077.

[37] Pierce K.L., Premont R.T., & Lefkowitz R.J. (2002) Seven-transmembrane receptors. *Nat. Rev. Mol. Cell Biol.*, **3,** 639-650.

[38] Hegener O., Prenner L., Runkel F., Leonhardt Baader S., Kappler J., & Häberlein H. (2004) Dinamics of β_2-Adrenergic Receptor-Ligand Complexes on Living Cells. *Biochemistry*, **43,** 6190-6199.

[39] Xiang Y., Rybin V.O., Steinberg S.F., & Kobilka B. (2002) Caveolar localization dictates physiologic signaling of β_2-adrenoceptors in neonatal cardiac myocytes. *J. Biol. Chem.*, **277,** 34280-34286.

[40] Barak L.S., Ferguson S.S.G., Zhang J., Martenson C., Meyer T., & Caron M.G. (1997) Internal trafficking and surface mobility of a functionally intact β_2-adrenergic receptor-green fluorescent protein conjugate. *Mol. Pharmacol.*, **51,** 177-184.

[41] Thomsen P., Roepstorff K., Stahlhut M., & Bo van Deurs (2002) Caveolae Are Highly Immobile Plasma Membrane Microdomains, Which Are not Involved in Constitutive Endocytic Trafficking. *Molecular Biology of the Cell*, **13,** 238-250.

[42] Douglass A.D. & Vale R.D. (2005) Single-Molecule Microscopy Reveals Plasma Membrane Microdomains Created by Protein-Protein Networks that Exclude or Trap Signaling Molecules in T Cells. *Cell*, **121,** 937-950.

[43] Bray D. (1998) Signalling complexes: biophysical constraints on intracelllar communication. *Annu. Rev. Biophys. Biomol. Struct.*, **27,** 59-75.

[44] Felsenfeld D., Choquet D., & Sheetz M.P. (1996) Ligand binding regulates the directed movement of beta 1 integrins on fibroblasts. *Nature*, **383,** 438-440.

[45] Holowka D. & Baird B. (1996) Antigen-mediated IGE receptor aggregation and signalling: a window on cell surface structure and dynamics. *Annu. Rev. Biophys. Biomol. Struct.*, **25,** 79-112.

[46] Kusumi A., Ike H., Nakada C., Murase K., & Fujiwara T. (2005) Single-molecule tracking of membrane molecules: plasma membrane compartmentalization and dynamic assembly of raft-philic signaling molecules. *Seminars in Immunology*, **17,** 3-21.

[47] Murase K., Fujiwara T., Uemura Y., Suzuki K., Iino ,R., Yamashita H., Saito M., Murakoshi H., Ritchie K., & Kusumi A. (2004) Ultrafine membrane compartments for molecular diffusion as revealed by single molecule techniques. *Biophys. J.*, **86,** 4075-4093.

[48] Sako Y. & Kusumi A. (1994) Compartmentalized structure of the plasma membrane for receptor movements as revealed by a nanometer-level motion analysis. *J. Cell Biol.*, **125,** 1251-1264.

[49] Sako Y. & Kusumi A. (1995) Barriers for lateral diffusion on transferrin receptor in the plasma membrane as characterized by receptor dragging by laser tweezers: fence versus tether. *J. Cell Biol.*, **129,** 1559-1574.

[50] Sheetz M.P. (1983) Memrane skeleton dynamics: role in modulation of red cell deformability, mobility of transmembrane proteins, and shape. *Semin. Hematol.*, **20,** 175-188.

[51] Kenworthy A.K., Nichols B.J., Remmert C.L., Hendrix G.M., Kumar M., Zimmerberg J., & Lippincott-Schwartz J. (2004) Dynamics of

putative raft-associated proteins a the cell surface. *J. Cell Biol.*, **165,** 735-746.

[52] Vrljic M., Nishimura S.Y., Moerner W.E., & McConnell H.M. (2005) Cholesterol Depletion Suppresses the Translational Diffusion of Class II Major Histocompatibility Complex Proteins in the Plasma Membrane. *Biophysical Journal*, **88,** 334-347.

[53] Daumas F., Destainville N., Millot C., Lopez A., Dean D., & Salome L. (2003) Confined diffusion without fences of a G-protein-coupled receptr as revealed by single particle racking. *Biophys. J.*, **84,** 356-366.

[54] Lommerse P.H., Blab G.A., Congnet L., Harms G.S., Snaar-Jagalska B.E., Spaink H.P., & Schmidt T. (2004) Single-molecule imaging of the H-ras membrane-anchor reveals domains in the cytoplasmic leaflet of the cell membrane. *Biophys. J.*, **86,** 609-616.

[55] Hancock J.F. & Parton R.G. (2005) Ras plasma membrane signalling platforms. *Biochem. J.*, **389,** 1-11.

[56] Lommerse P.H., Snaar-Jagalska B.E., Spaink H.P., & Schmidt T. (2005) Single-molecule diffusion measurements of H-Ras at the plasma membrane of live cells reveal microdomain localization upon activation. *J. Cell Science*, **118,** 1799-1809.

[57] Murakoshi H., Iino R., Kobayashi T., Fujiwara T., Ohshima C., Yoshimura A., & Kusumi A. (2004) Single-molecule imaging analysis of Ras activation in living cells. *PNAS*, **101,** 7317-7322.

[58] Prior I.A., Muncke C., Parton R.G., & Hancock J.F. (2003) Direct visualization of as proteins in spatially distinct cell surface microdomains. *J. Cell Biol.*, **160,** 165-170.

[59] Niv H., Gutman O., Kloog Y., & Henis Y.I. (2002) Activated K-Ras and H-Ras display different interactions with saturable nonraft sites at the surface of live cells. *J. Cell Biol.*, **157,** 865-872.

[60] Rotblat B., Prior I.A., Muncke C., Parton R.G., Kloog Y., Henis Y.I., & Hancock J.F. (2004) Three separable domains regulate GTP-dependent association of H-Ras with the plasma membrane. *Mol. Cell. Biol.*, **24,** 6799-6810.

[61] Ladha S., Mackie A.R., Harvey L.J., Clark D.C., Lea E.J., Brullemans M., & Duclohier H. (1996) Lateral diffusion in planer lipid bilayers: a fluorescence recovery after photobleaching investigation of its modulation by lipid composition, cholesterol, or alamethicin content and divalent cations. *Biophys. J.*, **71,** 1364-1373.

[62] Lee G.M., Zhang F., Ishihara A., McNeil C.L., & Jacobson K. (1993) Unconfined lateral diffusion and an estimate of pericellular matrix viscosity revealed by measuring the mobility of gold-tagged lipids. *J. Cell Biol.*, **120,** 25-35.

[63] Lindblom G., Johansson L.B., & Arvidson G. (1981) Effect of cholesterol in membranes. Pulsed nuclear magneic resonance measurements of lipid lateral diffusion. *Biochemistry*, **20,** 2204-2207.

[64] Sonnleitner A., Schütz G.J., & Schmidt T. (1999) Free Brownian motion of individual lipid molecules in biomembranes. *Biophys. J.*, **77,** 2638-2642.

[65] Swaisgood M. & Schindler M. (1989) Lateral diffusion of lectin receptors in fibroblast membranes as a function of cell shape. *Exp. Cell Res.*, **180,** 515-528.

[66] Kurzchalia T.V. & Parton R.G. (1999) Membrane microdomains and caveolae. *Curr. Opin. Cell Biol.*, **11,** 424-431.

[67] Fridriksson E.K., Shipkova P.A., Sheets E.D., Holowka D., Baird B., & McLafferty F.W. (1999) Quantitative analysis of phospholipids in functionally important membrane domains from RBL-2H3 mast cells using tandem high-resolution mass spectrometry. *Biochemistry*, **38,** 8056-8063.

[68] Schroeder R., London E., & Brown D. (1994) Interactions between saturated acyl chains confer detergent resistance on lipids and glycosylphosphatidylinositol (GPI)-anchored proteins: GPI-anchored proteins in liposomes and cells show similar behavior. *Proc. Natl. Acad. Sci. USA*, **91,** 12130-12134.

[69] Simons K. & Vaz W.L. (2004) Model systems, lipid rafts, and cell membranes. *Annu. Rev. Biophys. Biomol. Struct.*, **33,** 269-295.

[70] Edidin M. (2003) The state of lipid rafts: from model membranes to cells. *Annu. Rev. Biophys. Biomol. Struct.* , **32,** 257-283.

[71] Pralle A., Keller P., Florin E.L., Simons K., & Horber J.K. (2000) Sphingolipid-cholesterol rafts diffuse as small entities in the plasma membrane of mamalian cells. *J. Cell Biol.*, **148,** 997-1008.

[72] Simons K. & Ikonen E. (1997) Functional rafts in cell membranes. *Nature*, **387,** 569-572.

[73] Simons,K. & Toomre,D. (2000) Lipid rafts and signal transduction. *Nat. Rev. Mol. Cell Biol.*, **1,** 31-39.

[74] Kusumi A., Koyama-Honda I., & Suzuki K. (2004) Molecular dynamics and interactions for creation of stimulation-induced stabilized rafts from small unstable steady-state rafts. *Traffic*, **5,** 213-230.

[75] Sharma P., Varma R., Sarasij R.C., Ira Gousset K., Krishnamoorthy G., Rao M., & Mayor S. (2004) Nanoscale organization of multiple GPI-anchored proteins in living cell membranes. *Cell*, **116,** 577-589.

[76] Orr G., Hu D., Özcelik S., Opresko L.K., Wiley H.S., & Colson S.D. (2005) Cholesterol Dictates the Freedom of EGF Receptors and HER2 in the Plane of the Membrane. *Biophys. J.*, **89,** 1362-1373.

[77] Puri C., Tosoni D., Comai R., Rabellino A., Segat D., Caneva F., Luzzi P., Fiore P.P.D., & Tacchetti C. (2005) Relationships between EGFR Signalling-competent and Endocytosis-competent Membrane Microdomains. *Mol. Biol. of the Cell*, **16,** 2704-2718.

[78] Biedi C., Panetta D., Segat D., Cordera R., & Maggi D. (2003) Specificity of insulin-like growth factor I and insulin on Shc

phosporylation and Grb2 recruitment in caveolae. *Endocrinology,* **144,** 5497-5503.

[79] Ridyard M.S. & Robbins S.M. (2003) Fibroblast growth factor -2-induced signaling through lipid raft-associated fibroblast growth factor receptor substrate 2 (FRS2). *J. Biol. Chem.*, **278,** 13803-13809.

[80] Yang N., Huang Y., Jiang J., & Frank S.J. (2006) Caveolar and lipid raft localization of the growth hormone receptor and its signalling elements: impact on growth hormone signalling. *J. Biol. Chem.*, **279,** 20898-20905.

[81] Gingras D., Gauthier F., Lamy S., Desrosiers R.R., & Beliveau R. (1998) Localization of RhoA GTPase to endothelial caveolae-enriched membrane domains. *Biochem. Biophys. Res. Commun.*, **247,** 888-893.

[82] Michaely P.A., Mineo C., Ying Y.S., & Anderson R.G. (1999) Polarized distribution of endogenous Rac1 and RhoA at the cell surface. *J. Biol. Chem.*, **274,** 21430-21436.

[83] Harder T. & Engelhardt K.R. (2004) Membrane domains in lymphocytes-from lipid rafts to protein scaffolds. *Traffic*, **5,** 265-275.

[84] Harder T., Scheiffele P., Verkade P., & Simons K. (1998) Lipid domain structure of the plasma membrane revealed by patching of membrane components. *J. Cell Biol.*, **141,** 929-942.

[85] Brown D. & Rose J.K. (1992) Sorting of GPI-anchored proteins to glycolipid-enriched membrane subdomains during transport to the apical cell surface. *Cell*, **68,** 533-544.

[86] Heerklotz H. (2002) Triton promotes domain formation in he lipid raft mixtures. *Biophys. J.*, **83,** 2693-2701.

[87] Munro S. (2003) Lipid rafts:elusive or illusive? *Cell*, **115,** 377-388.

[88] Fra A.M., Williamson E., Simons K., & Parton R.G. (1995) De novo formation of caveolae in lymphocytes by expression of VIP21-caveolin. *Proc. Natl. Acad. Sci. USA*, **92,** 8655-8659.

[89] Pelkmans L. & Helenius A. (2002) Endocytosis via caveolae. *Traffic*, **3,** 311-320.

[90] Nichols B.J. (2003) GM1-containing lipid raft are depleted within clathrin-coated pits. *Curr. Biol*, **13,** 686-690.

[91] Holowka D., Sheets E.D., & Baird B. (2000) *J. Cell Sci.*, **113,** 1009-1019.

[92] Langlet C., Bernard A.M., Drevot P., & He H.T. (2000) *Curr. Opin. Immunol*., **12,** 250-255.

[93] Nagy P., Jenei A., Kirsch A.K., Szöllösi J., Damjanovich S., & Jovin T.M. (1999) *J. Cell Sci.*, **112,** 1733-1741.

[94] Korlach J., Schwille P., Webb W.W., & Feigenson G.W. (1999) *Proc. Natl. Acad. Sci. USA*, **96,** 8461-8466.

[95] Bacia K., Schwille P., & Kurzchalia T. (2005) Sterol structure determines the separation of phases and the curvature of the liquid-ordered phase in model membranes. *PNAS*, **102,** 3272-3277.

[96] Baumgart T., Hess S.T., & Webb W.W. (2003) *Nature*, **425,** 821-824.

[97] Dietrich C., Volovyk Z.N., Levi M., Thompson N.L., & Jacobson K. (2001) *Proc. Natl. Acad. Sci. USA*, **98,** 10642-10647.

[98] Janes P.W., Ley S.C., & Magee A.I. (1999) *J. Cell Biol.*, **147,** 447-461.

[99] Lencer W.I., Hirst T.R., & Holmes R.K. (1999) *Biochim. Biophys. Acta*, **1450,** 177-190.

[100] Kwik J., Boyle S., Fooksman D., Margolis L., Sheetz M.P., & Edidin M. (2003) Membrane cholesterol, lateral mobility, and the phosphatidylinositol 4,5-bisphosphate dependent organization of cell actin. *Proc. Natl. Acad. Sci. USA*, **100,** 13964-13969.

[101] Feder T.J., Brustmascher I., Slattery J.P., Baird B., & Webb W.W. (1996) Constrained diffusion o immobile fraction on cell surfaces: a new interpretation. *Biophys. J.*, **70,** 2767-2773.

[102] Ghosh R.N. & Webb W.W. (1994) Automated detection and tracking of individual and clusered cell-surface low-density lipoprotein receptor molecules. *Biophys. J.*, **66,** 1301-1318.

[103] Smith P.R., Morrison I.E.G., Wilson K.M., Fernandez N., & Cherry R.J. (1999) Anomalous diffusion of major histocompatibility complex class I molecules on HeLa cells determined by single prticle tracking. *Biophys. J.*, **76,** 3331-3344.

[104] Kusumi A. & Sako Y. (1996) Cell surface organization by the membrane skeleton. *Curr. Opin. Cell Biol.*, **8,** 566-574.

[105] Saxton M.J. (1994) Anomalous diffusion due to obstacles: a Monte Carlo study. *Biophys. J.*, **66,** 394-401.

[106] Iino R., Koyama I., & Kusumi A. (2001) Single molecule imaging of green fluorescent proteins in living cells: E-cadherin forms oligomers on the free cell surface. *Biophys. J.*, **80,** 2667-2677.

[107] Kerr J.F.R., Wyllie A.I., & Currie A.R. (1972) *Cancer*, **26,** 239-257.

[108] Nagata S. (1997) Apoptosis by death factor. *Cell*, **88,** 355-365.

[109] Grell M. (1990) Identification of a 60-kD TNF recptor as the major signal transducing component in TNF responses. *J. Exp. Med.*, **172,** 1019-1023.

[110] Banner D.W., D'Arcy A., Janes W., Gentz R., Schoenfeld H.J., Broger C., Loetscher H., & Lesslauer W. (1993) Crystal structure of the soluble human 55 kd TNF receptor-human TNF complex: implications for TNF receptor activation. *Cell*, **73,** 431-445.

[111] Hsu H., Xiong J., & Goeddel D. (1995) The TNF receptor 1-associated protein TRADD signals cell death and NF-B activation. *Cell*, **81,** 495-504.

[112] Samuilov V., Oleskin A., & Lagunova E. (2000) Programmed Cell Death. *Biochemistry*, **65,** 873-887.

[113] Hsu H., Shu H., Pan M., & Goeddel D. (1996) TRADD-TRAF2 and TRADD-FADD interactions define two distinct TNF receptor 1 signal transduction pathways. *Cell*, **84,** 299-308.

[114] Tartaglia L. & Goeddel D. (1992) Two TNF receptors. *Immunol. Today*, **13,** 151-153.

[115] Boldin M., Mett I., Varfolomeev E., Chumakov I., Shemer-Avni Y., Camonis J., & Wallach D. (1995) Self-association of the "death domains" of the p55 tumor necrosis factor (TNF) receptor and Fas/APO1 prompts signaling for TNF and Fas/APO1 effects. *J. Biol. Chem.*, **270,** 387-391.

[116] Wang J., Chun H., Wong W., Spencer D., & Lenardo M. (2001) Caspase-10 is an initiator caspase in death receptor signaling. *Proc. Natl. Acad. Sci. U. S. A*, **98,** 13884-13888.

[117] Shi Y. (2002) Mechanisms of Caspase Activation and Inhibition during Apoptosis. *Cell*, **9,** 459-470.

[118] Locksley R., Killeen N., & Lenardo M. (2001) *Cell*, **104,** 487-501.

[119] Grell M., Douni E., Wajant H., Lohden M., Clauss M., Maxeiner B., Georgopoulos S., Lesslauer W., Kollias G., Pfizenmaier K., & Scheurich P. (1995) The transmembrane form of tumor necrosis factor is the prime activating ligand of the 80 kDa tumor necrosis factor receptor. *Cell*, **83,** 793-802.

[120] Tang P., Hung M.-C., & Klostergaard J. (1996) Human pro-tumor necrosis factor is a homotrimer. *Biochemistry*, **35,** 8216-8225.

[121] Black R.A., Rauch C.T., Kozlosky C.J., Peschon J.J., Slack J.L., Wolfson M.F., Castner B.J., Stocking K.L., Reddy P., Srinivasan S., Nelson N., Boiani N., Schooley K.A., Gerhart M., Davis R., Fitzner

J.N., Johnson R.S., Paxton R.J., March C.J., & Cerretti D.P. (1997) A metalloproteinase disintegrin that releases tumournecrosis factor-alpha from cells. *Nature*, **385,** 729-733.

[122] Fesik S.W. (2000) Insights into programmed cell death through structural biology. *Cell*, **103,** 273-282.

[123] Krippner-Heidenreich A., Tubing F., Bryde S., Willi S., Zimmermann G., & Scheurich P. (2002) Control of receptor-induced signaling complex formation by the kinetics of ligand/receptor interaction. *J. Biol. Chem.*, **277,** 44155-44163.

[124] Eck M.J. & Sprang S.R. (1989) The structure of tumor necrosis factor-alpha at 2.6Å resolution. Implications for receptor binding. *J. Biol. Chem.*, **264,** 17595-17605.

[125] Eissner G., Kolch W., & Scheurich P. (2004) Ligands working as receptors: reverse signaling by members of the TNF superfamily enhance the plasticity of the immune system. *Cytokine & Growth Factor Reviews*., 15 (5), 353-366.

[126] Micheau O. & Tschopp J. (2003) Induction of TNF receptor I-mediated apoptosis via two sequential signaling complexes. *Cell*, **114,** 181-190.

[127] Humphrey W., Dalke A., & Schulten K. (1996) VMD-Visual Molecular Dynamics. *Journal of Molecular Graphics*, **14 (1),** 33-38.

[128] Grell M., Zimmermann G., Hulser D., Pfizenmaier K., & Scheurich P. (1994) TNF receptors TR60 and TR80 can mediate apoptosis via induction of distinct signal pathways. *J. Immunol.*, **153,** 1963-1972.

[129] Rothe M., Wong S.C., Henzel W.J., & Goeddel D.V. (1994) A novel family of putative signal transducers associated with the cytoplasmic domain of the 75 kDa tumor necrosis factor receptor. *Cell,* **78,** 681-692.

[130] Park Y.C., Burkitt V., Villa A.R., Tong L., & Wu H. (1999) Structural basis for selfassociation and receptor recognition of human TRAF2. *Nature,* **398,** 533-538.

[131] Wajant H., Grell M., & Scheurich P. (1999) TNF receptor associated factors in cytokine signaling. *Cytokine Growth Factor Rev.,* **10,** 15-26.

[132] Park Y.C., Ye H., Hsia C., Segal D., Rich R.L., Liou H.C., Myszka D.G., & Wu H. (2000) A novel mechanism of TRAF signaling revealed by structural and functional analyses of the TRADD-TRAF2 interaction. *Cell,* **101,** 777-787.

[133] Tsien R.Y. (1998) The green fluorescent protein. *Annu. Rev. Biochem.,* **67,** 509-544.

[134] Yang F., Moss L.G., & Phillips G.N. (1996) *Nat. Biotechnol.,* **14,** 1246-1251.

[135] Billinton N. & Knight A.W. (2001) Seeing the Wood through the Trees: A Review of Techniques for Distinguishing Green Fluorescent

Protein from Endogenous Autofluorescence. *Analytical Biochemistry,* **291,** 175-197.

[136] Goodenough D.A. & Revel J.P. (1970) A fine structural analysis of intercellular junctions in the mouse liver. *J. Cell Biol.*, **45,** 272-290.

[137] Kumar N.M. & Gilula N.B. (1986) Cloning and characterization of human and rat liver cDNAs coding for a gap junction protein. *J. Cell Biol.*, **103,** 767-776.

[138] Larsen W.J. (1977) Structural diversity of gap junctions. A review. *Tissue Cell,* **9,** 373-394.

[139] Makowski L., Caspar D.L.D., Phillips W.C., & Goodenough D.A. (1977) Gap junction structures: Analysis of the x-ray diffraction data. *J. Cell Biol.*, **74,** 629-645.

[140] Evans W.H., Ahmad S., Diez J., George C.H., Kendall J.M., & Martin P.E. (1999) Trafficking pathways leading to the formation of gap junctions. *219,* Novartis Found Symp., 44-54.

[141] Laing J.G., Tadros P.N., Westphale E.M., & Beyer E.C. (1997) Degradation of Connexin43 Gap Junctions Involves both the Proteasome and the Lysosome. *Experimental Cell Research,* **236,** 482-492.

[142] Jordan K., Solan J.L., Dominguez M., Sia M., Hand A., Lampe P.D., & Laird D.W. (1999) Trafficking, Assembly, and Function of a Connexin43-Green Fluorescent Protein Chimera in Live Mammalian Cells. *Molecular Biology of the Cell,* **10,** 2033-2050.

[143] Lauf U., Giepmans B.N., Lopez P., Braconnot S., Chen S.C., & Falk M.M. (2002) Dynamic trafficking and delivery of connexons to the plasma membrane and accretion to gap junctions in living cells. *Proc. Natl. Acad. Sci. USA*, **99,** 10446-10451.

[144] Falk M.M. (2000) Connexin-specific distribution within gap junctions revealed in living cells. *J. Cell Sci.*, **113,** 4109-4120.

[145] Falk M.M. (2000) Biosynthesis and structural composition of gap junction intercellular membrane channels. *Eur. J. Cell Biol.*, **79,** 564-574.

[146] Falk M.M. (2002) Genetic tags for labelling live cells: gap junctions and beyond. *Trends Cell Biol.*, **12,** 399-404.

[147] Schwille P. & Haustein E. (2003) Fluorescence Correlation Spectroscopy. *http://www. biophysics. org/education/schwille. pdf.*

[148] Minsky M. (1961) Microscopy apparatus. [US patent 3013467].

[149] Webb R.H. (1997) *Rep. Prog. Phys.*, **59,** 427-471.

[150] Pawley J.B. (1991) *Handbook of Biological Confocal Microscopy*, 2. edn. Plenum, New York.

[151] Aragón S.R. & Pecora R. (1975) Fluorescence Correlation Spectroscopy and Brownian Rotational Diffusion. *Biopolymers*, **14,** 119-137.

[152] Schwille P., Korlach J., & Webb W.W. (1999) *Cytometry*, **36 (3),** 176-182.

[153] Wachsmuth M., Waldeck W., & Langowski J. (2000) Anomalous diffusion of fluorescent probes inside living cell nuclei investigated by spatially-resolved fluorescence correlation spectroscopy. *Journal of Molecular Biology*, **298,** 677-689.

[154] Feder T.J., Brust-Mascher I., Slattery J.P., Baird B., & Webb W.W. (1996) *Biophysical Journal*, **70 (6),** 2767-2773.

[155] Teruel M.N. & Meyer T. (2000) Translocation and Reversible Localization of Signaling Proteins: A Dynamic Future for Signal Transduction. *Cell*, **103,** 181-184.

[156] Saffman P.G. & Delbrück M. (1975) *Proc. Nat. Acad. Sci. USA*, **27(8),** 3111-3115.

[157] Saffman P.G. (1976) *Journal of Fluid Mechanics*, **73(4),** 593-602.

[158] Cherry R. (1979) *Biochem. et Biophys. Acta*, **559,** 289-327.

[159] Conner S.D. & Schmid S.L. (2003) Regulated portals of entry into the cell. *Nature*, **422,** 37-44.

[160] Ko Y.-G., Lee J.-S., Kang Y.-S., Ahn J.-H., & Seo J.-S. (1999) TNF-α-Mediated Apoptosis Is Initiated in Caveolae-Like Domains. *J. Immunol.*, 7217-7223.

[161] Legler D.F., Micheau O., Doucey M.-A., Tschopp J., & Bron C. (2003) Recruitment of TNF Receptor 1 to Lipid Rafts Is Essential for TNF-α-Mediated NF-κB Activation. *Immunity*, **18,** 655-664.

[162] Cottin A., Doan J.E.S., & Riches D.W.H. (2002) Restricted Localization of the TNF Receptor CD120a to Lipid Rafts: A Novel Role for the Death Domain. *J. Immunol.*.

[163] Feng X., Gaeta M.L., Madge L.A., Yang J.-H., Bradley J.R., & Pober J.S. (2001) Caveolin-1 Associates with TRAF2 to Form a Complex That Is Recruited to Tumor Necrosis Factor Receptor. *J. of Biol. Chem.*, **276,** 8341-8349.

[164] Ledgerwood E.C., Pober J.S., & Bradley J.R. (1999) Recent advances in the molecular basis of TNF signal transduction. *Lab. Invest.*, **79,** 1041-1050.

Acknowledgements

The present work was carried out at the 3rd Institute of Physics in collaboration with the Department of Biophysics and the Institute of Cell Biology and Immunology.

At this place I would like to thank all those people, who contributed to my work. First of all I wish to thank Prof. Jörg Wrachtrup for inviting me to his lab and for supervising my work. I would like to thank Dr. Carsten Tietz and Dr. Fedor Jelezko for the excellent mentoring and technical assistance as well as Dr. Uwe Gerken and Dr. Elmar Thews for their help and support throughout my entire thesis.

I wish to thank all members of the 3rd Institut of Physik for being very amiable colleagues, for their help and interesting and fruitful discussions during countless coffe-breaks. Special thanks to Andrew Aird for the molecular modelling and preparing all the nice pictures with VMD.

Thanks a lot to Britta Götze, Alexandra Elli and Monika Düser. They made daily life in the institute extremely nice, smooth and interesting, apart for being such good friends!

I would also like to thank Dr. Reiner Eckert for preparing the samples for the experiment with gap-junction channels and Prof. Robin Ghosh for the dye-labelled lipids.

I would like to thank Prof. Peter Scheurich for being my second supervisor and all the help from him and his institute. A special thank to Dr. Anja Krippner-Heidenreich, Sylvia Willi and Gudrun Zimmermann for preparing numberless samples and support. You were a great help to me.

I would like to thank Dr. Suren Felekyan for providing me the opportunity to write my thesis in Germany and for his help and support.

Finally, I am indebted to my family, and especially to my husband Uwe Gerken, for their support and advice throughout my education.